A Spectroscopic Survey of Young Massive Star-Forming Regions

Shiwei Wu
Max-Planck-Institut für Astronomie

Heidelberg 2016

Dissertation in Astronomy
submitted to the
Combined Faculties of the Natural Sciences and Mathematics
of the Ruperto-Carola-University of Heidelberg, Germany,
for the degree of
Doctor of Natural Sciences

Put forward by
M.Sc. *Shiwei Wu*
born in Guiyang, China

Oral examination: 01.02.16

A Spectroscopic Survey of Young Massive Star-Forming Regions

Referees: **Prof. Dr. Thomas Henning**
Prof. Dr. Ralf Klessen

To my family

Abstract

Massive stars form on different scales, ranging from large, dispersed OB associations to compact, dense starburst clusters. The question whether one single star formation mechanism is responsible for this wide range of properties is not answered yet. The complex structure of regions of massive star formation, and the involved short timescales provide a challenge for our understanding of their birth and early evolution. In this thesis, I study the formation process of the massive stellar content in two of the most massive and luminous star forming regions in our Galaxy: W49 and W51. I analyse near-infrared (NIR) observations obtained with state-of-the-art ground based telescopes. NIR spectroscopic observations provide reliable classification on the nature of massive stars still heavily embedded in Giant Molecular Clouds (GMCs). With the derived physical properties of the massive stars, we aim to investigate and determine the star formation history of the star forming regions.

A very massive star (VMS) (M > 100 $M_{\odot}$) is discovered in the central cluster of W49. It is classified as an O2-3.5If* star based on its *K*-band spectrum. By comparing with Geneva stellar evolutionary models, the initial mass of this star is estimated as between 100 $M_{\odot}$ and 180 $M_{\odot}$. With the complete spectroscopic observations of W49, thirteen O type stars as well as two Young Stellar Objects (YSOs) are identified. The age of the cluster is estimated as ~1.5 Myrs, with star formation still ongoing in different parts of the region. The stellar content of W51 is also studied in this thesis. Evidence has been found that the star formation in W51 has started ~5 Myrs ago and still active until now. The distinct environments and properties of sub-clusters are discussed. Despite the fact that the W51 and W49 GMCs have similar mass, we find very different massive stellar population and star formation history. W51 does not contain any VMS, while W49 has 3-4 stars more massive than 100 $M_{\odot}$. This might be related to differences in the star formation process between these two regions.

Zusammenfassung

Massereiche Sterne entstehen in Strukturen auf verschiedener Größenskalen, von ausgedehnten OB Assoziationen bis hin zum kompakten "Starburst Cluster" Die Frage, ob ein einzelner Sternentstehungsmechanismus diese weit gefächerten Eigenschaften erklären kann ist noch nicht geklärt. Die komplexe Struktur der Regionen in denen sich die Entstehung massereicher Sterne abspielt, sowie deren kurze Zeitskalen, stellen eine Herausforderung für unser Verständnis der Entstehung und frühzeitlichen Entwicklung dar. In dieser Arbeit untersuche ich die Entstehungsmechanismen des massereichen stellaren Anteils von zwei der massereichsten und leuchtkräftigsten Sternentstehungsgebiete in unserer Galaxis: W49 und W51. Ich analysiere mit modernsten Teleskopen aufgenommene Infrarotbeobachtungen. Spektroskopische Nahinfrarotaufnahmen erlauben eine zuverlässige Klassifizierung massereicher Sterne, die noch stark in einer riesigen Molekülwolke eingebettet sind. Es ist unser Ziel mit den abgeleiteten physikalischen Eigenschaften der massereichen Sterne die Sternentstehungsgeschichte der Sternentstehungsgebiete zu bestimmen.

Im zentralen Sternhaufen in W49 wurde ein sehr massereicher Stern ($M > 100\ M_{\odot}$) entdeckt. Über ein Spektrum im *K*-Band wird der Stern als O2-3.5If* klassifiziert. Durch Vergleich mit den Genfer Sternentwicklungsmodellen lässt sich die ursprüngliche Masse des Sterns zwischen 100 $M_{\odot}$ und 180 $M_{\odot}$ eingrenzen. Insgesamt werden aufgrund der spektroskopischen Beobachtungen in W49 13 O-Sterne und zwei junge stellare Objekte identifiziert. Das Alter des Sternhaufens wird auf ~ 1.5 *MioJahre* geschätzt, wobei Sternentstehung weiterhin in unterschiedlichen Teilen von W49 stattfindet. Weiterhin wird in dieser Arbeit die Sternpopulation in W51 untersucht. Dabei werden Belege dafür gefunden, dass in W51 seit 5 Mio Jahren Sterne entstanden sind und weiter entstehen. Die Sternentstehungsumgebung und die Eigenschaften diverser stellarer Untergruppen werden diskutiert. Obwohl die riesigen Molekülwolken um W49 und W51 vergleichbare Massen aufweisen, unterscheiden sich die Populationen an massereichen Sternen und die Sternentstehungsgeschichten deutlich. In W51 finden sich keine sehr massereichen Sterne, während sich in W49 drei bis vier Stern mit über 100 Sonnenmassen befinden. Eine mögliche Erklärung dafür könnten unterschiedliche Sternentstehungsprozesse in den beiden Regionen sein.

Contents

List of Figures

List of Tables

Chapter 1

Introduction

As one of the fundamental building blocks of galaxies, stars are key in understanding the nature of the world. The essential questions on where and how they form come up almost naturally. Millenia of astronomical exploration, in particular, the enormous progress on astronomical instruments and technologies in the past decades, have contributed significantly to our knowledge of stars. Stars originate deeply embedded in GMCs, where molecular cores gravitationally collapse to initiate their formation.

Stars rarely form isolated, but instead in stellar groups or clusters where they interact with each other during the star formation process. Thus, in order to properly understand the stellar formation process, the formation of stellar clusters needs to be understood as well. Galactic star formation sites, hosting the so-called "embedded clusters", are the ideal targets to closely study star formation in different environments. Studying embedded clusters can improve our understanding of the massive star formation mechanism, stellar evolution, feedback from massive stars, and provide the basis for a better understanding of the formation of extra-galactic star clusters.

1.1 Clustered star formation

Observations suggest that most stars do not form in isolation but form in a clustered environment (Lada & Lada 2003). The protostars are deeply embedded inside GMCs, and invisible at optical wavelengths. Only after the stars are being formed and the molecular cloud has started to disperse, do these regions become visible as embedded clusters. These embedded clusters are the end products of massive star formation (Zinnecker & Yorke 2007), usually associated with HII regions of different scales, and still partially embedded within the gas and dust of the molecular clouds. They are recognized as the probes of star formation in extreme environments, where an intense Lyman continuum radiation field, large extinction, and high stellar densities are shaping the morphologies and dominate the physical processes of the star-forming regions (Fig. 1.1).

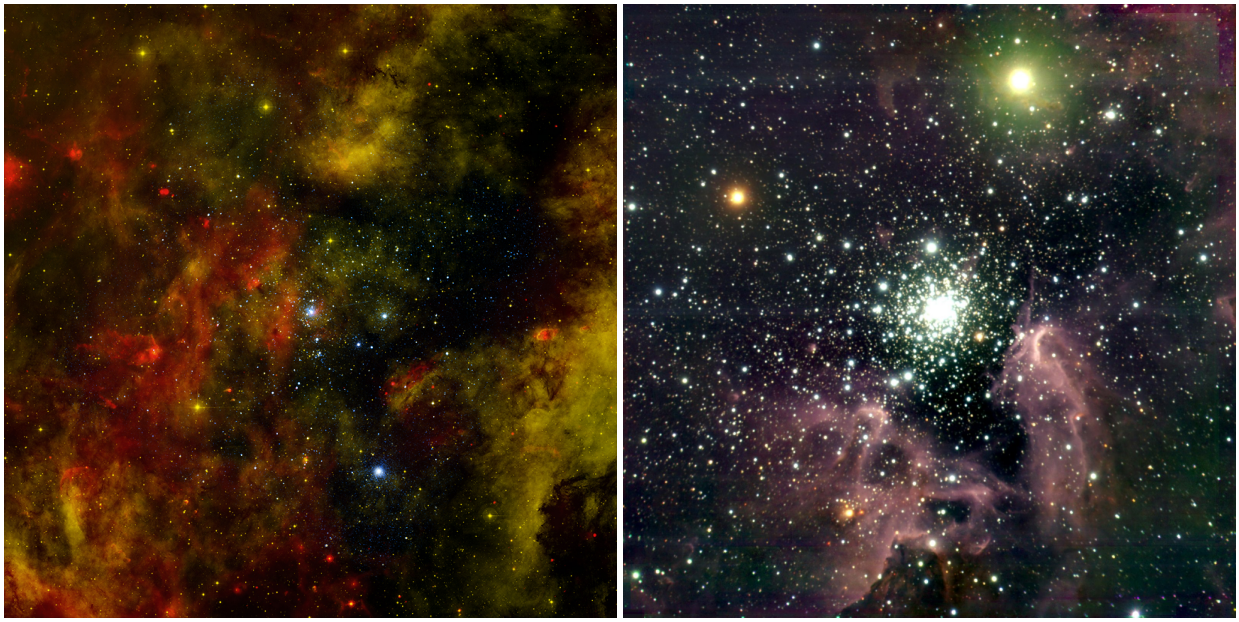

Figure 1.1: *Left:* Cyg_OB2 as an example of loose OB associations. Credit: X-ray: NASA/CXC/SAO/J.Drake et al, Optical: Univ. of Hertfordshire/INT/IPHAS, Infrared: NASA/JPL-Caltech *Right: JHK* composite color image of NGC 3603 obtained with VLT/ISAAC (Stolte et al. 2004), with similar mass of the Cyg_OB2 region.

While clustering is an important feature of star formation with only very few exceptions (de Wit et al. 2004, 2005), embedded clusters are the best places to study the early evolution and initial physical conditions of massive stars, since they are the birthplaces of the majority of most massive stars in our Galaxy (Lada & Lada 2003). From the observational point of view, VMSs are usually found in such young star-forming regions (Crowther et al. 2010; Bestenlehner et al. 2011; Wu et al. 2014).

The stellar members of embedded clusters have masses ranging from the bottom to the top of the stellar mass function all residing in a relatively small volume, ranging from $\sim$ 10 pc to less than a pc (Lada & Lada 2003), and most likely formed together in the same molecular cloud. The distributions of stars in mass, age, and space trace the formation history of their parental regions. For some clusters, the overwhelming majority of stars are formed in a single star burst (Kudryavtseva et al. 2012), on the other hand, age spread between different subregions is also found in other clusters (Negueruela et al. 2010; Bik et al. 2012). For some clusters, the centres are very compact, harbouring the most massive stars of the star forming regions (NGC 3603 (Rochau et al. 2010) and W49, which is studied in chapter 3 of this thesis), while some other clusters extend over a larger volume with multiple compact cores (Carina Nebula Complex (Preibisch et al. 2012) and W51, which is studied in chapter 4 of this thesis).

In the dense, gravitationally bound Young Massive Clusters (YMCs), where the stars are packed closely together, dynamical interactions between the cluster members become important. Each cluster is a many-body system where interactions between members are complex, thus, it is a laboratory for studies of stellar dynamical evolution. The N-body evolutionary effect can either leads to the concentration of massive stars in the centre of a cluster, or the ejection of OB stars with velocities in excess of 40 km s^{-1} (Blaauw 1961; Hoogerwerf et al. 2001).

Since mass and size of YMCs is between those of open and globular clusters, studying them is a natural bridge between star/planet formation in the solar neighbourhood to the oldest structures in the local universe (Longmore et al. 2014). Another aspect is that they may serve as a local analog to the extra-galactic starburst clusters with respect to the similar total mass and stellar density. Through research on the local YMCs, we can determine properties of extra-galactic clusters, even though the stellar content (in particular in their cores) in general cannot be resolved with the current generation of telescopes.

In summary, the research on embedded clusters is important because: (i) Clustering is a normal feature for stars, especially for the most massive ones; (ii) Stellar members in the clusters cover a large mass range and thus provide the samples to study the formation histories of the star-forming regions; (iii) Due to the small spatial scale and high stellar density in YMCs, complex gravitational interaction can be studied in detail; (iv) They provide templates for the studies of the extra-galactic clusters.

1.2 Why study the massive stellar content?

Although it is well known that the birthplace in particular of massive stars are GMCs, stars with different masses are thought to form in different ways. For stars with masses no more than 8 $M_\odot$, their precursors are the dense molecular cores within molecular clouds. The dense cores will collapse and finally form protostars, which will keep accreting the surrounding infalling gas and dust until they reach the main sequence. The widely accepted picture of low-mass star formation is described in Larson (1969) and Shu et al. (1987). On the other hand, their high mass counterparts, i.e. stars with masses higher than 8 $M_\odot$, have a more complicated formation mechanism instead of just being a scaled-up version of low-mass star formation. New physical processes are introduced into high-mass star formation including the more important role of radiative forces (stellar feedback), much shorter time of the pre-main-sequence phase, greater effect of gravitational dynamics, and bigger influence on triggering further star formation (Zinnecker & Yorke 2007).

The formation mechanisms of massive stars are by no means fully understood (Krumholz 2014).

The two main scenarios explaining the formation of very massive stars involve accretion of stellar matter (e.g. Kuiper et al. 2010, 2012) and mergers of lower-mass stars in tight binaries (Bonnell & Bate 2005). For a long time, it was entirely unknown if or how very massive stars with masses in excess of 150 $M_\odot$ could form at all. Observational evidence was presented hinting at an upper mass limit of 150 $M_\odot$ (Figer 2005). However, recently Crowther et al. (2010) suggested the existence of very massive stars of up to 300 $M_\odot$, especially in and around young massive clusters, such as NGC 3603, the Arches cluster, and R136 in the Large Magellanic Cloud. The discovery of such objects would provide observational constraints on numerical simulations investigating the formation of massive stars (e.g. Kuiper et al. (2010, 2011)).

By investigating the stellar content of young massive star-forming regions, we can try to understand how environmental effects such as morphology influence the star formation history. We can address the question whether clusters form in a single burst with stars all of the same age (Kudryavtseva et al. 2012), or form over a longer time with star formation happening in different parts of the clouds (Blaauw 1991; de Zeeuw et al. 1999). For instance, the Galactic Centre and disk are assembling gas into massive clusters in different ways. For star formation in the disk, large scale gas flows feeding the progenitor cloud via filaments is important. While in the Galactic Centre, gas is able to reach very high densities without forming stars until possibly cloud-cloud collisions or tidal forces trigger the collapse of gas under its own gravity (Longmore et al. 2014; Johnston et al. 2014).

With the help of stellar evolutionary models, it is possible to get physical parameters of the stellar content such as the age and the mass, which allows us to understand the mass function and star formation history of YMCs (Bastian et al. 2010). By investigating the massive stellar content, the feedback of massive stars on their surroundings can be studied. The massive stars are the main sources of the ionising flux injected into GMCs, and are also responsible for stellar wind and supernova shockwave, thus dominating the feedback process in molecular clouds. Questions concerning the role of feedback in star formation and whether massive stars trigger or stop further star formation (Zinnecker & Yorke 2007) remain to be answered.

Studying the spatial distribution of massive stars will provide clues on the formation mechanisms of clusters and massive stars. If all massive stars form in clusters or if OB stars can form in isolation is still under debate (Bressert et al. 2012; de Wit et al. 2005; Bonnell et al. 2004; Banerjee et al. 2012). This topic can be addressed by identifying the location of the massive stars and comparing them to their possible birth sites.

1.3 Observational point of view

The key technology facilitating studies of embedded stellar clusters is the NIR detectors. The visual extinction towards YMCs is usually very high and make stars invisible in the optical band. We can only count on observations in longer wavelengths since according to the interstellar extinction curve, the near-infrared radiation from young stars is subject to much lower extinction and can penetrate larger columns of dust in star forming regions and on the way to Earth. As the apparent NIR magnitudes of the massive cluster members are considerably brighter than the limiting magnitude observed with large groundbased telescopes like the LBT and the VLT, the highest mass members can be characterised by spectroscopy.

The major part of the spectroscopic data I used in this thesis is coming from the LOBSTAR project (PI: A. Bik), which is a near-infrared spectroscopic survey of the stellar content of a number of most massive star formation complexes in our Galaxy, including W3 Main, W49 and W51. In W3 Main Bik et al. (2012) classified 15 OB stars and three YSOs, which is indicative of an age spread of at least 2 to 3 Myr between different subregions. The evolutionary sequence observed in the low-mass stellar population via photometry shows that W3 Main is still actively forming stars (Bik et al. 2014) (Fig. 1.2). In this thesis, the other two regions are studied in detail.

LUCI is an infrared multi-mode instrument mounted on the LBT, Mount Graham, near Tucson, Arizona, at an altitude of about 3200 m. In seeing-limited mode, it has a 4′ square field of view and is capable of long-slit and multi-slit spectroscopy as well as imaging in the near infrared $zJHK$-bands from 0.85 to 2.4 μm. In seeing limited mode, the image scale is 0.12" pix^{-1} (N3.75 camera) for imaging and 0.25" pix^{-1} (N1.8 camera) for spectroscopy. Various gratings provide resolutions from 2000 for H+K to 6500-8500 in single band z, j, H, K in the basic modes [1]. The multi-object spectroscopy of LUCI is particularly well-suited to study very crowded star fields like deeply embedded young cluster centres. Within the spectral range of the K-band, many important diagnostic lines can be used to distinguish between stars of different spectral types and luminosity classes. In the following chapters of this thesis, observations from LUCI provide the major information of our science targets.

The two other instruments contributing to the work shown in this thesis are the European Southern Observatory (ESO) instruments VLT/ISAAC and NTT/SOFI. ISAAC is an IR (1 - 5 μm) imager and spectrograph mounted to the Nasmyth of one of the VLT Unit Telescopes, equipped with a 1024 x 1024 Hawaii Rockwell array used at short wavelengths (1 - 2.5 μm) [2]. It provides us with long-slit spectroscopy of some of the massive stars in W49. SOFI is the infrared spectrograph and imaging camera on the NTT. It is also equipped with a Hawaii HgCdTe 1024x1024

[1] http://abell.as.arizona.edu/~lbtsci/Instruments/LUCIFER/lucifer.html
[2] http://www.eso.org/sci/facilities/paranal/decommissioned/isaac.html

Figure 1.2: LUCI JHK_s color image of W3 Main, the first star-forming region studied in the project of LOBSTAR (Bik et al. 2012).

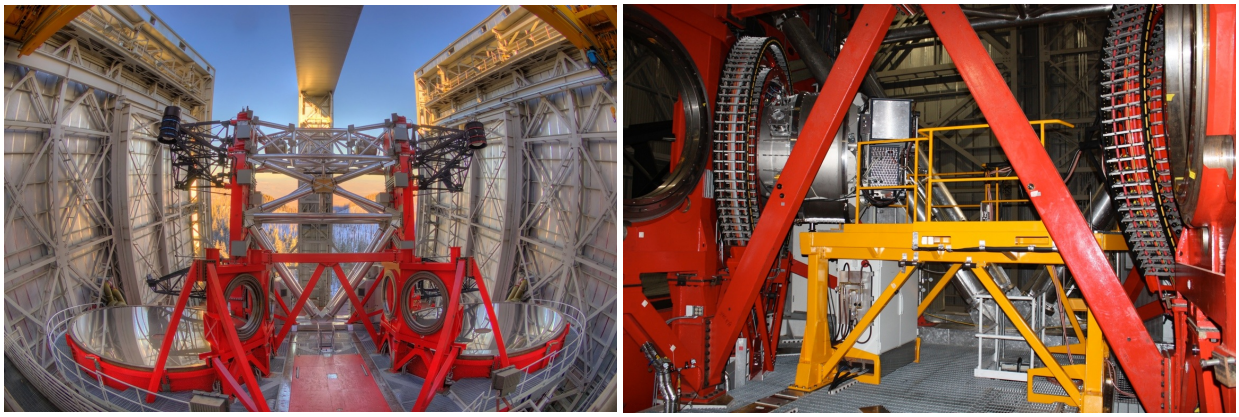

Figure 1.3: *Left:* The image of LBT taken form the LBT webpage (http://www.lbto.org). *Right:* LUCI, the main instrument used in the LOBSTAR project. Credit: Arjan Bik.

array [3]. Images of both W49 and W51 taken with SOFI are utilized in this thesis.

1.4 The focus of this thesis

My work over the past three years was aimed at understanding the formation process of the massive stellar content in young stellar clusters through NIR observation using the state of the art equipments described in Sect. 1.3. Previous observations toward Ultracompact HII (UCHII) regions have been made in radio and infrared regimes, which only provide indirect probes of properties of the central massive stars. The radio flux is proportional to the number of ionizing photons emitted from the hot and massive stars embedded in clouds. By the help of stellar models, the spectral types of central stars can be derived. The infrared luminosity reradiated from the warm dust around the young massive stars provides an indirect estimate of the luminosity of the stars themselves.

Based on our NIR imaging and spectroscopic observations of W49 and W51 – the two most massive and luminous star forming regions in our Galaxy – I investigate the massive stellar content of these regions. The spectral types of massive stars can be classified. Physical parameters, including extinction, ionizing flux, effective temperature, and luminosity can be derived. By comparing with stellar evolutionary models, mass, and age of stars can be estimated. With the derived properties of the massive stars, the age of the different regions can be estimated and the star formation history of W49 and W51 can be reconstructed.

1.4.1 W49

With dozens of massive stars in its core, W49 is one of the most important Galactic sites for studying the formation and evolution of VMSs. Given its location in the plane of the Milky Way and distance of $11.1\ ^{+0.8}_{-0.7}$ kpc (Zhang et al. 2013), W49 is obscured optically by intervening interstellar dust, and subject to large amounts of crowding and field star contamination by foreground stars.

Using deep near-infrared imaging, Alves & Homeier (2003) and Homeier & Alves (2005) studied its stellar population and mass function, and reported the detection of massive stellar clusters still deeply embedded in the GMC of the W49 complex. The observations reveal high extinction towards W49 and large internal extinction variations. They derive a total stellar mass of $5-7\times10^4$ $M_\odot$, which makes W49 comparable to extragalactic giant star-forming regions.

[3] http://www.eso.org/sci/facilities/lasilla/instruments/sofi.html

W49 was also the subject of several radio and submillimeter studies (de Pree et al. 1997; Roberts et al. 2011; Nagy et al. 2012; Galvan-Madrid et al. 2013; Nagy et al. 2015), which revealed complex kinematics of the molecular gas in W49, with a mixture of infall and outflow motions. There are several clumps of cool and dense gas surrounding and possibly infalling onto the centre of the region (Roberts et al. 2011). With only 1% of the gas being photoionized, star formation in W49 is ongoing and the feedback from the cluster is not (yet) strong enough to halt the process (Galvan-Madrid et al. 2013). As comparable physical conditions have been measured in extragalactic starburst regions, W49 could serve as a template for the luminous, embedded star clusters in normal and starburst galaxies.

In Chapter 2, we present the discovery of the brightest star in the dense core of the central cluster of W49, which we hereafter refer to as W49nr1. The near-infrared observations of W49nr1 are shown. Based on its VLT/ISAAC K-band spectrum, W49nr1 is classified as an O2-3.5If* star. Its physical conditions including the extreme mass range over 100 $M_\odot$ are derived by comparing with stellar evolution models.

In Chapter 3, our spectroscopic survey of W49 is described. With the K-band spectroscopic observation from LBT/LUCI together with JHK_s images from observation of NTT/SOFI and LBT/LUCI, massive stars are identified and analysed. Thirteen O-type stars as well as two YSOs are classified in this region. The astrophysical properties of these stars are derived. Three of the O-type stars show strong wind features and are considered to be Of-type supergiants with masses beyond 100 $M_\odot$. The massive stars are placed in an HRD, and their physical conditions and the formation history of the cluster are discussed.

1.4.2 W51

As another important part of our LOBSTAR project, we present in Chapter 4 the results of NIR spectroscopy and photometry of the W51 region. The W51 GMC, located in the Sagittarius arm in the Galactic disk, is known as one of the most luminous star forming regions in the Galaxy. Its elongated shape of 83×114 pc is stretched out along the galactic plane. The total mass estimate is 1.2×10^6 $M_\odot$ (Carpenter & Sanders 1998). The distance of W51 is 5.4 ± 0.3 kpc according to maser trigonometric parallax observations (Sato et al. 2010).

Radio observations support the scenario that infall in the W51 region is taking place in several localized regions as opposed to globally over the entire region (Sollins et al. 2004). The volume density within the forming W51 proto-clusters is $> 10^5$ cm^{-3}, indicating that some regions in W51 have their gas densities above normal "threshold" for star formation. The star forming activity is still ongoing in W51A, while it has mostly ended in W51B (Ginsburg et al. 2015).

In Chapter 4, we identify nine OB-type massive stars and a YSO based on K-band spectroscopic data from LBT/LUCI combined with an analysis of JHK_s images obtained with NTT/SOFI. Spectral types of stellar objects ranging from late O to late B subtypes are determined according to different features in their K-band spectra. Placing them in an HRD give us clues on the formation of the clusters. Taking into consideration the previous radio observations of this region, the formation scenario of the W51 is discussed and compared to that of W49.

Chapter 2

The Discovery of a Very Massive Star: W49nr1

Based on S.-W. Wu, A. Bik, Th. Henning, A. Pasquali, W. Brandner, A. Stolte
Published in Astronomy & Astrophysics, 2014, 568, L13

2.1 Introduction

Even though VMSs (M > 100 $M_{\odot}$) are very rare, they have a strong influence on their environment via powerful winds and ionizing radiation, injecting large quantities of momentum and energy into the surrounding interstellar medium. Their fast evolution and the steep slope of the Initial Mass Function (IMF) imply that one has to study the most massive star-forming regions to identify them.

In this chapter we present the discovery of a VMS in one of the most luminous Galactic HII regions: W49 (Fig 2.1). With dozens of OB-type stars in its core, W49 is one of the most important Galactic sites for studying the formation and evolution of massive stars in the local universe (Alves & Homeier 2003; Homeier & Alves 2005). Given its location in the plane of the Milky Way and a distance of 11.11 $^{+0.79}_{-0.69}$ kpc (Zhang et al. 2013), W49 is optically obscured by intervening interstellar dust. This makes an optical identification and spectral classification of the stellar content close to impossible, leaving the near-infrared window (primarily *K*-band) for spectral classification of the highly obscured stars.

Here, we report on the spectroscopic identification of a VMS in W49. We first present our near-infrared observations (imaging and spectroscopy) of W49 (Sect. 2.2). The spectral features as well as the classification of W49nr1 are described in Sect. 2.3, where we also derive its stellar parameters like effective temperature (T_{eff}), initial mass and age. Finally, we briefly discuss the implications of our results in Sect. 2.4 and end with conclusions in Sect. 2.5.

2.2 Observation and data reduction

A medium-resolution (R=10,000) K-band spectrum of W49nr1 was obtained with ISAAC mounted on Antu (UT1) of ESO's VLT, Paranal, Chile. J- and H-band images were obtained with SOFI at the NTT, La Silla, Chile and a K-band image was acquired with LUCI mounted on the LBT, Mount Graham, Arizona.

2.2.1 Observations

SOFI J- and H-band imaging observations of W49 were performed on 2001, June 7 (PI: J. Alves) providing a $5' \times 5'$ field of view with $0.''288$ $pixel^{-1}$. The data were taken with a detector integration time (DIT) (detector integration time) of 6 s and number of integrations (NDIT) of 5 per saved frame. The number of exposures for J and H-band are 20 and 15 respectively, which lead to a total exposure time of 600 s (J-band) and 450 s (H-band). The spatial resolution is $\sim 0.5 - 0.7''$.

The LUCI K-band data were taken on 2009, September 29 with the N3.75 camera, providing a $5' \times 5'$ field of view with $0.''12$ $pixel^{-1}$. The spatial resolution of the K image is $\sim 0.6 - 0.7''$. The observations were taken with a DIT of 2 s and NDIT of 10. Forty-two frames were observed, resulting in a total exposure time of 840 s. Sky frames were taken at an offset positions centred at $\alpha(2000) = 19^h08^m35.8^s, \delta(2000) = +08°50'52.7''$.

The most luminous star in the central cluster of W49, W49nr1 (Table 2.1), was observed with ISAAC in the K-band on 2004, August 6 (PI: J. Alves), with 3 exposures each with a DIT of 300s. The wavelength range covered by the spectrum is 2.08 μm to 2.20 μm. The sky frame and science frames were taken with an object-sky-object pattern, and the nodding offset between the two science frames was set to $20''$. HR 6572, an A0V star, was used as the standard star to correct for the telluric features from the atmosphere. It was observed about one hour before the science frames, in the same wavelength range as the science observations and with an integration time of 5 s.

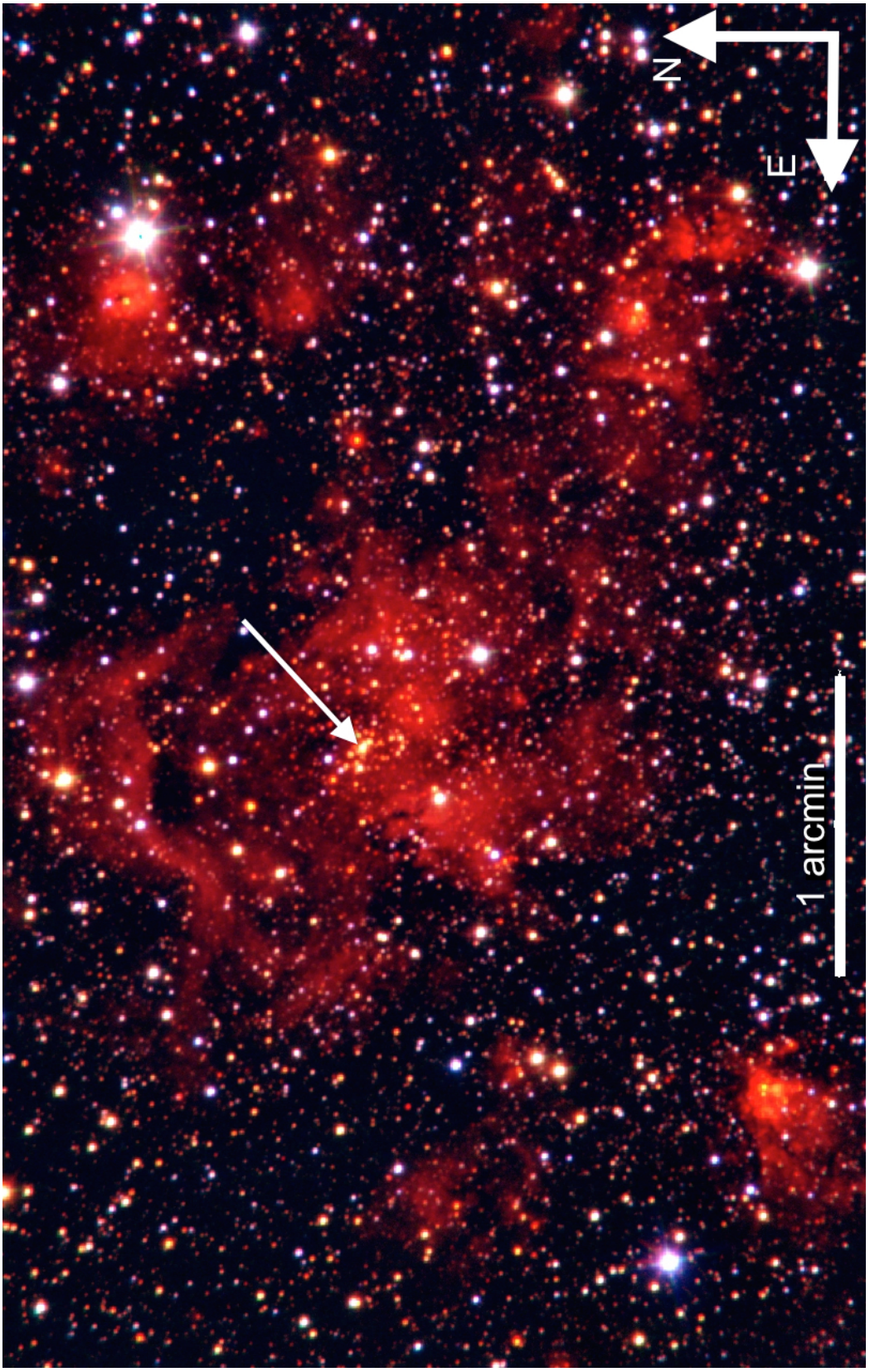

Figure 2.1: *JHK* three color image of the central area of W49. The massive star W49nr1 is indicated with a white arrow.

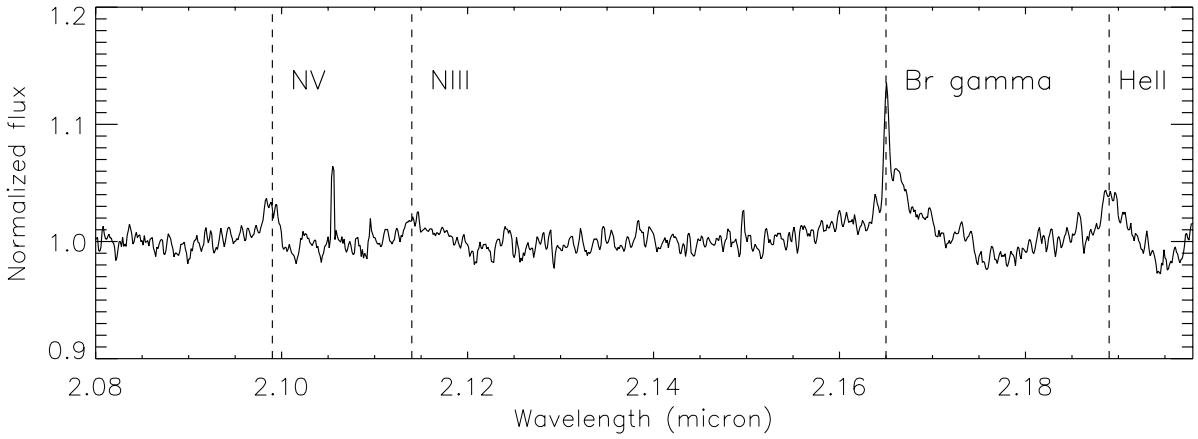

Figure 2.2: Normalised *K*-band spectrum of W49nr1 with the emission lines annotated.

2.2.2 Data reduction

Imaging

The *J*- and *H*-band images were reduced using the ESO SOFI pipeline v1.5.2. and the *K* data with standard IRAF[1] routines (see also Pasquali et al. 2011; Bik et al. 2014). The images were dark and flat field corrected. For the *JH* data, a sky frame was created from the science frames by rejecting the brightest pixels while combining the frames in pixel coordinates. A sky frame for the *K*-band data was created by combining images taken at the offset position and rejecting the 3 lowest and 6 highest values.

Photometry on the *JHK* images was performed with `DAOPHOT` (Stetson 1987) under IRAF. Stars are detected with *daofind* with a threshold of 3σ above the background. Aperture photometry was performed with *phot* in a radius of (1-2) $\times$ the Full Width at Half Maximum (FWHM) of the point spread function (PSF). For each filter a reference PSF model was constructed by combining the PSF of at least 20 objects. PSF-fitting photometry was performed with *allstar*, using the PSF model to fit all objects identified with a 3σ confidence level over the local background.

The *K* image of W49 has severe nebular contamination strongly affecting the photometry of the point sources. To reduce the effect of the nebulosity in the *K* image, we first removed the stars by means of PSF fitting. The residual frame, with all the stars subtracted, was then smoothed with a kernel of 12 pixels, resulting in a frame containing only the smooth nebular emission. This smoothed frame is subtracted from the original frame. After that, we performed PSF photometry

[1]IRAF is distributed by the National Optical Astronomy Observatory, which is operated by the Association of Universities for Research in Astronomy, Inc., under cooperative agreement with the National Science Foundation

Table 2.1: Observed and derived properties of W49nr1

α(J2000) (h m s)	19:10:17.43
δ(J2000) (° ′ ″)	+9:06:20.93
J(mag)	16.57±0.18
H(mag)	13.47±0.12
K(mag)	11.93±0.10
Equivalent Width (EW)(Brγ) (Å)	8.2 ± 1.7
EW(HeII) (Å)	2.4 ± 0.7
EW(NIII) (Å)	2.3 ± 1.0
EW(Nv) (Å)	2.6 ± 0.9
Spectral type	O2-3.5If*
T_{eff}(K)	40,000 – 50,000
BC (mag)	-5.2 – -4.55
A_K(mag)	2.9 [a] / 2.6 - 3.5 [b]
Initial mass ($M_\odot$)	100 – 180 [a] / 90 – 250 [b]
Luminosity ($L/L_\odot$)	1.7 - 3.1×10^6 [a] / 1.2 - 4.9×10^6 [b]

a. With extinction law of Indebetouw et al. (2005)
b. Considering other extinction laws (see text).

on the nebular subtracted image, resulting in a more accurate photometry.

W49nr1 is located in the centre of a compact cluster and its photometry is affected by crowding from the neighbouring stars. To quantify the effect of the crowding, we performed aperture photometry at the position of W49nr1 on the residuals in the PSF-subtracted frame. This gives an error of 15.8, 6.4 and 8.6 % for J, H and K respectively.

Finally, we cross-matched the obtained catalogs for each filter to identify the sources detected in more than one band. We calibrated the SOFI and LUCI photometry with 2MASS (Skrutskie et al. 2006). The final calibration resulted in errors in the zero points of 0.0063, 0.0071 and 0.0055 mag for J, H and K-band respectively. We did not find a color dependence of the derived zero points. The final errors of the JHK photometry, as listed in Table 2.1, are a combination of the photometry uncertainty, errors in the zero points and the errors due to crowding.

Spectroscopy

The ISAAC observations of W49nr1 were reduced using standard IRAF routines. The wavelength calibration was performed using the Xe and Ar arc frames. After the flat fielding and wavelength calibration, the sky was removed by subtracting the frames taken at the A and B nodding position. The spectra were extracted using *doslit* and the different exposures are combined to one final spectrum. To remove the narrow Brγ emission from the diffuse nebular emission surrounding the cluster, the background was estimated using a Legendre function, sampling a region close to the star, and subtracted from the spectrum.

The spectrum of the telluric standard star was reduced in the same way as the spectrum of W49nr1. Before correcting the spectrum of W49nr1 with the standard star, the Brγ line of the standard star was removed by fitting a Lorentzian profile. The resulting atmospheric transmission spectrum was used to correct the science spectrum for telluric absorption using the IRAF task *telluric*. The Sinal-to-Noise Ratio (SNR) of the final spectrum is ~90.

2.3 Results

2.3.1 Spectral classification of W49nr1

The final, normalized K-band spectrum of W49nr1 is shown in Fig 2.2. The spectrum is dominated by broad emission lines of Brγ (2.166 μm), HeII (2.189 μm), NIII (2.116 μm) and NV (2.10 μm). The narrow emission component of Brγ is a residual of the nebular subtraction. The HeII and NV lines are indicative of an early spectral type (Hanson et al. 2005). The broad emission profiles imply an origin in the stellar wind. These properties suggest similarities with the spectral classes O2-3.5If*, O2-3.5If*/WN5-7 ("slash" stars) and WN5-7 stars (Crowther & Walborn 2011). The sum of the EWs of Brγ and HeII can be used as a discriminator between these classes. For the WN5-7 stars, the summed EWs are expected to be above 70 Å, while O2-3.5If* stars have a total EW between 2 and 20 Å, with the "slash" stars lying in between. The total EW of both lines for W49nr1 (Table 2.1) is (10.6 ± 1.8 Å), resulting in a classification of W49nr1 as O2-3.5If*.

2.3.2 HRD

Based on the classification of W49nr1 as an O2-3.5If* star, we estimated T_{eff} between 40,000 and 50,000 K and the bolometric correction (BC_K) between -5.2 and -4.55 mag adopting the

derived values for an O2f*, O3I and an O4I star as representative for this class (Crowther & Walborn 2011). From our HK photometry the absolute K-band magnitude was derived to be -6.27 ± 0.1 mag by assuming the distance of 11.11 kpc (Zhang et al. 2013), applying the extinction law of Indebetouw et al. (2005) and adopting the intrinsic color of $(H - K) = -0.1$ mag for O3I stars from Martins & Plez (2006). After applying the BC_K, the bolometric magnitude of W49nr1 was derived to be between -11.47 and -10.82 mag, and the corresponding bolometric luminosity between 1.7×10^6 and 3.1×10^6 $L_\odot$.

We plotted the likely parameter space of W49nr1 in the HRD as shown in Fig 2.3. As T_{eff} and BC_K are correlated, the likely location of W49nr1 is a diagonal ellipse. The possible locations of W49nr1 in the HRD was estimated by calculating the luminosity for the three spectral types in this class (O2If*, O3I and O4I), using their T_{eff} and corresponding BC_K. To estimate the initial mass and age of W49nr1, the likely parameter space in the HRD was compared with the Geneva theoretical stellar evolution models (Ekström et al. 2012; Yusof et al. 2013), using models with and without stellar rotation.

From the evolutionary tracks, the initial mass of W49nr1 was estimated to be in the range between ~110 and ~180 $M_\odot$ for models without rotation and between ~100 and ~170 $M_\odot$ for models with rotation (Fig 2.3, left panel, vertically hashed area). While the initial mass estimate for W49nr1 is insensitive to rotation, the isochrones for the models with and without rotation for the same age are very different (Fig 2.3, right panel). The position of W49nr1 suggests an upper age limit of ~2 Myrs after comparison with the "non-rotating" isochrones, however, considering the models with rotation, an age between 2 and 3 Myrs is more likely.

As the extinction towards W49nr1 is high ($A_K = 2.9$ mag) the choice of the extinction law can have a large effect on the derived luminosity and therefore on its initial mass and age. To select the best fitting extinction laws, we applied a similar analysis to the color-color diagram of W49 as Bik et al. (2012) and found that the slopes of the Cardelli et al. (1989) and Román-Zúñiga et al. (2007) laws were not consistent with the observations (discussed also in Sect. 3.3.1).

The extintion law of Indebetouw et al. (2005) was the best fitting law, but also the slopes of Fitzpatrick (1999), Nishiyama et al. (2009) and Rieke & Lebofsky (1985) are consistent with the observed colors. Taking into account all the 4 extinction laws, the estimated initial mass range widens to 90 - 250 $M_\odot$(see Fig 2.3).

2.4 Discussion and future prospectives

In this chapter we report the discovery of a VMS in the centre of the main cluster in W49. In the following we discuss the uncertainties in the derivation of the stellar parameters and the

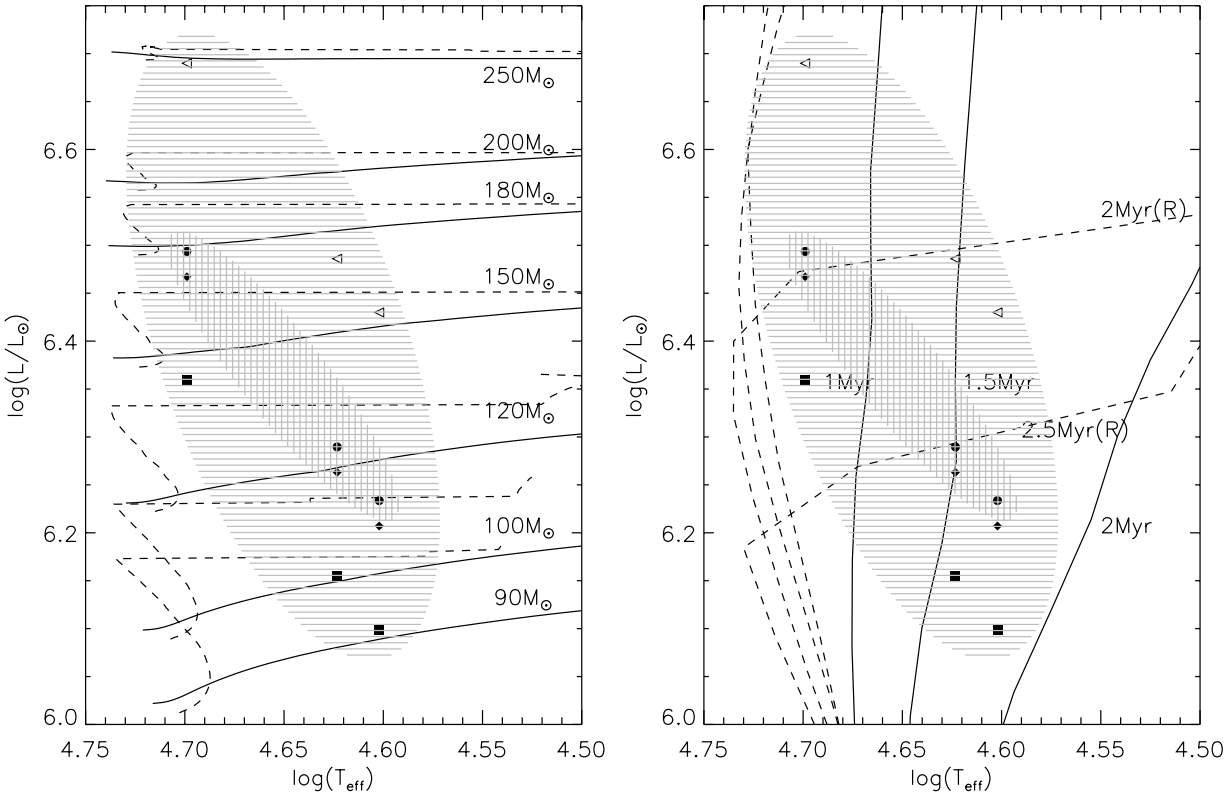

Figure 2.3: HRD with the possible location of W49nr1 marked as a vertically hashed area and horizontally hashed, taking into account different extinction laws. The three black filled circles stand for an O2If*, an O3I and an O4I star respectively. *Left panel:* The Geneva evolution tracks (Ekström et al. 2012; Yusof et al. 2013) without stellar rotation (solid line) and with rotation (dashed line) for different masses are over plotted. *Right panel:* The main sequence isochrones with different ages, again without stellar rotation (solid line) and with rotation (dashed line).

implications for the properties of the central cluster in W49. We end with a suggestion for further characterization of this object.

2.4.1 Stellar paramaters

Our classification of W49nr1 depends on the empirical relation between the spectral type and the equivalent width of the emission lines as well as the calibration of K-band bolometric corrections for early-O stars based upon atmosphere models derived by Crowther & Walborn (2011). Due to the very few objects used in this study, it is hard to predict the uncertainty of this classification and a larger number of stars is needed to make this calibration more reliable.

The evolution of the VMSs is mostly governed by their stellar wind and mass-loss rate. These input parameters for stellar evolution models add uncertainties to the estimated initial mass and age. As a comparison to the Geneva models we use the relation between the luminosity and the maximum stellar mass for homogeneous hydrogen burners (Gräfener et al. 2011), resulting in a present-day mass estimate of 110 - 175 $M_\odot$ (and 95 - 250 $M_\odot$ for taking into account all 4 extinction laws as discussed in Sect. 2.3.2).

The stellar rotation only plays an important part in estimating the age of W49nr1 from the HRD, as the rotational models predict longer time scales for the different evolutionary phases of the massive stars. The K-band spectrum is fully dominated by emission lines originating in the stellar wind, hence no estimate of the rotation can be made. High resolution spectroscopy of possible absorption lines to derive its rotation is key to understand the evolutionary status of this extreme star as well as the cluster. By monitoring the radial velocity of the emission lines, multi-epoch spectroscopy could probe for a possible binary nature.

2.4.2 Cluster properties

W49nr1 is located in the centre of the compact central cluster in W49 (Fig 2.1), and thus supports the theoretical expectation of rapid dynamical mass segregation (e.g. Allison et al. (2009)). Homeier & Alves (2005) estimate the mass of this cluster as 10^4 $M_\odot$. This suggests that W49nr1 is located in an environment quite similar to other VMSs located in (Crowther et al. 2010). It adds to the growing number of stars with initial masses at or above 150 $M_\odot$, suggesting the absence of a strict upper mass limit for massive stars as also suggested by numerical simulations (Kuiper et al. 2010, 2011).

Comparing the cluster mass and the derived stellar mass for W49nr1 to theoretical relations between cluster mass and mass of the most massive star (Weidner et al. 2010) shows that the

presence of such a massive star is consistent with a normal initial mass function. A full study of the upper end of the IMF requires a spectroscopy classification of many more massive stars.

2.5 Conclusions

In this chapter we present JHK imaging and K-band spectroscopy observations of W49nr1, the brightest star in the central cluster of W49. According to classification criteria based on the equivalent widths of Brγ and He II given by Crowther & Walborn (2011), W49nr1 is classified as an O2-3.5If* star. We estimate the effective temperature to be between 40,000 and 50,000 K and the bolometric luminosity between 1.7×10^6 and 3.1×10^6 $L_\odot$. Comparison with the Geneva stellar evolutionary tracks suggests an initial mass range of 100 - 180 $M_\odot$ in the case of a single star, relatively independent of rotational velocity. We study the effect of variations in the extinction law on the stellar parameters, resulting in a large initial mass range of 90 - 250 $M_\odot$. Estimates of the present day mass delivers similar values. The age depends severely on rotational velocity and can only be constrained to less than 3 Myrs. The next step will be a full spectroscopic modelling of the near-infrared spectrum of W49nr1 resulting in stricter constraints on the effective temperature and luminosity. Spectral modelling will allow us to identify possible absorption lines at other wavelengths, suitable for measuring the rotational velocity.

Chapter 3

The Spectroscopic Survy of W49

Based on S.-W. Wu, A. Bik, J. M. Bestenlehner, Th. Henning, A. Pasquali, W. Brandner, A. Stolte, Submitted to Astronomy & Astrophysics, 2015

3.1 Introduction

Massive stars form in dense regions of giant molecular clouds, and interact strongly with their environment. The environments where massive stars form range from dense starburst clusters to loose OB associations. The former are very compact regions with half-mass radii of one parsec or less bound by self-gravity (e.g., (Rochau et al. 2010)), while in the latter OB stars spread over scale from a few to tens of parsec. Such a difference in morphology and physical scale could have a strong influence on the early evolution of the star-forming regions and the stars within them. In order to detect the deeply embedded, recently formed stars, the NIR spectral window provides the possibility to peer through the dust and provides the opportunity to detect the stellar photosphere of young massive stars.

Massive stars are the main sources of ionising flux and mechanical energy (by means of stellar winds and supernova shock waves) injected into GMCs. By identifying and characterising the massive stellar content, the feedback on the surroundings can be studied in detail. An important question is if and under what circumstances the feedback by massive stars might trigger or quench further star formation (Zinnecker & Yorke 2007).

A study of the spatial distribution of massive stars also provides clues on the formation mechanisms of clusters and massive stars. It is still under debate if all massive stars form in clusters or if individual OB stars could form in isolation (Bressert et al. 2012; de Wit et al. 2005; Bonnell et al. 2004; Banerjee et al. 2012).

Young massive clusters, where the majority of the VMSs form and reside during their short life

time (Crowther et al. 2010; Bestenlehner et al. 2011; Wu et al. 2014), are the best environment to study the physical conditions of the birthplaces and the early evolution of the most massive stars.

In the following sections, we present our near-infrared observation of W49 from LBT/LUCI and NTT/SOFI. The reduction of the imaging and spectroscopic data is presented in Sect. 3.2; in Sect. 3.3 we derive the astrophysical properties of the massive stars, and place them in an HRD; the fundamental properties of the cluster in W49, its formation history, feedback towards the environment and the spatial distribution of massive stars are discussed in Sect. 3.4. The result of our spectroscopic investigation towards W49 is summarised in Sect. 3.5.

3.2 Near-infrared observations and data reduction

The observations have been carried out with LUCI mounted on the LBT (Hill et al. 2006), Mount Graham, Arizona. LUCI is a near-infrared multi-mode instrument capable of Multi-Object Spectroscopy (MOS), long-slit spectroscopy and imaging (Seifert et al. 2010; Ageorges et al. 2010; Buschkamp et al. 2010). The spectra of the massive stars in W49 have been taken in MOS mode based on a pre-imaging K-band image also obtained with LUCI. Additional archival data were used to complement the LUCI data. Medium-resolution (R=10,000) K-band spectra of five massive stars in W49 obtained with ISAAC mounted on Antu (UT1) of ESO's VLT, Paranal, Chile, and , J- and H-band images obtained with SOFI at the NTT, La Silla, Chile, were downloaded from the ESO archive.

3.2.1 Observations

Imaging Observations

The K-band image of W49 was taken on 2009, September 29 with the N3.75 camera of LBT/LUCI with a total exposure time of 840 s. More details on the imaging observations can be found in Wu et al. (2014).

The archival J and H-band data (first published in Alves & Homeier 2003) were downloaded from the ESO archive and are the same we used in Chapter 2. The observations were performed on 2001, June 7 with NTT/SOFI for a total exposure time of 600 s and 450 s in J and H, respectively. All data were taken under good atmospheric conditions with a typical angular resolution of 0.5 to 0.7 ″.

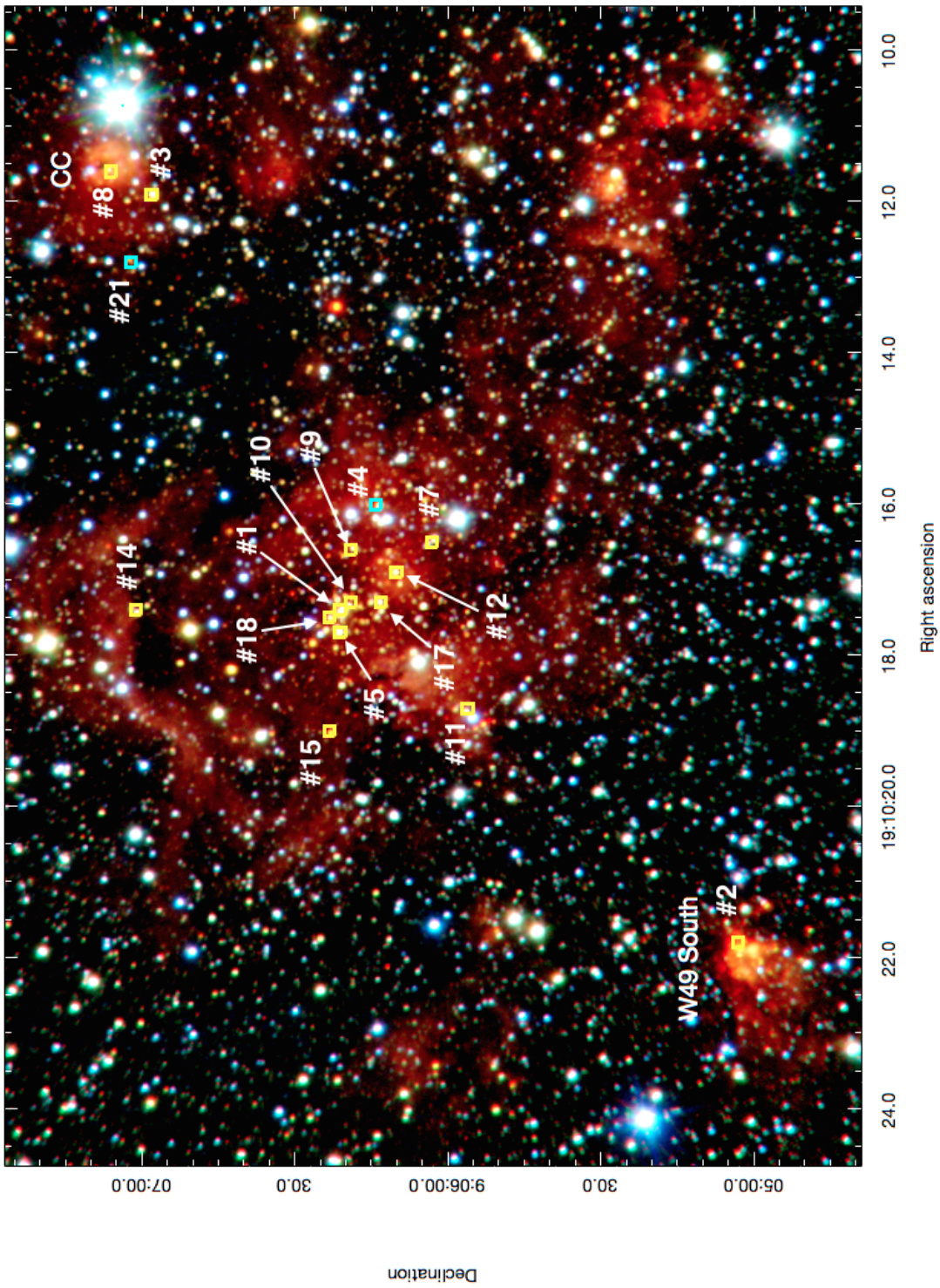

Figure 3.1: *JHK* composite color image of the central 12 pc × 9 pc of W49. North is up, and east is to the left. The red, green, and blue channels are mapped to the *K*, *H*, and *J*, respectively. The *J* and *H*-band image are from NTT/SOFI and the *K*-band image is from LBT/LUCI. The spectroscopically identified OB-type stars are marked by yellow squares. Two YSOs are marked with blue squares. Two radio sources (W49 South and CC, also associated with sub-clusters) are labeled with white numbers.

Spectroscopic Observations

We observed W49 with the MOS mode of LUCI in the K-band from 2010 May 14 to June 11 and from 2011 April 11 to May 15 under varying atmospheric conditions. We used the 210_zJHK grating and slit width of 0.7″ for the masks targeting the brighter stars, and 1″ for the remaining stars. The angular sampling of the spectra is 0.″25 $pixel^{-1}$ with the N1.8 camera, which provides the largest wavelength coverage ($\Delta\lambda = 0.328\mu$). The spectroscopic targets were selected by their $H - K$ color. Following Alves & Homeier (2003), sources with $H - K > 1.2$ mag were pre-selected as candidate cluster members. Additional stars with less red $H - K$ color were added in cases where the selected targets did not fill all the slits available in the mask.

In addition to the MOS spectra from LUCI, we reduced a set of archival long-slit spectra taken with ISAAC in the K-band on 2004 August 6, providing a wavelength coverage between 2.08 μm and 2.20 μm. The spectra were collected with a angular sampling of 0″.147 $pixel^{-1}$. The K-band spectrum of the VMS W49nr1 (studied in Chapter 2), is also part of this dataset. More details on the ISAAC spectra are presented in Chapter 2.

3.2.2 Data reductionon

The reduction of the imaging data and the ISAAC long-slit spectra is described in Sect. 2.2.2. The LUCI spectra were reduced with a modified version of *lucired*, which is a collection of IRAF routines developed for the reduction of LUCI MOS spectra. The raw frames were first corrected for the tilt and distortion using spectroscopic sieve and pinhole masks, respectively. The science and standard star spectra were divided by the normalized flat field. The MOS spectra were cut into individual slits and the wavelength calibration was carried out using the Ar and Ne wavelength calibration frames. After the wavelength calibration, the sky background was removed by subtracting two frames adjacent in time or using the procedure by Davies (2007), depending on which one of these two methods was more successful in minimizing sky-lines residuals. Then the one-dimensional spectra were extracted using IRAF task *doslit*. The local background was estimated by fitting a region close to the star with a Legendre function, so that the narrow Brγ emission from the surrounding diffuse nebular structure can be removed from the final spectra. At last the individual exposures for each star are combined into the final spectra.

In preparation for telluric correction, the Brγ absorption line in the spectrum of the telluric standard star was removed by fitting the line with a Lorentzian profile. The resulting atmospheric transmission spectrum was used with the IRAF task *telluric* to correct the science spectra. After comparing the science spectra corrected with the telluric standard stars taken before and after the science exposure, we selected the science spectra with the least telluric residuals. Finally, the

spectra of the science targets are normalized and displayed in Fig. 3.4, Fig. 3.5 and Fig. 3.6. A residual Brγ emission component remains due to intensity variations of the nebular emission on small spatial scales.

In total, good quality spectra of 44 stars have been obtained with identifiable features in their continuum. Half of them have spectra dominated by CO absorption bands and other atomic absorption lines. They are identified as late-type foreground dwarf and giant stars and are not members of W49 and therefore not discussed in this Chapter. The remaining 22 stars show the spectral features of massive stars and YSOs and are candidate members of W49. In the following, their membership to W49 is discussed in more detail.

3.3 Results

In this section we present the near-infrared photometry as well as the K-band spectroscopy data for W49. Based on both the imaging and spectroscopy we derive the effective temperature and luminosity of the identified massive stars, and place them in the HRD.

3.3.1 Photometry

Near-infrared imaging of the W49 star-forming region shows that this region is dominated by a dense central cluster surrounded by smaller sub-clusters (Fig. 3.1). Due to the large distance of W49, high extinction and high foreground contamination make it impossible to reliably determine cluster membership on photometry alone. This is clearly demonstrated by the observed JHK CMD (Fig. 3.2), showing a continuous spread in color, without a clearly identifiable reddened main sequence as the reddened cluster population. The $J-H$, $H-K$ CCD (Fig. 3.3) shows that the large range in the $H-K$ color corresponds to an extinction range $A_K = 0$ to 5 mag when applying the extinction law of Indebetouw et al. (2005).

To get an idea of the stellar population in W49, Alves & Homeier (2003) and Homeier & Alves (2005) applied a $H-K \geq 1.2$ mag color cut (equivalent to $A_K = 2.1$ mag), based on the clustering stars. For our spectroscopic survey we selected stars in a similar fashion: based on their red color and association to one of the clusters identified by Alves & Homeier (2003). Their observed JHK magnitudes are listed in Table. 3.4. Almost all stars are detected in JHK, allowing a characterization of the sources using the CMD and CCD. Exceptions including source #10, which is only detected in K, and is blended with brighter stars in J and H. The crowding in the K band still results in a high uncertainty of the photometry. Source #15 is not detected in J as this source is highly reddened and hence too faint. The locations of the spectroscopically identified

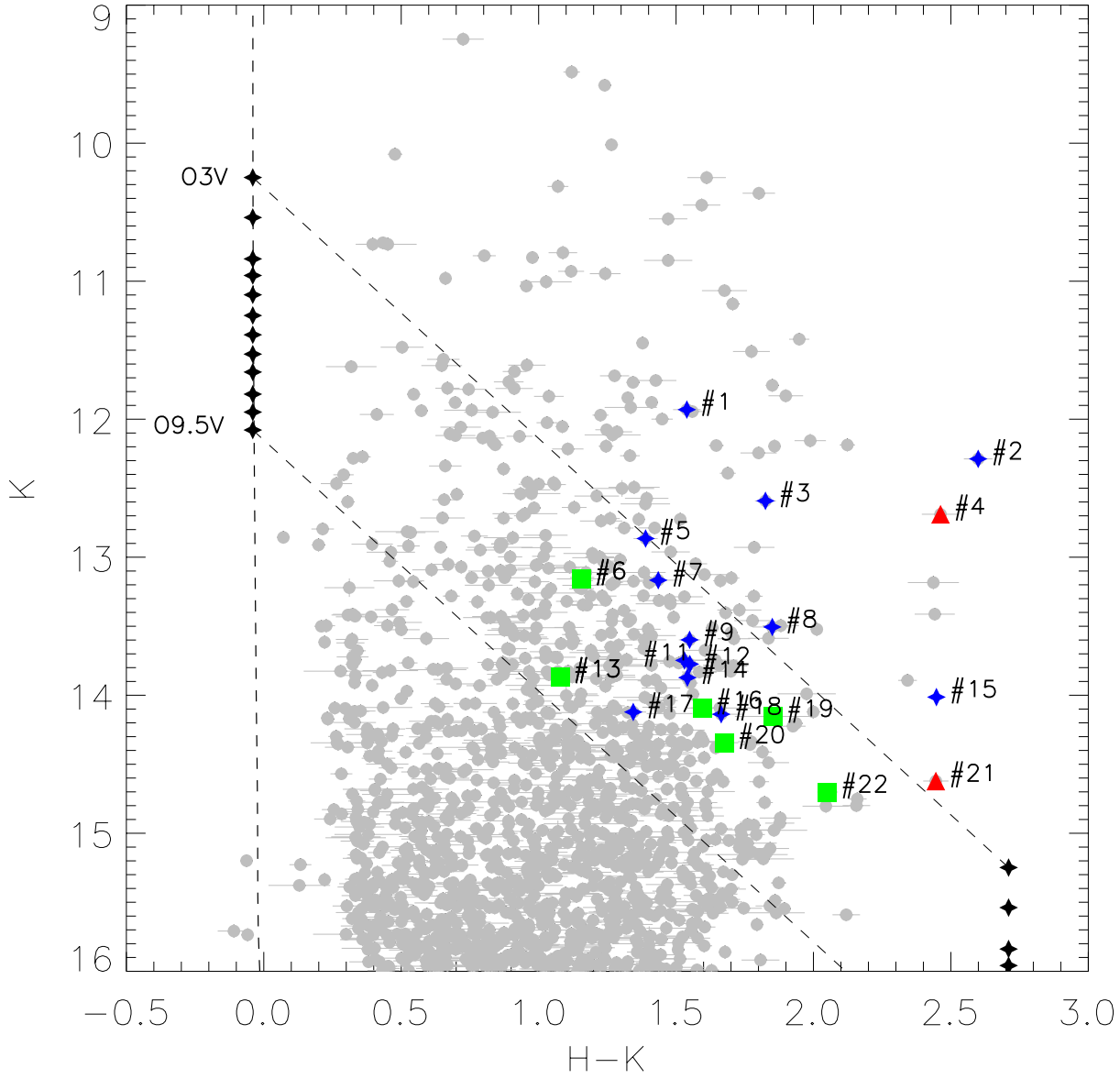

Figure 3.2: $H-K$ vs. K CMD of W49. All sources identified in JHK and with $K \leq 16$ mag are plotted in grey. The blue star symbols represent the spectroscopically identified OB stars, red triangles are the YSOs with CO emission in their spectra, while the green squares mark the locations of the stars with Brγ absorption lines as the most obvious feature, and which cannot be classified due to a lack of other features (see discussion in the text). The dashed vertical line represents the un-reddened isochrone for main sequence stars with an age of 1 Myrs (Ekström et al. 2012; Yusof et al. 2013). The black star symbols in the bottom right mark the locations of O stars of different subtypes for A_K =5 mag. The two diagonal dashed lines mark the reddening directions of an O3V and O9.5V star according to the extinction law of Indebetouw et al. (2005).

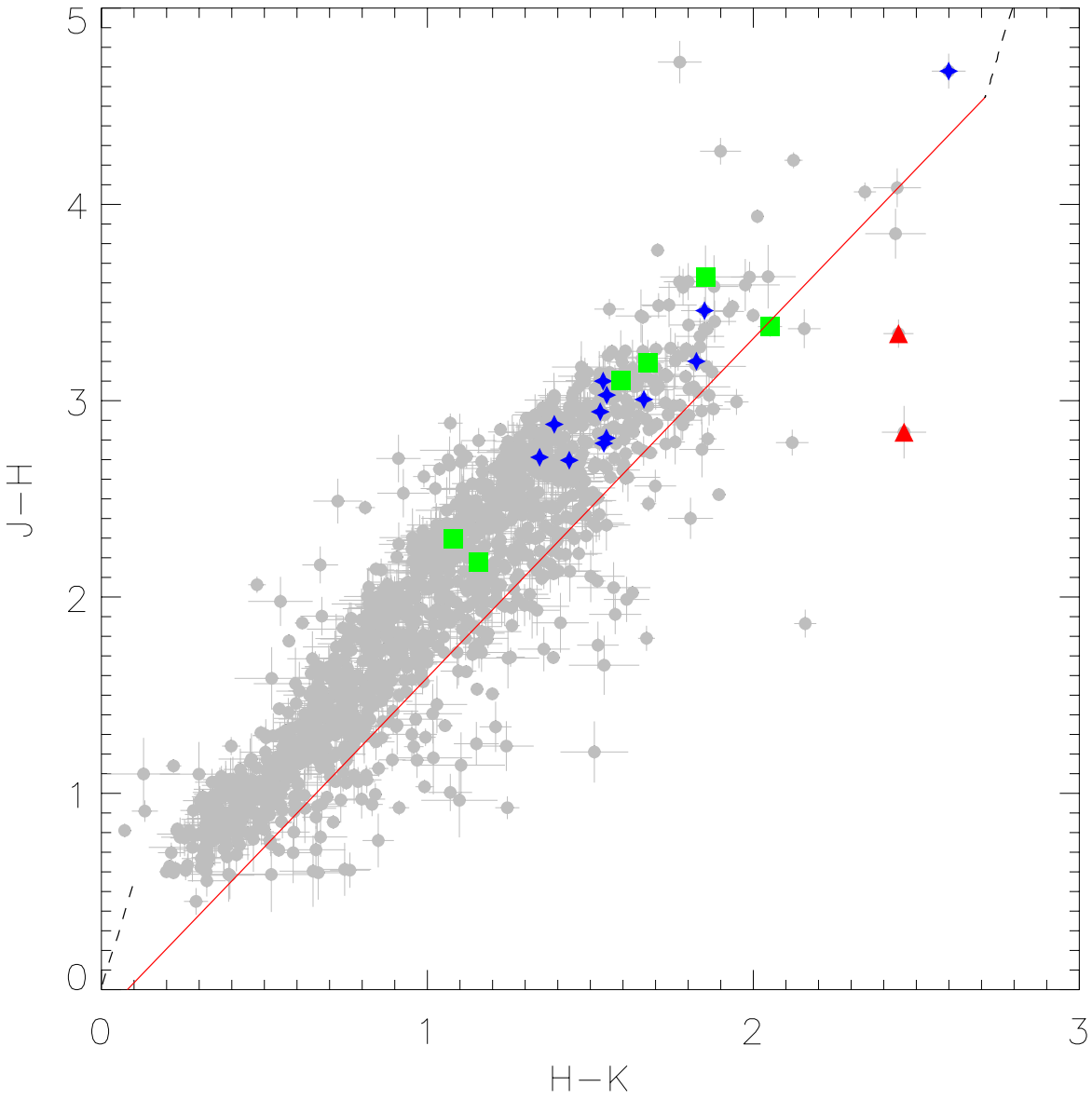

Figure 3.3: $J-H$, $H-K$ CCD of W49 for the same sources as shown in Fig. 3.2. The symbols have the same meaning as described in Fig. 3.2. The two black dashed lines represent main sequence isochrones with the age of 1 Myrs from Ekström et al. (2012) and Yusof et al. (2013) without being reddened (bottom left) and being reddened with A_K =5 mag (upper right). The red diagonal line represents the reddening law according to Indebetouw et al. (2005).

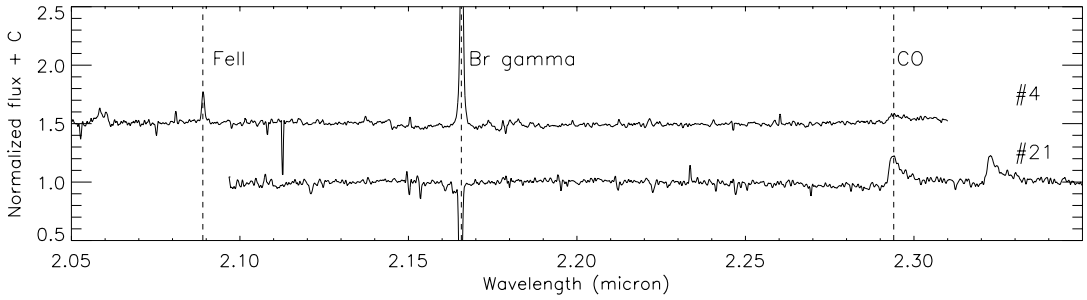

Figure 3.4: Normalized K-band spectrum of two stars identified as YSOs in W49. The most important features are the CO emission lines at the long wavelength end of their K-band spectra.

massive stars (see section 3.3) are marked in the CMD and CCD and show that indeed the cluster is extremely reddened and that extinction within W49 is highly varying.

In the CMD, the black star symbols mark the positions of different subtypes of main sequence stars ranging from O3V to O9.5V taken from Martins & Plez (2006), adopting the extinction law of Indebetouw et al. (2005) and assuming a distance of 11.1 kpc (Zhang et al. 2013) for W49. The reference points are then reddened by $A_K = 5$ mag. The spectral types of the candidate massive stars can be estimated by comparing the positions of the observed stars in the CMD with the reddened main sequence. The resulting photometric spectral types are given in Table. 3.1 and can be compared to our spectral classification based on the LUCI spectra (Section 3.3). Most stars are classified between O3V and O9.5V suggesting that they are massive stars inside W49. Some stars appear to be more luminous than a single O3V star. In these cases a spectral classification is mandatory to reveal the true nature.

As discussed in Sect. 2.3.2 the choice of the extinction law will have a significant effect on the dereddened magnitudes and therefore on the photometric spectral type. We use the extinction laws of Indebetouw et al. (2005); Fitzpatrick (1999); Nishiyama et al. (2009) and Rieke & Lebofsky (1985), whose slopes are consistent with the observed colors in W49, to estimate the uncertainty due to different extinction laws on the photometric spectral type. Different extinction laws result in 2 to 3 subtype uncertainty in the photometric spectral type determination. The extinction law by Fitzpatrick (1999) yields earlier subtypes, Nishiyama et al. (2009) yields later subtypes, while Indebetouw et al. (2005) and Rieke & Lebofsky (1985) give comparable results in between the previous two.

Table 3.1: Spectral types of the massive stars in W49: Photometric classification derived from CMD shown in the left column and spectroscopic classification from LUCI *K*-band spectra shown in the right column; the numbering of massive stars is according to their *K*-band magnitude from bright to faint.

Star	Ph. Class.	Sp. Class.
#1	<O3	O2-3.5If*
#2	<O3	O2-3.5If*
#3	<O3	O3-O7V
#4	O[a]	YSO
#5	O3-O4	O3-O5V
#6	O5.5-O6	B2-B3V
#7	O3-O4	O3-O5V
#8	< O3	O3-O7V
#9	O4-O5	O3-O7V
#10	-	O5-O7V
#11	O5-O5.5	O3-O5V
#12	O5-O5.5	O5-O7V
#13	O8-O8.5	B0-B2V
#14	O5.5-O6	O3-O5V
#15	<O3	O2-3.5If*
#16	O6-O6.5	Brγ abs
#17	O7.5-O8	O7-O9.5
#18	O5.5-O6	O8-O9.5
#19	O4-O5	Brγ abs
#20	O6-O6.5	Brγ abs
#21	O[a]	YSO
#22	O5-O5.5	Brγ abs

a. Luminous YSOs with intrinsic IR excess.

3.3.2 Excess sources

In addition to stars located on or near the reddening line of the CCD (Fig. 3.3), several sources are located to the right of the reddened main sequence. These stars possibly possess an intrinsic infrared excess due to circumstellar material. In general the fraction of infrared excess sources is a strong function of the age of a stellar cluster, e.g. (Hernández et al. 2008). Additionally, dispersion of circumstellar material is driven by external factors like photo evaporation (Hollenbach et al. 2000) or dynamical interactions with surrounding stars (Olczak et al. 2010), resulting in a much lower disk fraction in massive stellar clusters (e.g. Stolte et al. 2010; Fang et al. 2012; Bik et al. 2014; Stolte et al. 2015).

For W49 we cannot determine a reliable disk fraction, as with the current data we cannot separate the cluster members from the fore- and background stars. However we can identify individual YSOs and discuss their likelihood to be a member of the cluster. Two of the most extreme excess sources in the CCD are covered by our LUCI spectra (Fig. 3.4). Both sources (#4 and #21) have an extremely red color $H - K > 2.4$ mag. Source #4 has been identified by Conti & Blum (2002, their nr 2) as a candidate OB star, by Homeier & Alves (2005) as a candidate for VMS with a mass in excess of 120 $M_\odot$, and by Saral et al. (2015, nr 7 in their Table. 10) as a candidate YSO with a mass estimate of $\approx 8.9\,M_\odot$. We note that the latter result is based on SED fitting and relies on 2MASS and UKIDSS photometry, and hence might be affected by crowding and blending. The YSOs are marked by red triangles in the CMD and CCD of Fig. 3.2 and Fig. 3.3. Their location in the upper right corner of the CCD suggests that they have a similar extinction as the candidate O stars in W49 and that their extreme $H - K$ color is caused by the infrared excess emission.

The K-band spectra show the CO v = 2-0 and 3-1 overtone bands at around 2.3 μm in emission, which is frequently observed in YSOs (Bik & Thi 2004; Bik et al. 2006; Stolte et al. 2010; Wheelwright et al. 2010). In addition to CO, star #4 also shows Brγ and Fe II 2.089 μm emission. The Brγ absorption line in the spectrum of #21 is caused by over subtraction of the diffuse nebular Brγ emission.

The CO emission likely arises from the neutral($\sim$ 2000 K) dense inner regions of the disk (Bik & Thi 2004; Wheelwright et al. 2010), while the Brγ emission is originating from the surrounding H II region as well as the ionised regions of the circumstellar disk. The Fe II emission in the spectrum of #4 is seen in several high-luminosity objects and could be caused by UV fluorescence (McGregor et al. 1988).

As we do not know the relative contribution of the disk and the star to the total observed flux we cannot determine the spectral type of the underlying star via photometry. The presence of Brγ and Fe II lines in the spectrum suggests that the central source is a hot and probably massive

star. Similar to Bik et al. (2006), we try to estimate the spectral type of the underlying star by comparing its location in the CMD with that of well studied massive YSOs. Bik et al. (2006) construct a CMD from the de-reddened J-K color and the absolute K magnitude (their Fig. 1). By applying an average extinction towards W49 of A_K = 3 mag (Table. 3.2) and a distance modulus of 15.22 mag, we derive absolute magnitudes of M_K = -5.5 mag and M_K = -3.9 mag for #4 and #21 respectively. The de-reddened J-K colors are 0.8 mag (#4) and 1.3 mag (#21). Placing the objects into the diagram of Bik et al. (2006) shows that their central stars are most likely late O stars and that they have a rather blue SED with little dust present. Bik et al. (2006) explain this as a result of disk dispersal. The outer regions of the disk are dispersed faster than the inner region and a small and hot inner disk remains before the disk is totally destroyed by the UV photons.

3.3.3 Spectral classification of the massive stars

Apart from the two YSO spectra, all the other spectra presented in this Chapter are photospheric spectra showing absorption and emission lines typical for OB stars. The normalized K-band spectra of the massive stars are shown in Fig. 3.5 and Fig. 3.6. The majority of the spectra show Brγ absorption originating in the stellar photosphere. Some Brγ profiles show a narrow emission component in the center originating in the surrounding HII region. As discussed in the data reduction section, we tried to correct the spectra for nebular emission by fitting and subtracting the background. Nevertheless, residuals are still left in some spectra because of the small-scale variations of the nebular emission. Other lines used for the derivation of the spectral type are the 2.10 μm (NV), 2.113 μm (HeI), 2.116 μm (NIII) and 2.189 μm (HeII) lines.

Our spectral classification is supported by synthetic spectra computed with the non-LTE radiative transfer code CMFGEN (Hillier & Miller 1998). The stellar atmosphere models contain the following model atoms HI, HeI-II, CI-IV, NI-V, OI-VI, SiII-IV and FeI-VII. We set the surface gravity $\log g = 4$, the wind parameter $\beta = 1.0$, the volume filling factor $f_v = 0.25$, the luminosity to $\log L/L_\odot = 6$ and the terminal velocity to typical values for O dwarfs. The effective temperature (T_{eff}) and the mass-loss rate ($\dot{M}$) were varied between 30,000 and 50,000K and $\log(\dot{M}/M_\odot) = -5$ and -6.5, respectively. The luminosity of our targets were estimated by extracting absolute magnitudes and intrinsic colors from the synthetic spectra.

OB main sequence stars

The LUCI spectra of the massive stars have been visually compared to high resolution K-band spectra of reference O and B type stars with optical classification from Hanson et al. (1996, 2005) and Bik et al. (2005). The high resolution spectra of Hanson et al. (2005) and Bik et al. (2005)

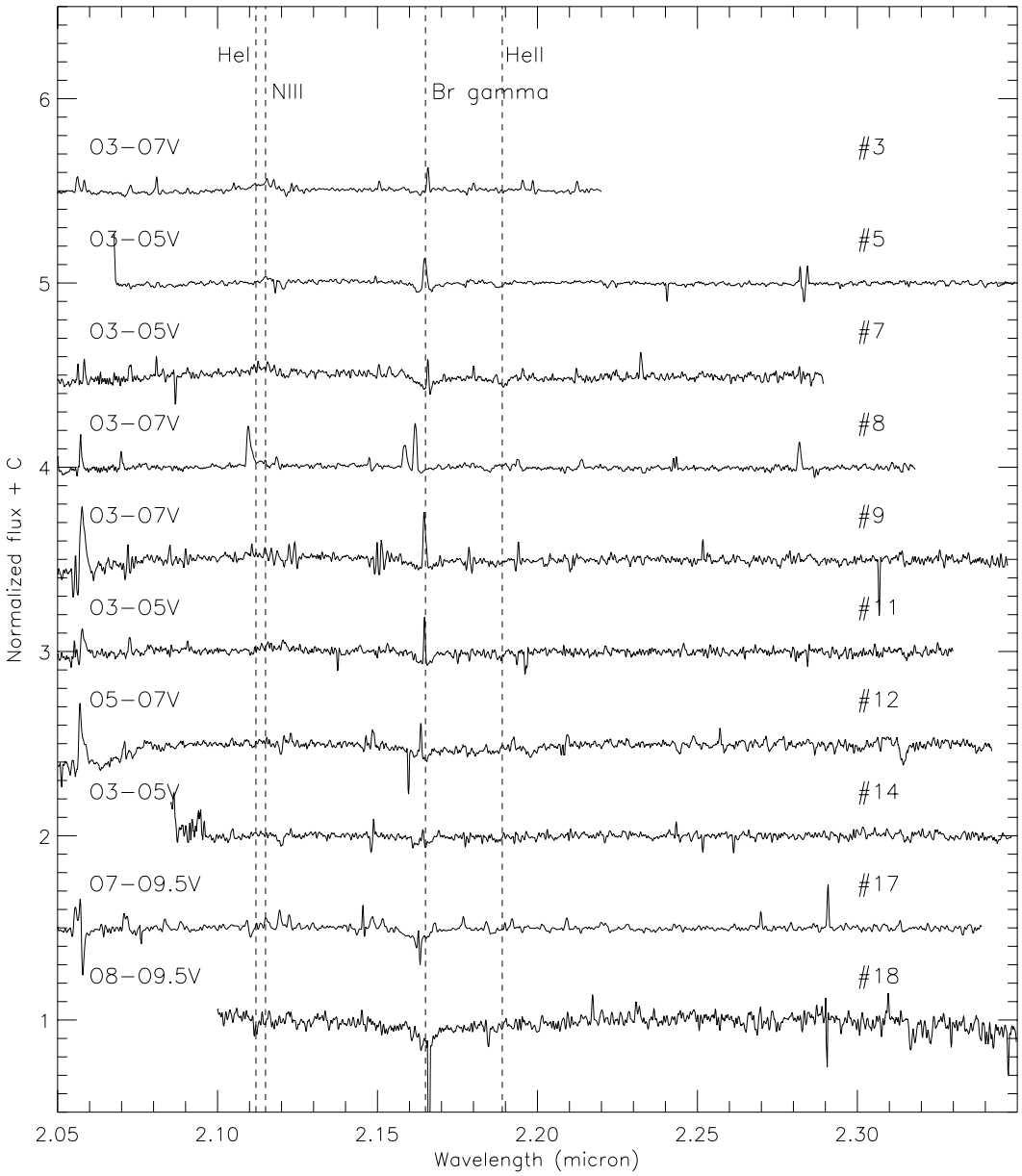

Figure 3.5: Normalized *K*-band spectrum of OB-type stars in W49 as taken with the multi-object mode of LUCI. The star number and the spectral type based on the spectroscopic classification are indicated above the corresponding spectrum. Indicated with dashed lines are the spectral features crucial for spectroscopic classification.

are rebinned to the resolution of the LUCI spectra and artificial noise was added to the reference spectra to degrade them to the SNR level of the LUCI spectra. The errors on the spectral types are derived where visual comparison shows clear mis-matches between the observed and reference spectra. Typically, the error is 1 or 2 sub types.

As shown in Table. 3.2, 10 out of the 22 stars are identified as OB main sequence star. Almost all spectra are classified as early type O stars (earlier than O7V) as they all show HeII and NIII in their spectra, indicative of a high effective temperature. To better refine the spectral classification we used the absence of the HeI (2.11 μm) line as an indicator for stars with spectral types between O3V and O5V. The strength of the Brγ and HeII absorption lines varies from star to star (see also Hanson et al. 1996, 2005), probably due to stellar wind variations. Therefore matching the strength in the spectra with those of reference spectra will not result in a good spectral type estimate.

Some stars (e.g. #3 and #8) show strong contamination by nebular emission of HeI and therefore this line cannot be used as discriminant between early O and mid O stars. Two stars (#6 and #13) are classified as early B stars. Three objects (including W49nr1 (#1) of Chapter 2) show spectra dominated by stellar wind (Fig. 3.6) and their classification is discussed separately (Sect. 3.3.3).

The SNR of our observations is not good enough for a tailored spectroscopic analysis of all sample stars. We only estimated effective temperature for the O stars of earlier spectral type (#3,5,7,8,9), where we could identify signatures of Brγ and HeII (2.189 micron) in emission or absorption. Some targets show a broad NIII / HeI complex at ~2.11 micron, which is not reproduced by the synthetic spectra and is likely a result of the poor SNR of the observation and the blending of several lines. The derived $T_{\rm eff}$ confirm the spectral classification based on the reference spectra.

Four relatively faint stars among our sample (#16, #19, #20 and #22) have low SNR. No obvious features except the broad Brγ absorption lines are found in their spectra. This would classify them as early type, however a more detailed classification is not possible. As they are fainter than the stars classified above, we suspect that they are lower-mass cluster members and possibly late-O or early-B stars.

Five stars are observed both with LUCI and with VLT/ISAAC and are marked by an asterisk after their name in Table. 3.2. The first one is the VMS reported in Chapter 2 as W49nr1. The other four were identified as O3V to O5V stars according to their ISAAC spectra. The ISAAC spectra confirm the spectral classification derived from the LUCI spectra.

We now can compare our photometric spectral types derived in Sect. 3.3.1 to those derived from the LUCI spectroscopy. Most of O-type stars have photometric spectral types similar to the spectral types derived from spectroscopy, like #3, #5, #7, #9, #11, #12 and, #17. For the two B

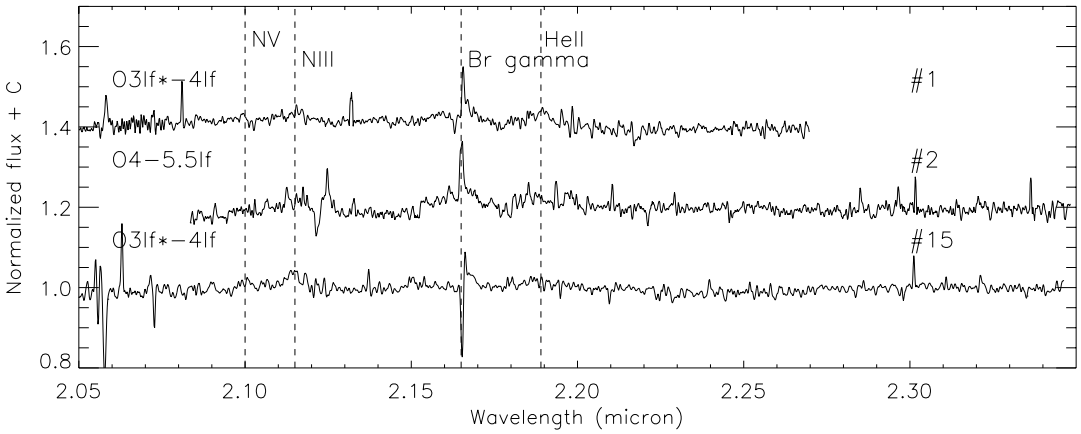

Figure 3.6: Normalized *K*-band spectra of Of type stars in W49 as taken with the multi-object mode of LUCI. The star number and the spectral type from spectroscopic classification are marked above the corresponding spectrum. Indicated with dashed lines are the spectral features crucial for classification.

stars (#6 and #13), however, we find a large discrepancy. The difference between the photometric and spectroscopic spectral type suggests that these stars are located at a closer distance than W49. In fact, their location in the CCD (Fig. 3.3) shows that they have a lower extinction than the other massive stars, consistent with a closer distance. Therefore we identify stars #6 and #13 as foreground stars.

Spectral classification of VMSs

In addition to W49nr1 (#1 in this Chapter) presented in Chapter 2, we have identified two additional stars (#2 and #15) whose spectra display broad Brγ and HeII emission lines. Additional lines of HeI and NIII are visible. We do not detect the Nv line at 2.10 μm in #2; it is only detected in #1 and #15. These spectral features are indicative of a strong stellar wind and a high effective temperature and we apply the same classification criteria as done for #1 in Chapter 2.

The sum of the equivalent widths of their Brγ and HeII lines (14.3 ±2.5 Å for #2 and 4.4 ±1.2 Å for #15, respectively) corresponds to a spectral type O2-3.5If* in the classification scheme proposed by Crowther & Walborn (2011), while the value for slash-stars (Of/WN) is in the range of $\sim$ 20 – 70 Å and lager than $\sim$ 70 Å for Wolf-Rayet stars. This criterion classifies #2 as a slash-star with strong wind features. The absence of the Nv line in the spectrum of #2 implies a later subtype and a lower temperature when compared to #1 and #15.

A comparison with reference stars with spectral types O3If*, O4If, O5If and O5.5If from Hanson

Table 3.2: Physical parameters of the OB stars in W49

Nr.	A_k (mag)	Sp. Type (Hanson)[a]	Sp.Type (Crowther)[b]	logT_{eff} (K)	log$L$ ($L_\odot$)	Mass ($M_\odot$)	Upper[c] ($M_\odot$)	Lower[c] ($M_\odot$)	logQ_0 (s^{-1})
#1*	2.83 ± 0.29**	O3If*-O4If	O2-3.5If*	4.65 ± 0.02**	6.28 ± 0.15**	130 ± 30**	130	50	50.03-50.10**
#2	4.78 ± 0.53**	O4If-O5.5If	> O3.5If*	4.55 ± 0.02**	6.64 ± 0.25**	250 ± 120**	240	90	50.03-50.27**
#3	3.50 ± 0.04	O3-O7V	-	4.61 ± 0.05	6.18 ± 0.13	105 ± 20	-	-	49.58-50.11
#5*	2.71 ± 0.13	O3-O5V	-	4.63 ± 0.02	5.82 ± 0.10	64 ± 8	-	-	49.47-49.72
#7*	2.79 ± 0.08	O3-O5V	-	4.63 ± 0.02	5.73 ± 0.09	57 ± 5	-	-	49.39-49.62
#8*	3.55 ± 0.17	O3-O7V	-	4.61 ± 0.05	5.83 ± 0.15	65 ± 13	-	-	49.21-49.78
#9*	2.99 ± 0.06	O3-O7V	-	4.61 ± 0.05	5.58 ± 0.13	47 ± 7	-	-	48.98-49.51
#11	2.96 ± 0.09	O3-O5V	-	4.63 ± 0.02	5.57 ± 0.09	48 ± 4	-	-	49.23-49.46
#12	3.00 ± 0.08	O5-O7V	-	4.59 ± 0.02	5.45 ± 0.09	40 ± 4	-	-	48.89-49.29
#14	2.98 ± 0.03	O3-O5V	-	4.63 ± 0.02	5.53 ± 0.08	46 ± 4	-	-	49.20-49.41
#15	4.52 ± 0.16**	O3If*-O4If	O2-3.5If*	4.64 ± 0.01**	6.11 ± (0.10)**	96 ± 14**	100	40	49.85-49.90**
#17	2.63 ± 0.20	O7-O9.5V	-	4.54 ± 0.03	5.01 ± 0.13	24 ± 3	-	-	47.79-48.68
#18	3.21 ± 0.16	O8-O9.5V	-	4.52 ± 0.02	5.20 ± 0.11	28 ± 3	-	-	48.02-48.69

*Stars also observed by VLT/ISAAC (PI: N. Homeier, Program ID: 073.D-0837)

**Parameters from photospheric model fitting

a Spectral types obtained by comparison with reference stars from Hanson et al. (2005)

b Spectral types for Of stars according to criteria from Crowther & Walborn (2011)

c The upper and lower mass limits of #1, #2 and #15 for the assumption of chemical homogeneous hydrogen and helium burners using the mass-luminosity relation from Gräfener et al. (2011) (see Sect. 3.3.4).

et al. (2005) shows the presence of the Nv line at 2.10 μm in O3If* stars and some of the O4If stars. Accordingly #2 is classified as a later type (O4If-O5.5If), while #15 has an earlier type (O3If*-O4If). Even though the reference stars do not include the spectral type O2If*, the temperature range obtained from the spectroscopic analysis suggest that stars #1 and #15 can be as early as O2If*.

3.3.4 HRD

After the spectroscopic classification, the massive stars are placed in the HRD and we compare their locations with stellar evolution models. The effective temperature of O-type main sequence stars is taken from Martins et al. (2005), while the bolometric correction and the intrinsic $H-K$ colors are from Martins & Plez (2006). By assuming the Indebetouw et al. (2005) extinction law, A_K was derived. With these parameters in hand, we can determine both the absolute bolometric magnitude and luminosity of the newly discovered massive stars (Fig. 3.7). We use the stellar evolution tracks from the Geneva models (Ekström et al. 2012; Yusof et al. 2013) to derive the masses of the stars. Those numbers as well as other parameters derived for the massive stars are compiled in Table. 3.2. The large uncertainties in the locations of the stars are dominated by the uncertainty in the spectral classification. The HRD is shown in Fig. 3.7, where the isochrones for 1 Myrs, 1.5 Myrs, 2 Myrs and 3 Myrs (Ekström et al. 2012; Yusof et al. 2013) are plotted as dashed lines together with the ZAMS (Lejeune & Schaerer 2001).

Due to limitations of empirical spectral libraries, the earliest spectral type available for classification is O3V. Using stellar parameters taken from Martins et al. (2005, Table. 1), this spectral type corresponds to an effective temperature of 44,600 K. Because of this limitation, our O3 spectral classification includes also all stars hotter than 44,600 K. In the HRD for W49 (Fig. 3.7), stars with spectral type classification O3 to O5 could be located at higher effective temperature than indicated, which would also affect their location with respect to the isochrones. A dedicated spectral modelling of the observed spectra is the way to overcome this limitation. A comparison with evolutionary tracks from stellar models (Fig. 3.8) yields the masses for the O-type main sequence stars (Table. 3.2). The derived masses range from ~20 $M_\odot$ to ~120 $M_\odot$ for these stars.

To place #1, #2 and #15 on the HRD, we derived T_{eff} and luminosity based on our grid of synthetic spectra (see Sect. 3.3). From the best fitting models we estimated T_{eff} and extracted the intrinsic $H-K$ color. The intrinsic color was used to determine the extinction in the K-band (A_K) by applying the extinction law of Indebetouw et al. (2005). The absolute K-band magnitudes were calculated by subtracting A_K and the distance modulus from the apparent magnitudes. The actual luminosity of the three stars was obtained by rescaling the stellar model spectrum with a luminosity of $\log L/L_\odot = 6$ to match the observed absolute magnitudes.

As a comparison to Geneva models, we apply the relation between the luminosity and the present-day stellar mass with the upper limit from homogeneous hydrogen burners and lower limit from helium burners (Gräfener et al. 2011). When adopting a hydrogen fraction of $0.7^{+0.05}_{-0.1}$, the upper mass limit would be in the range of 110-130 $M_\odot$ for #1, 200-240 $M_\odot$ for #2 and 90-100 $M_\odot$ for #15, in agreement with the masses estimated from tracks of massive star evolution. In case the three stars are helium burners, lower limits on their masses would be around 50 $M_\odot$, 90 $M_\odot$, and 40 $M_\odot$, respectively.

While the estimated upper mass limit of #2 is considerably higher than the widely accepted mass limit of 150 $M_\odot$ (Figer 2005; Koen 2006), the likelihood of VMSs to be binary or multiple systems is also very high. X-ray observations can serve as diagnostics under the assumption that the intrinsic X-ray luminosity of single O stars can be approximated by $L_X/L_{Bol} \sim 10^{-7}$ (Chlebowski et al. 1989; Crowther et al. 2010). Colliding supersonic stellar winds in early type binaries will produce additional X-ray flux from the shock heated material in the wind interaction region (Stevens et al. 1992). In our OB stars sample, only stars #1, #2 and #12 are detected as bright X-ray sources by XMM and Chandra (Leisa Townsley, private communication) suggesting that they might be colliding-wind binaries. If this is the case, the masses of the individual components of these sources could be lower than the above estimate.

3.4 Discussion

3.4.1 Cluster properties of W49

Cluster age

On the HRD (Fig. 3.7), we overplotted the main sequence isochrones for different ages from the Geneva evolutionary model (Ekström et al. 2012; Yusof et al. 2013) and compare the locations of the massive stars with the isochrones. Within the uncertainties, all stars (maybe with the exception of star #18) are consistent with a 1.5 Myrs isochrone. Smaller error bars would be required to make a definite statement about a possible age spread.

Cluster mass

From their photometric analysis, and by extrapolating the mass function to the mass range 1 to 20 $M_\odot$, Homeier & Alves (2005) deduced a total stellar mass of 5 to 7×10^4 $M_\odot$ for a $5' \times 5'$ (16 $\times$ 16 pc) region centered on cluster 1. This estimate is limited by contamination with field stars,

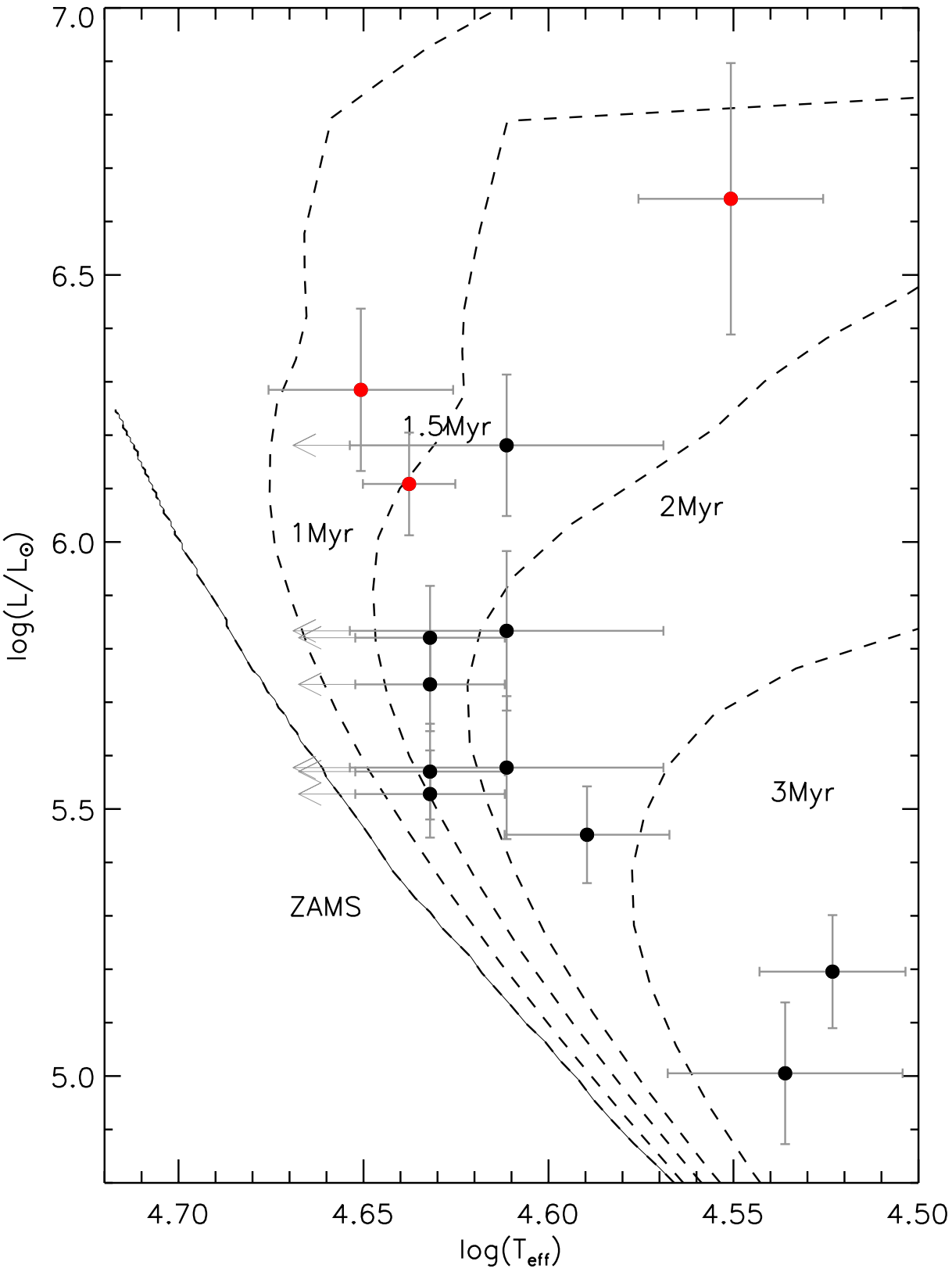

Figure 3.7: HRD of the massive stars in W49. The solid line represents the zero age main sequence isochrone from Lejeune & Schaerer (2001). The dashed lines are main-sequence isochrones for 1, 1.5, 2 and 3 Myrs from Ekström et al. (2012) and Yusof et al. (2013). The stars are de-reddened using the extinction law of Indebetouw et al. (2005). Three VMSs are indicated by red dots while OB main sequence stars are indicated by black dots.

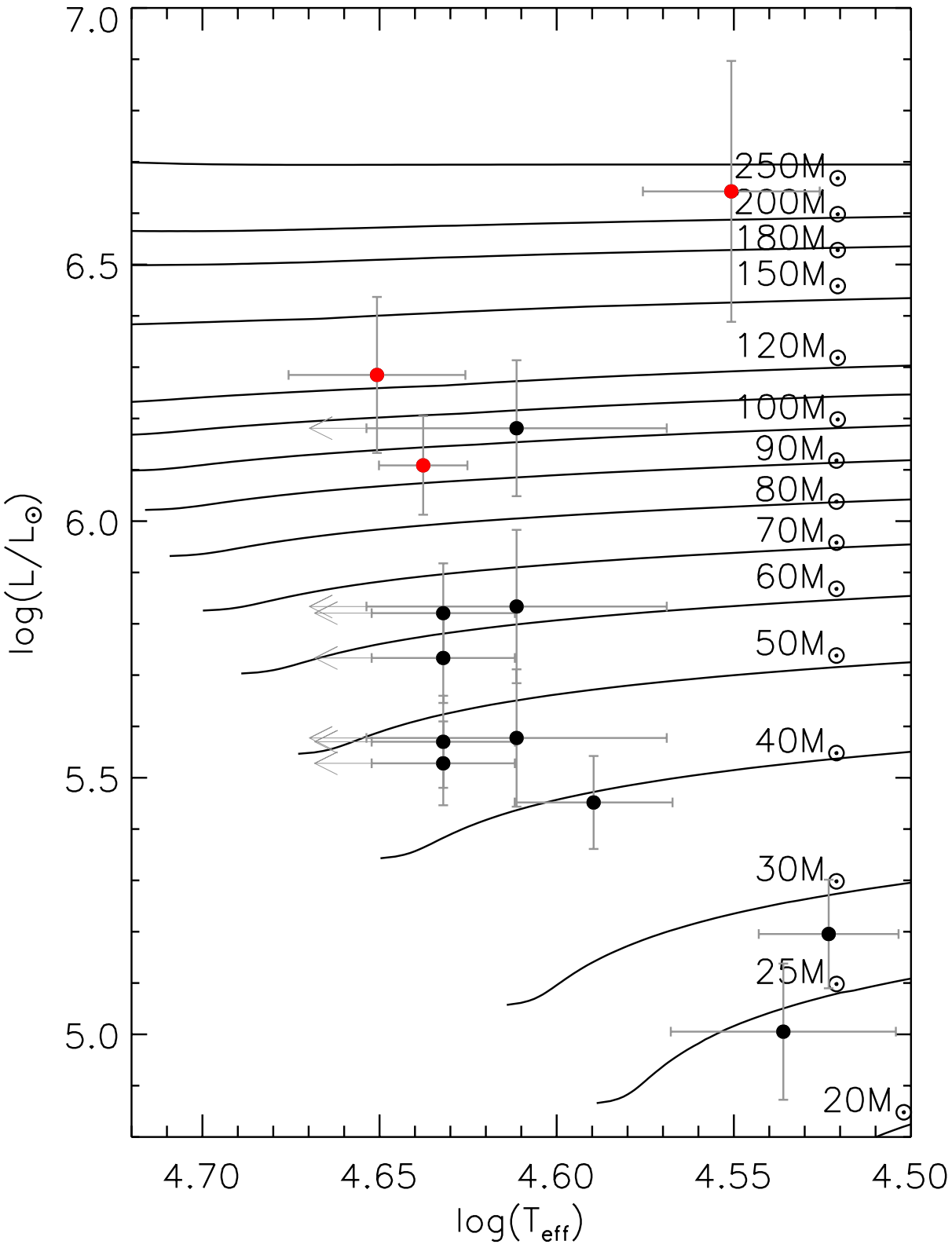

Figure 3.8: HRD of the massive stars in W49. The solid lines represent the evolutionary tracks from Ekström et al. (2012) and Yusof et al. (2013). See Fig. 3.7 for an explanation of the symbols.

even after color selection. To quantify this contamination requires spectroscopy of every star or proper motion measurements to remove the fore- and background stars by their different spatial velocities (e.g. Stolte et al. 2015).

We can still try to place constraints on the shape of the IMF of W49 and determine whether the presence of 3 VMSs is consistent with the derived cluster mass by Homeier & Alves (2005) and a typical high-mass slope of -2.35 of the IMF (Salpeter 1955; Kroupa 2001). We randomly sample 1000 times a Kroupa (2001) type mass function by drawing 200 high-mass stars between 20 and 400 $M_\odot$, corresponding to a total cluster mass between $5-7\times10^4$ $M_\odot$. We find that of these 200 stars, on average 10 ± 3 stars are expected to be more massive than 150 $M_\odot$. In W49 we have detected 3 VMSs spectroscopically, suggesting that this detection is perfectly normal, and does not suggest any oddity in the mass function of W49. As we cannot quantify our spectroscopic completeness, we might have missed several VMSs. The CMD (Fig. 3.2) shows several bright stars near the location of the spectroscopically detected VMSs.

3.4.2 Feedback

Massive stars have a strong impact on their formation sites. The ionizing radiation and stellar winds of the massive stars are able to alter the state of the interstellar medium (ISM) and halt star formation or trigger new episodes. Observations of the ISM (e.g. Peng et al. (2010); Galvan-Madrid et al. (2013)) show the effect of the stellar feedback on the ISM. Simulations suggest that the hydrogen ionizing photons have a more destructive effect than the mechanical feedback of the stellar winds of massive stars (Dale et al. 2013), however none of the two mechanisms is sufficient to fully destroy a giant molecular cloud of $\approx 10^6\,M_\odot$ surrounding a massive cluster.

The energy and momentum input in the ISM can be quantified by a characterisation of the massive stars. The spectral classification of the massive stars in W49 also results in an estimate of the number of ionizing photons (Q_0) emitted by each star and the stellar wind parameters. From Martins et al. (2005), we take the numbers of ionising photons emitted from stars with a certain spectral type. The ionising fluxes are rescaled with luminosities of individual stars and the final result listed in Table. 3.2 (#1, #2 and #15 have the ionizing flux directly from photospheric modelling). The total amount of ionizing photons emitted in W49 is dominated by the 3 VMSs and adds up to a total of $10^{50.45\sim50.59}$ s^{-1} (see Table. 3.2).

We can compare the number of ionizing photons with the radio flux emitted by W49. The radio free-free flux of the HII region is a direct proxy of the number of ionizing photons and therefore can be compared with the stellar ionizing photons according to the spectral types we have derived. Low spatial resolution radio observations from Kennicutt (1984) provide us with the total integrated radio flux of the entire HII region. Kennicutt (1984) derives a size of the radio

emitting region of 60 pc, which includes all the massive stars we have identified.

Based on their radio data, Kennicutt (1984) estimates the number of Lyman continuum photons to be $10^{51.20} s^{-1}$ (adopting the distance of 14.1 kpc). When we scale this number to the currently most accurate distance of 11.1 kpc, the value decreases to $10^{50.99} s^{-1}$. The upper limit on the total number of ionizing photons emitted by our massive star sample is of the same order ($10^{50.94} s^{-1}$), though slightly lower, also suggesting that our massive star sample is still incomplete.

High spatial resolution radio continuum observations of W49 (de Pree et al. 1997) resolve the large HII region detected by Kennicutt (1984) and reveal the presence of many smaller HII regions which are harbouring one or more O stars. After comparing the spatial locations of the O stars with those of the HII regions, we could identify two HII regions where we have found a central O star: #2 located in W49 South, and #8 associated with the radio shell source CC (de Pree et al. 1997). We recalculated the number of ionizing photons in the two HII regions based on de Pree et al. (1997), and scaled to a distance of 11.1 kpc. The Lyman continuum photon flux derived from radio observations of W49 South and CC are $10^{49.73} s^{-1}$ and $10^{48.96} s^{-1}$, respectively.

As listed in Table. 3.2, the O stars #2 and #8 emit $10^{50.03\sim50.27}$ s^{-1} and $10^{49.21\sim49.78}$ s^{-1} Lyman continuum photons, respectively. In both cases, the early O-type stars provide sufficient Lyman continuum flux to completely ionize the local HII region, which is consistent with the assumption that the stars are the main, if not the only source of ionization in each region.

In W49, the luminosity output from massive stars dominates the feedback towards the cloud. At the current stage, neither over-pressurized ionized gas nor radiation pressure from the central cluster have cleared the entire molecular cloud. According to Galvan-Madrid et al. (2013) only 1% of the total gas mass (10^6 $M_\odot$) is ionized. This is in agreement with simulations of cluster formation in massive molecular clouds (Dale et al. 2014). Consequently, a large amount of photons must either be leaking out of W49 or must be absorbed by the dust still present in the region. Neither of these photons would contribute to the ionization of the nebula. We note that a large fraction of escaping ionizing photons is commonly observed in regions of massive star formation (Kurtz et al. 1994).

Smaller scale effects of feedback inside the molecular cloud, however, can be seen in W49. Fig. 3.1 shows the presence of a nebular arc north of the central cluster. This arc appears to be part of a ring structure seen in Spitzer images as well as CO line emission (Peng et al. 2010). Rings are likely the result of the feedback by stellar winds or ionizing photons of a few massive stars in W49.

3.4.3 Do massive stars in W49 form in isolation?

When looking at the spatial distribution of the massive stars (Fig. 3.1) and the HII regions (also tracing the locations of the more embedded O stars) it becomes clear that several star formation sites are present in W49. In the near-infrared a central cluster (cluster 1) becomes evident which contains "only" 10^4 $M_\odot$ within a radius of 45″ (2.4 pc) (Homeier & Alves 2005), while the total mass of the 16 x 16 pc studied area is estimated to be $5 - 7 \times 10^4$ $M_\odot$. Apart from the clusters detected in the infrared, a proto-cluster is still forming and detected only at radio wavelength at about 3 pc distance of the center of cluster 1 and the so-called Welch ring (Welch et al. 1987) can be found, which harbours dozens of strong radio continuum sources (de Pree et al. 1997), implying the presence of an even younger event of massive star formation.

The majority of the massive stars are concentrated towards cluster 1. Within a radius of 45″ (2.5 pc) we identify 10 OB stars and a massive YSO. Homeier & Alves (2005) used this radius to determine the total mass of cluster 1 to 10^4 $M_\odot$. The four other stars are located in two of the subclusters identified by Alves & Homeier (2003); one star in cluster 2 near the HII region W49 South and three stars in cluster 3 associated with HII region CC.

The environments of the two YSOs differ from each other. One of them (#21) is in the subcluster to the northwest of the center (shown with blue squares in Fig. 3.1). The other YSO (#4) resides in the middle of the main cluster, thus showing that circumstellar disks can survive even in extreme environments, with high stellar density and strong UV radiation field.

The distribution of the 11 massive stars in cluster 1 shows that not all massive stars are located in a compact cluster – unlike in NGC3603, where all the massive stars are within 1 pc of the center (Moffat et al. 1994). Only 7 stars are within a projected distance less than 1 pc of the center of cluster 1, while 5 stars are located outside, including #14 located at a projected distance of 2.2 pc. The Spitzer images obtained with the IRAC camera (Fazio et al. 2004) suggest the presence of a bow shock to the north of star #14. This would indicate that #14 is a candidate run-away OB star, possibly originating from the core of the central cluster (Gvaramadze et al. 2010). Assuming an age of 1 to 2 Myrs (Sect. 3.4.1) we can calculate a projected velocity of 1 to 2 $\mathrm{km\,s^{-1}}$, which is required to reach 2.2 pc. This velocity is very low compared to the upper limit for OB runaway velocities of a few hundreds $km\ s^{-1}$ (Philp et al. 1996). Considering that bowshocks typically appear around stars with velocities of $> 10\ km\ s^{-1}$, it might have been kicked out at a later state of the cluster lifetime.

Using the above argument, also the massive stars associated with the W49 South and CC HII regions might be considered to be runaway stars from the central cluster. However, other arguments suggest that they might have formed there as members of a small sub cluster. The stars are inside an HII region, still surrounded by the molecular material where they might have formed in.

The shape of the W49 South HII region (de Pree et al. 1997) is cometary, but directed towards the center of cluster 1. The HII region CC is classified as irregular, and thus unlike a cometary shape created by the interaction of moving O stars with an HII region. Additionally, Alves & Homeier (2003) show that small sub clusters, consisting of more than one massive star are associated with W49 South and CC.

3.4.4 W49 as an extragalactic template?

Eleven of the 15 massive stars from our catalog are located in the central compact region (cluster 1) of W49, while several sub-clusters harbour the remaining four massive stars. The total gas mass within a radius of 60 pc and the stellar mass of W49 are estimated to be 1.1×10^6 $M_\odot$ (Galvan-Madrid et al. 2013) and $5 - 7 \times 10^4$ $M_\odot$ (Homeier & Alves 2005), respectively. This classifies W49 as one of the most massive star-forming regions in the Galaxy outside the Galactic center, and makes it a templates for extragalactic giant HII regions, which have masses in the range $M_{\rm gas} = 10^4 - 10^7\,M_\odot$ and $M_{\rm stars} = 10^3 - 10^5$ $M_\odot$ (Kennicutt 1984). W49 is reminiscent of the well-studied clusters NGC 3603 YC, W43, Westerlund 1 (Wd 1), Westerlund 2 (Wd 2) and the Carina Nebula Complex (CNC). Their physical parameters are shown in comparison with W49's in Table. 3.3. The NGC 3603 young cluster (YC, (Rochau et al. 2010)) is very compact in the center and has ~40 high-mass O- and WR stars confined into a very compact region of $\leq$ 1pc (Moffat et al. 1994). The stellar cluster of Wd2 reveals a morphology similar to NGC 3603 YC, but the former's size is a few times larger and has a more extended scale. CNC consists of several dense clusters including Trumpler 14 and Trumpler 16, embedded in a large amount of gas and dust within the region extending over at least 80 pc (Preibisch et al. 2012). The central region of W49 with massive stars confined into a single dense core shows a similar morphology to NGC 3603 (Moffat et al. 1994), but its extent over more than 60 pc in diameter makes it less compact. Overall, the morphology of W49 is comparable to the Carina Nebula region, with some dense clusters embedded in a more distributed region of ongoing star formation, with the key difference that CNC is closer to us, and hence can be studied at higher spatial resolution (Ascenso et al. 2007b).

The morphologies of star formation regions give us clues to understand their formation mechanisms. Different patterns of star formation exist among these regions. For NGC 3603, cloud-cloud collision might be the potential trigger of starburst (Fukui et al. 2014), and the resulting monolithic collapse could explain the formation of a ultra-compact core of NGC 3603. This is probably not the case for W49, where the star formation event seems to be taking place over a larger volume with individual subclusterings. Star formation in W49 might have been triggered by the density waves of a spiral arm forming a giant molecular cloud, which subsequently via hierarchical fragmentation morphed into several cores of different mass and density, and finally

Table 3.3: Physical properties of those famous star-forming regions

Star-forming region	Distance (kpc)	Extinction (mag)	Age (Myrs)	Cluster Mass ($10^4 M_\odot$)	Reference pc
W49	$11.1^{+0.8}_{-0.7}$	$A_K \sim 3$	1-2	5-7	1, 2, 3, 4
NGC 3603	6.0 ± 0.3	$A_V \sim 4.5$	1-2	1.3 ± 0.3	5, 6, 7, 8
W43	$5.49^{+0.39}_{-0.34}$	$A_V \sim 30$	5-10	-	9, 10, 11
Westerlund 1 (Wd 1)	4.0 ± 0.2	$A_{K_s} = 0.91 \pm 0.05$	3-6	5-15	7, 12, 13, 14, 15
Westerlund 2 (Wd 2)	4.16 ± 0.33	$A_V = 6.51 \pm 0.38$	< 3	>0.7	16, 17
Carina Nebula Complex (CNC)	2.3	$A_V = 3.5$	2-8	>10	18, 19
NGC 346 (in SMC)	60.6	-[a]	~ 3	39	20, 21, 22

a. The extinction towards NGC 346 is very low due to its location in the SMC; it is spatially highly variable and mainly comes from the star-forming region itself.

(1) Kennicutt (1984); (2) Alves & Homeier (2003); (3) Homeier & Alves (2005); (4) Zhang et al. (2013); (5) Grabelsky et al. (1988); (6) Stolte et al. (2004); (7) Kudryavtseva et al. (2012); (8) Moffat et al. (1994); (9) Zhang et al. (2014); (10) Blum et al. (1999); (11) Bally et al. (2010); (12) Gennaro et al. (2011); (13) Clark et al. (2005a); (14) Crowther et al. (2006); (15) Brandner et al. (2008) (16) Vargas Álvarez et al. (2013); (17) Ascenso et al. (2007a) (18) Preibisch et al. (2012); (19) Ascenso et al. (2007b) (20) Hilditch et al. (2005); (21) Bouret et al. (2003); (22) Sabbi et al. (2008).

resulting in cluster 1 and other subclusters in W49. For CNC, and very likely also for W49, star formation occurred not only in the core of the region, but originated independently in multiple cores away from the centre. Several young clusters formed and exist simultaneously in the Carina Nebula star formation complex. For W49, with several sub-clusters outside of the main cluster, the formation process seems not to be strictly coeval. The presence of the Welch ring also indicates non-coeval star formation. Considering the comparable size of W49 and CNC, and the presence of multi-seed star formation sites in W49, CNC with its several compact clusters may represent a more evolved state of a W49-type starburst region.

3.5 Conclusions

In this Chapter we present JHK imaging (NTT/SOFI and LBT/LUCI) and K-band spectroscopy (LBT/LUCI) of the massive stellar content in W49, one of the most massive and young star-forming regions in our Galaxy located at a distance of 11.1 kpc from us. Our main findings are as follows.

1. Our photometry confirms the high extinction (on average $A_K \sim 3$ mag) as well as large extinction variations. The presence of two infrared excess sources implies the existence of circumstellar disks around massive YSOs.

2. Thirteen O-type stars and two stars with CO disks are identified according to their NIR spectra. With the derived spectral types, their physical parameters, including effective temperature and bolometric luminosities are estimated. Along with the magnitudes derived from photometry and comparison with Geneva stellar evolution models, masses and ages of the massive stars are estimated. The most massive star found in our survey is #2, with an upper mass limit of $\approx$240 $M_\odot$.

3. The analysis of the stellar population enables us to study the properties of the cluster and the star formation region. Massive cluster members have a typical age of 1.5 Myrs, while the presence of embedded sources indicates still ongoing star formation in the region. The number of massive stars is consistent with previous estimates of a cluster mass of 50,000 to 70,000 solar masses. The massive stars are also capable of providing the vast majority of the ionizing photons powering the HII region. The spatial distribution of the massive stars indicates that some of the stars might have formed several half-mass radii away from the cluster center, though ejection from the clusters is also a possibility.

4. Considering its young age, abundant reservoir of gas, and high total mass, W49 is comparable to extragalactic giant HII regions. It can serve as a template and help us to understand

star formation in normal and starburst galaxies, which is poorly studied due to large distances.

Due to the extreme crowding in the cluster centre and the incompleteness of our spectroscopic survey sample, a complete stellar census of W49 is not possible at seeing limited angular resolution. This limits our ability to precisely reconstruct the formation history of W49. Higher angular resolution observation are required to achieve a comprehensive view of the formation of this young star cluster.

Appendix A: Comparison of spectra from different instruments

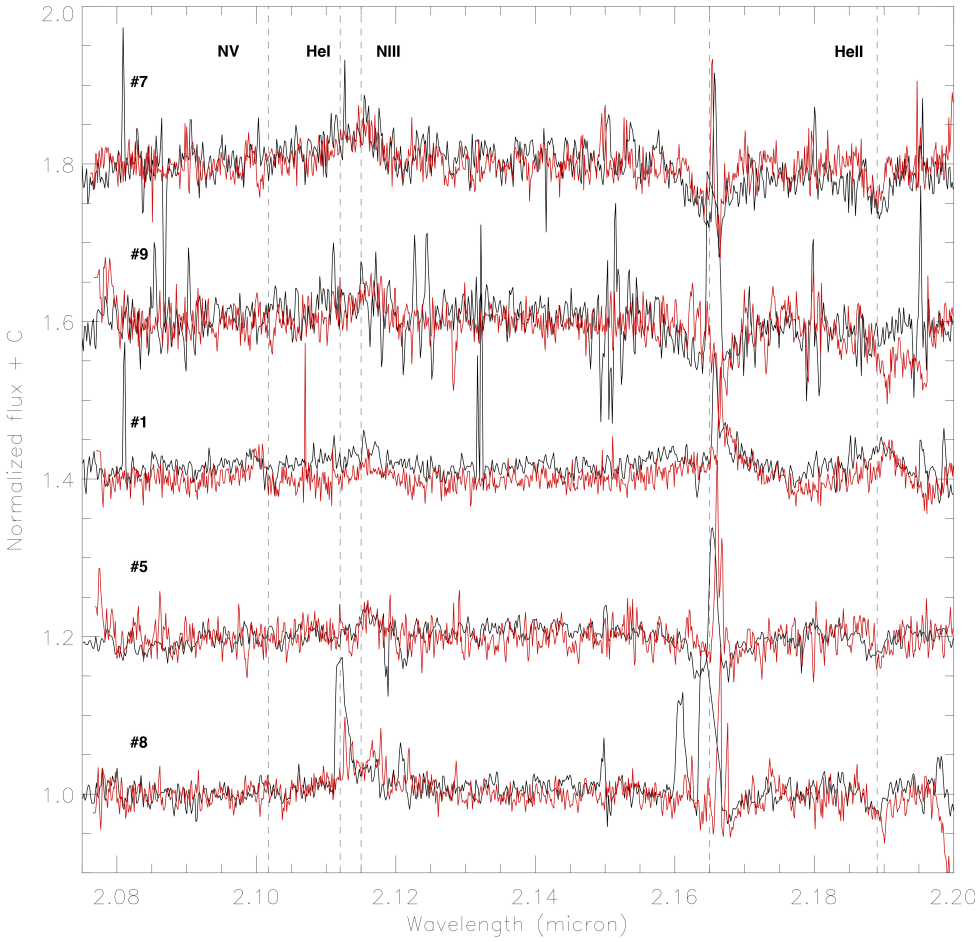

Figure 3.9: Normalized *K*-band spectrum of the five stars observed with both ISAAC (red) and LUCI (black) in W49. The important diagnostic lines are indicated with vertical dashed lines.

Appendix B: The observing log

Table 3.4: Spectroscopically observed massive stars in W49

Source	ID	RA(J2000)	dec (J2000)	J (mag)	H (mag)	K (mag)	Class
1	MOS08Klt135(VMS)*	19 10 17.4	+09 06 21	16.57 ± 0.18	13.47 ± 0.12	11.93 ± 0.10	Of
2	MOS07Klt135	19 10 21.8	+09 05 03	19.57 ± 0.14	14.89 ± 0.06	12.29 ± 0.29	Of
3	MOS13Klt135	19 10 11.9	+09 06 58	17.62 ± 0.01	14.42 ± 0.02	12.59 ± 0.01	OB
4	MOS12Klt135	19 10 16.0	+09 06 14	17.99 ± 0.07	15.15 ± 0.05	12.69 ± 0.01	YSO
5	MOS13Klt1407*	19 10 17.7	+09 06 21	17.13 ± 0.02	14.25 ± 0.05	12.86 ± 0.05	OB
6	MOS20Klt135	19 10 14.9	+09 06 49	16.49 ± 0.01	14.31 ± 0.02	13.16 ± 0.01	foreground
7	MOS11Klt135*	19 10 16.5	+09 06 03	17.30 ± 0.05	14.60 ± 0.02	13.17 ± 0.04	OB
8	MOS07Klt1412*	19 10 11.6	+09 07 06	18.81 ± 0.07	15.36 ± 0.07	13.51 ± 0.06	OB
9	MOS07Klt145m2r*	19 10 16.6	+09 06 19	17.96 ± 0.02	15.15 ± 0.02	13.60 ± 0.02	OB
10	MOS08Klt145m2	19 10 17.3	+09 06 19	-	-	13.69 ± 0.99	OB
11	MOS16Klt145	19 10 18.7	+09 05 56	18.22 ± 0.10	15.28 ± 0.02	13.74 ± 0.05	OB
12	MOS14Klt145	19 10 16.9	+09 06 10	18.35 ± 0.07	15.32 ± 0.04	13.77 ± 0.02	OB
13	MOS12Klt145m2r	19 10 12.7	+09 05 25	17.24 ± 0.02	14.94 ± 0.03	13.87 ± 0.01	foreground
14	MOS10Klt1411	19 10 17.4	+09 07 01	18.20 ± 0.03	15.41 ± 0.01	13.87 ± 0.01	OB
15	MOS12Klt15	19 10 19.0	+09 06 23	-	16.46 ± 0.08	14.01 ± 0.05	Of
16	MOS19OBS45left	19 10 17.5	+09 06 22	18.79 ± 0.11	15.69 ± 0.08	14.09 ± 0.12	$Br\gamma$ abs
17	MOS07Klt15	19 10 17.3	+09 06 13	18.18 ± 0.09	15.47 ± 0.08	14.12 ± 0.07	OB
18	MOS19OBS45mid	19 10 17.5	+09 06 23	18.81 ± 0.08	15.80 ± 0.05	14.14 ± 0.07	OB
19	MOS11Klt145m2	19 10 21.9	+09 05 03	19.64 ± 0.30	16.01 ± 0.10	14.15 ± 0.11	$Br\gamma$ abs
20	MOS19OBS45right	19 10 17.5	+09 06 24	19.21 ± 0.14	16.02 ± 0.04	14.34 ± 0.12	$Br\gamma$ abs
21	MOS16Klt15	19 10 12.8	+09 07 02	20.41 ± 0.16	17.07 ± 0.04	14.62 ± 0.06	YSO
22	MOS09Klt15	19 10 15.9	+09 06 05	20.13 ± 0.06	16.75 ± 0.08	14.70 ± 0.14	$Br\gamma$ abs

Chapter 4

Another Star Formation Scenario: W51

4.1 Introduction

The W51 GMC complex is an elongated molecular cloud complex, located in the Sagittarius spiral arm at a distance of 5.4 kpc (Sato et al. 2010). The complex spans a region on the sky of $45' \times 50'$ (Fig. 4.1), corresponding to 60×80 pc. The GMC complex contains 6 UCHII regions: G49.5-0.4 (the most luminous region in W51), G49.4-0.3, G49.2-0.3, G49.1-0.4, G49.0-0.3 and G48.9-0.3 (Kumar et al. 2004).The 21 cm radio continuum map of the W51 GMC complex shows two major HII regions named W51A (associated with G49.5-0.4 and G49.4-0.3) and W51B (associated with G49.2-0.3, G49.1-0.4, G49.0-0.3 and G48.9-0.3), and W51C, which is a large shell type supernova remnant to the east of W51B (Koo & Moon 1997). In Fig. 4.1, the dust distribution in W51 is shown with green contours in the left panel, the ionized gas is indicated by white contours in the right panel. High resolution radio continuum observation from Mehringer (1994) resolve as least eight components in G49.5-0.4 (W51a-h).

The distribution of clusters in the W51 region is non-uniform, and very different from the case of W49 (Chapter 3). In W51 they are spread over in a region of $45' \times 50'$, while in W49 a central massive cluster is present. Different subregions separated by dozens of pc from each other, suggesting a complex environment and formation scenario for this region. The NIR spectroscopic observations presented in this chapter focus on the clusters, which are associated with radio emission.

Several NIR studies of W51 were carried out in the past 20 years, and a number of embedded clusters containing candidate OB stars have been identified (Okumura et al. 2000; Kumar et al. 2004). Figuerêdo et al. (2008) obtained low resolution K-band spectra for five objects in the region of W51A, and could classify four of them as O-type stars. High resolution K-band spectra of two massive stars (associated with IRS2E and IRS2W, respectively) were obtained by Barbosa et al. (2008) in W51d (Fig. 4.3, middle panel). IRS2E was identified as a YSO, and IRS2W –

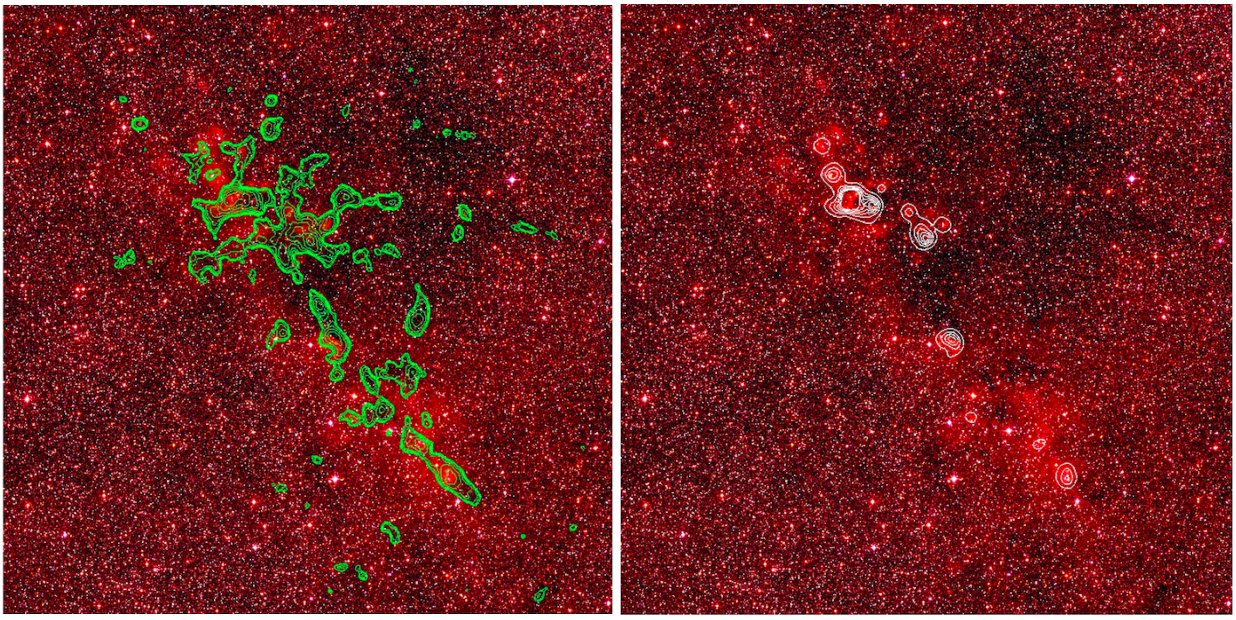

Figure 4.1: *Left:* The 1° × 1° degree *JHK*-band combined image of W51 overlaid by 1.1-mm dust continuum contour from the Bolocam survey in green. *Right:* The same NIR image with 1.4 GHz NRAO VLA Sky Survey (NVSS) contour overlaid in white.

which turns out to be the main ionizing source of W51d – was classified as an early O-type star (Barbosa et al. 2008).

In this chapter, we present the NIR observations obtained with LBT/LUCI and NTT/SOFI, and the reduction of the photometric and spectroscopic data in Sect. 4.2; in Sect. 4.3, we derive the properties of the identified massive stars and place them in an HRD; in Sect. 4.4, the physical status of the clusters as well as the entire GMC complex is discussed and we compare our findings to those of W49.

4.2 Observation and data reduction

4.2.1 Observations

The imaging observations were conducted in 2007 August 30 and September 30, (079.C-0248(A), PI: J. S. Clark) with the ESO NTT NIR spectrograph and imaging camera SOFI (Moorwood et al. 1998), which is equipped with a Hawaii HgCdTe 1024 × 1024 array, yielding a field of view of $\sim 4'.9 \times 4'.9$ with a plate scale of $0''.288$ pixel^{-1} in its large field (LF) imaging mode. In total, 8 fields were observed in J, H, and K_s-bands. Using dithered observations, each field was typically

Table 4.1. SOFI Observation of W51: Logs of Observations

Box	RA	Dec	Observing date	Exposure time(s)			Seeing(″)		
	(J2000)	(J2000)	(YYYY-MM-DD)	J	H	K_s	J	H	K_s
1	19:23:52.4	14:35:27	2007-08-30	288	288	288	1.05	1.16	1.29
2	19:23:33.0	14:37:36	2007-09-30	288	288	288	0.85	0.91	0.91
3	19:23:43.5	14:31:10	2007-09-28	288	288	288	1.07	1.04	0.95
4	19:23:09.4	14:28:05	2007-09-30	288	288	288	0.99	0.96	0.94
5	19:23:01.9	14:16:17	2007-09-30	288	288	288	1.00	0.88	1.08
6	19:22:53.0	14:09:57	2007-08-31	288	288	374	1.20	1.12	1.04
7	19:22:32.5	14:06:17	2007-08-31	288	288	288	1.05	1.23	1.00
8	19:22:13.7	14:02:09	2007-08-27	288	288	230	1.00	1.26	1.13

imaged ten times with individual exposure times of 28.8s (with DIT=1.2 s and NDIT=24) in all three bands. Table. 4.2.1 lists the centre coordinates, the observing date, the total integration time, and the average seeing for each field.

The *K*-band spectroscopic data of W51 were observed with LBT/LUCI in MOS mode from 2012 May 28 to 2012 October 11, with a DIT of 60 s and NDIT of 5 per frame. The same grating and camera (210_zJHK and N1.8) were used to get similar wavelength coverage and resolution as for the W49 dataset (Sect. 3.2.1). The slit width is ∼1 ″ for all the stars taken in the six successfully taken masks. Telluric standard stars were observed in each slit to ensure that wavelength coverage and other observational conditions were the same as for the scientific observations.

4.2.2 Data reduction

Imaging

The imaging data reduction was performed using an IDL pipeline which was improved by Gennaro et al. (2012) based on *eclipse* routines (Devillard 2001). The raw data were processed with dark subtraction, flat-fielding, cross-talk removal, and sky subtraction. We also removed the geometrical distortion on the dithered frames using the geometric distortion solution. Finally we combined the dithered frames in each filter for each field using the *eclipse jitter* task. The absolute astrometry was performed on the coadded frames by comparing the image with the 2MASS

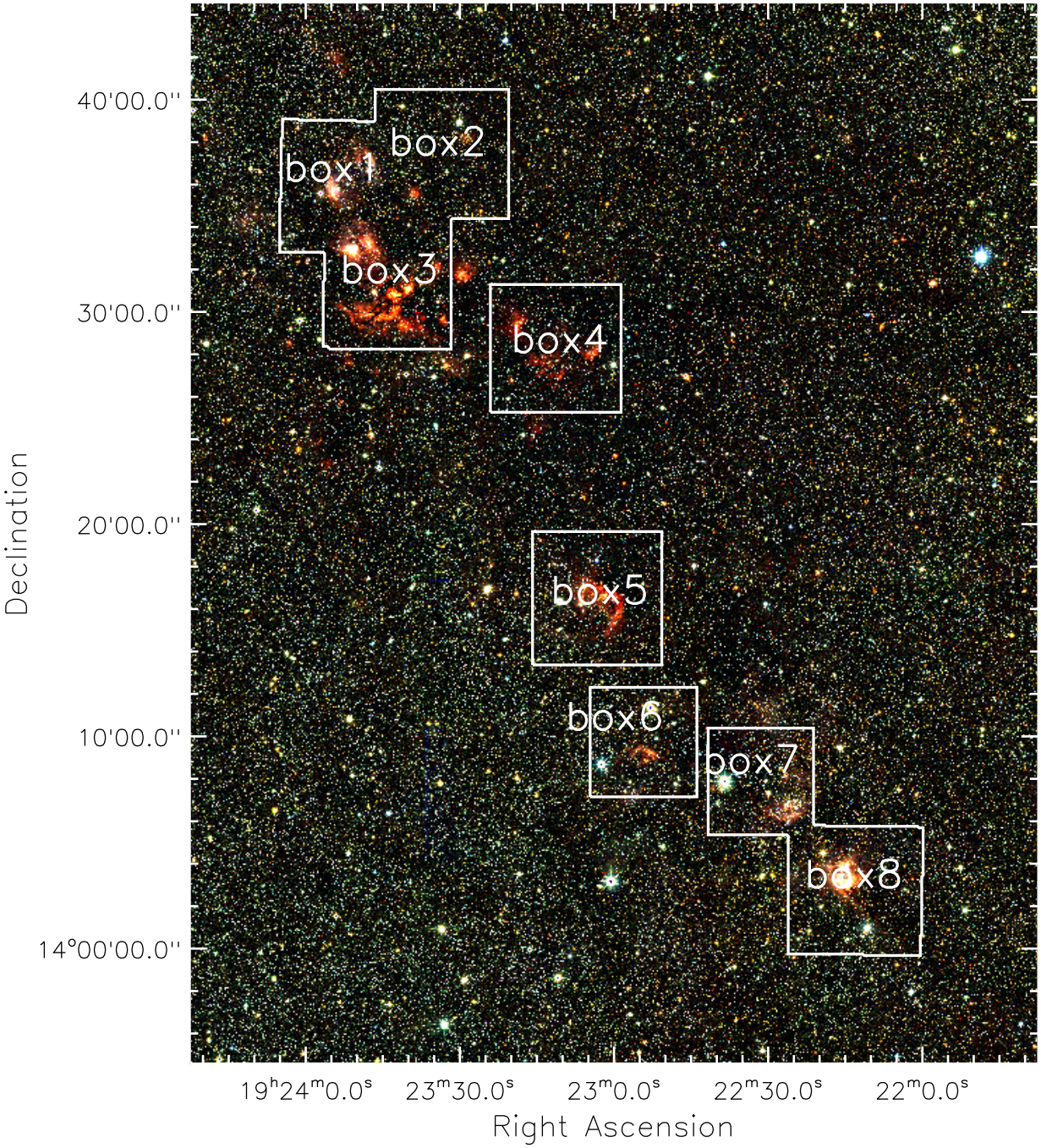

Figure 4.2: UKIDSS *JHK* composite colour image of the entire region of W51. Outlined by white boxes are the fields observed by NTT/SOFI.

reference catalog (Skrutskie et al. 2006) with IRAF *ccmap* and *cctran* tasks. We use UKIDSS[1] GPS (Lucas et al. 2008) catalog to estimate the accuracy of our astrometry. We find that the rms values of the difference of coordinates between the sources on the final mosaic images and UKIDSS catalog for all fields are below 0″.2.

Photometry was performed on the reduced frames using the IRAF `DAOPHOT` package (Stetson 1987). PSF photometry was conducted on the co-added images in each filter of each field. Photometric zero points and color terms were calculated by a comparison of the instrumental magnitudes of relatively isolated, unsaturated bright sources with the counterparts in the UKIDSS catalog. By comparing ~12,500 sources detected in both the SOFI and the UKIDSS observations, we find that the photometric reliability in all bands is ~0.04-0.14 mag, depending on the source brightness (Miaomiao Zhang, private communication).

Spectroscopy

The LUCI spectra were reduced with a modified version of *lucired*, using the same method as described in the previous chapter for the spectroscopic data of W49. After being extracted from the multi-object spectroscopic frame, the science spectra are corrected with the telluric standard stars taken before (Hip 90337, B9V) and after (Hip 104320, B3V) the science observation. The science spectra with the least residuals are selected as final results.

The only exception is OBS1, as the mask for the standard star observations of OBS1 was shifted with respect to the science observations and the flat field. This resulted in badly calibrated standard star data as the shifted flatfield did not anymore overlap with the position of the standard star on the detector. Instead, we corrected the absorption lines of the spectra taken in OBS1 with MOLECFIT (Smette et al. 2015; Kausch et al. 2015) by fitting synthetic transmission spectra to the observed spectra.

For this procedure, first the atmospheric conditions on the day of the observations for Mount Graham were downloaded [2]. After that the spectra were fitted with transmission models including H_2O, CO_2, O_3, N_2O, CO and CH_4. The resolution was fixed to 5.12 Å as measured on an OH sky line in the observed data. The fit was performed allowing for a wavelength shift, providing the best correction.

For OBS1slit17 the fit was performed in two stages. The region redwards of 2.29 μm in the

[1]The UKIDSS project is defined in Lawrence et al. (2007). UKIDSS uses the UKIRT Wide Field Camera (WFCAM; Casali et al. (2007)) and a photometric system described in Hewett et al. (2006). The pipeline processing and science archive are described in Irwin (2008) and Hambly et al. (2008). We have used data from the 7th data release, which is described in detail in Warren et al. (2007).

[2]`http://www.ready.noaa.gov/READYamet.php`

spectrum of OBS1slit17 is dominated by strong CO emission bands. A global fit of the entire K-band spectra resulted in badly over-subtracted spectra due to the lack of continuum at the red end of the spectrum. Instead we first fitted the spectra bluewards of 2.29 μm to obtain a realistic correction for all elements except CO (which is the dominant absorber redwards of 2.29 μm). After that we fixed the abundances of those elements as well as the wavelength shift and fitted the full spectrum allowing for only CO to vary. This resulted in a proper correction of the entire observed *K*-band spectrum (Fig 4.7).

In the next step, spectra dominated by CO absorption lines, which are coming from late type stars not likely to be members of the stellar clusters, were rejected. Only spectra with a SNR of at least 30 were selected. As a result, a sample of nine OB-type stars as well as one YSO with good quality spectra was identified. Their parameters and properties will be discussed in the following sections.

4.3 Results

4.3.1 Photometry

We imaged 8 fields in the W51 GMC in *JHK*. The imaged fields are associated with different UCHII regions containing embedded clusters (Fig. 4.2) with the following corresponding relations: Box 1, 2 and 3 - G49.5-0.4, Box 4 - G49.4-0.3, Box 5 - G49.2-0.3, Box6 - G49.1-0.4, Box7 - G49.0-0.3 and Box8 - G48.9-0.3, respectively.

The clusters are spread out over the entire GMC region and the different clusters are separated by tens of pc from each other. To get individual measurements of each cluster and their properties, we focus on the clusters themselves and select the areas where the stars still embedded in the nebular components, to reduce the contaminations by field stars. The regions we choose for the photometric analysis are shown in Fig 4.3. Stars located in the circles of different sub clusters are used to construct CMDs and CCDs for each sub cluster. In order to make the diagrams more clear and reliable, we selected only stars detected in all *JHK* bands and with photometric errors smaller than 0.2 mag. In the following we focus specifically on the best studied region IRS2 (associated with G49.5-0.4) and the regions with spectroscopic data observed in (G49.5-0.4 and G49.2-0.3).

Overplotted on the CMDs is the main sequence isochrones from Geneva Stellar Evolution Models [3] for an age of 1 Myrs (Ekström et al. 2012; Yusof et al. 2013) and assuming a distance of

[3] http://obswww.unige.ch/Recherche/evoldb/index/

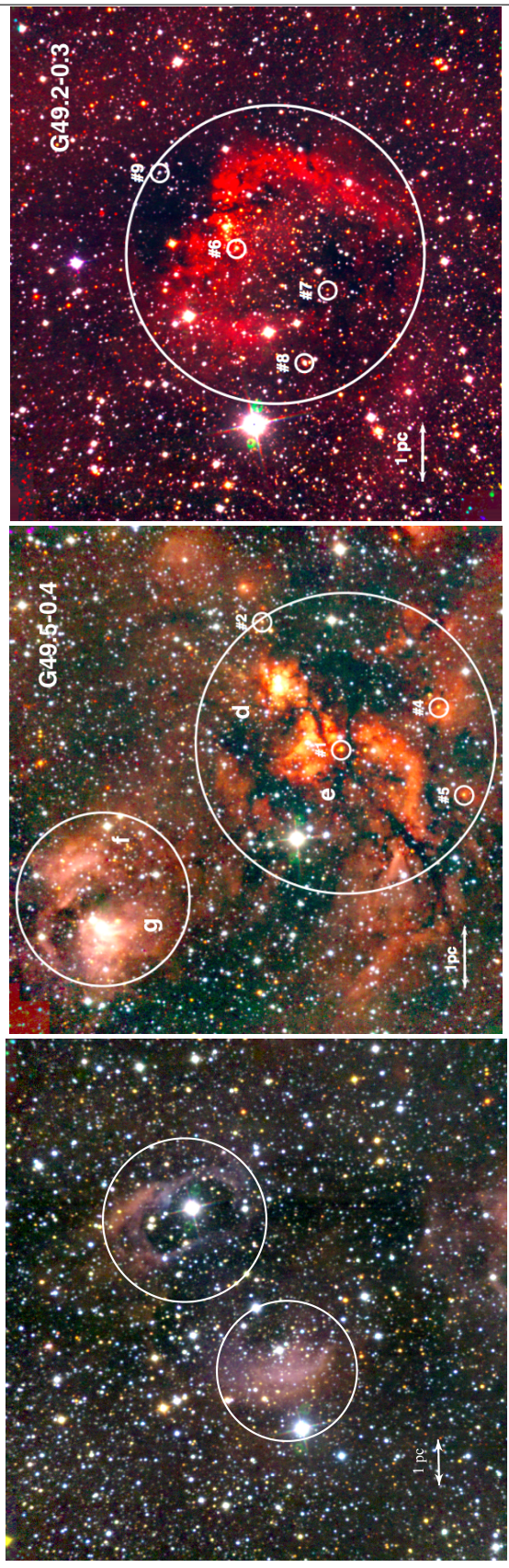

Figure 4.3: JHK_s composite color image of three different subregions of W51: Box1, Box 3 and Box 5. North is up, and east is to the left. The red, green and blue channels are mapped to the K, H and J, respectively. The regions selected for the photometric analysis are indicated with white circles. The OB stars as well as the YSO are marked with small green circles and labeled with their names.

5.4 kpc (Sato et al. 2010) . An unreddenend, blue main sequence at H-K = 0.5 is visible towards all of the clusters. This is very likely the unreddened foreground population towards W51. Each pannel shows a reddened cluster population starting at H-$K \approx 1$ mag and extending to H-$K \approx 3$ mag for the most embedded cluster. The positions of spectroscopically identified OB-type stars are marked with their IDs in the CMD and are all part of the reddened population confirming its nature as the W51 cluster population. Star #3 (OBS3slit15) is not detected in the J-band as it is heavily reddened, and therefore does not have a match in the combined JHK photometric catalog.

In the CCDs, the solid line and dashed line represent the main sequence stars isochrones and the reddening vector, respectively. Again foreground population is clearly visible at low extinction values. The cluster population is visible at higher extinction, reaching values up to $A_K = 4.7$ mag. The spectrally classified OB stars are located on the reddened main sequence line. The YSO in G49.5-0.4 shows a clear evidence for infrared excess and exhibiting higher $H - K$ color compare to other main sequence stars.

4.3.2 Spectral Classification of OB stars

From the spectroscopic analysis of our observed spectra, 9 stars are identified as OB-type stars. The normalized K-band spectra of them are shown in Fig 4.6. The major diagnostic lines available for classification of O to early A subtypes in this wavelength range are the 2.166 μm (Brγ), 2.113 μm (HeI) and 2.189 μm (HeII) lines. Similarly as discussed in the data reduction section of the W49 chapter, some Brγ profiles show a narrow emission in the centre of the broad stellar absorption line. This emission comes from the surrounding HII region. We tried to correct the nebular contaminations by fitting and subtracting the background around the positions of the spectra. Residual of the nebular emission are still present in the spectra of #1, #3, #4, #5 and #7.

To determine the spectral types of each star, their spectra have been visually compared to high resolution K-band spectra of reference OB-type stars with optical classification from Hanson et al. (1996, 2005) and Bik et al. (2005). The details of this method are demonstrated in Sect. 3.3.3.

Shown in the Fig 4.6 are the normalized K-band spectra of the OB-type stars. 2 out of 9 stars are classified as O-type stars according to the appearance of Brγ, HeI, HeII in both of them as well as NIII at 2.115 μm for star #6. The majority of stars in our sample are B type stars. The early B types show Brγ and HeI absorption lines in their K-band spectra. For mid and late B type stars, in the absence of the HeI line, the strength of the Brγ line is the only method to distinguish stars with different subtypes (Hanson et al. 1996). Star #9 is the only star classified as late B to early A type due to its very strong Brγ absorption with an EW of 14 Å.

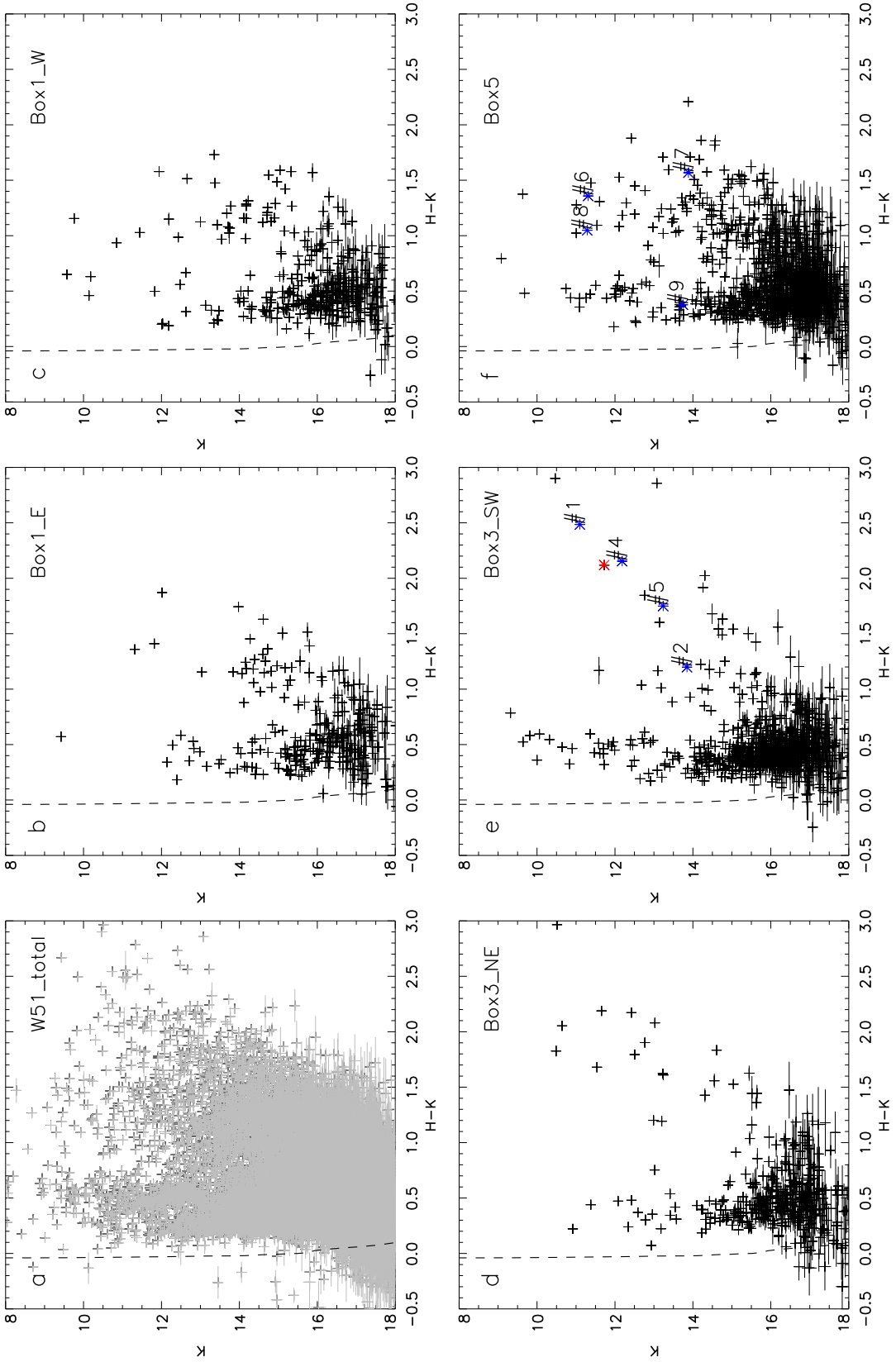

Figure 4.4: CMD of the entire region of W51 and subclusters defined by the circles on the images. The dashed vertical line represents the un-reddened isochrone for main sequence stars with an age of 1 Myrs Ekström et al. (2012) and Yusof et al. (2013)

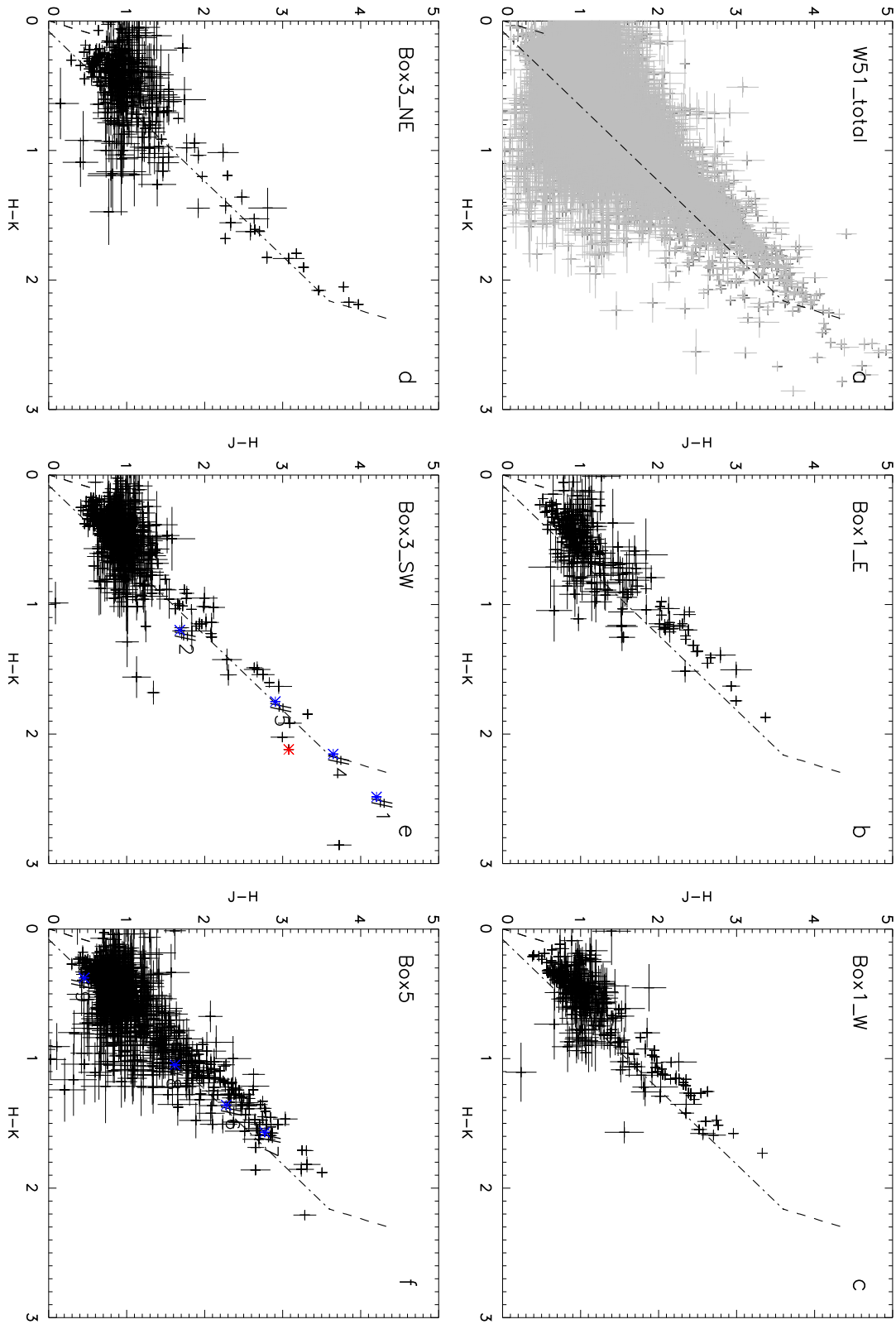

Figure 4.5: CCD of the entire region of W51 and subclusters defined by the circles on the images.

Table 4.2: Physical parameters of the OB stars in W51

Nr.	ID	Region	A_k (mag)	Sp. Type (Hanson)[a]	logT_{eff} (K)	log$L$ ($L_\odot$)	Mass ($M_\odot$)
#1	OBS2slit17	G49.5-0.4	4.70 ± 0.05	O7V-O8V	4.55 ± 0.01	6.47 ± 0.06	165 ± 15
#2	OBS3slit09	G49.5-0.4	2.27 ± 0.06	B0V-B2V	4.41 ± 0.09	4.06 ± 0.21	12 ± 1
#3	OBS3slit15[b]	G49.5-0.4	-	B3V-B7V	-	-	-
#4	OBS3slit16	G49.5-0.4	4.04 ± 0.07	O9.5V-B2V	4.42 ± 0.09	5.40 ± 0.20	32 ± 8
#5	OBS3slit17	G49.5-0.4	3.25 ± 0.06	B1V-B3V	4.33 ± 0.09	4.48 ± 0.23	13 ± 2
#6	OBS9slit08	G49.2-0.3	2.65 ± 0.02	O5V-O7V	4.59 ± 0.02	5.67 ± 0.08	50 ± 5
#7	OBS9slit15	G49.2-0.3	2.87 ± 0.03	B3V-B7V	4.19 ± 0.04	3.65 ± 0.12	7 ± 2
#8	OBS9slit17	G49.2-0.3	2.03 ± 0.07	O9V-B2V	4.43 ± 0.10	4.97 ± 0.21	20 ± 5
#9	OBS9slit23	G49.2-0.3	0.65 ± 0.05	B8V-A3V	4.02 ± 0.08	2.30 ± 0.18	3 ± 1

a. Spectral types obtained by comparison with reference stars from Hanson et al. (1996, 2005)
b. Not detected in J-band, hence it is not included in the combined JHK photometric catalog of W51.

The very luminous source (also called LS1 in Okumura et al. (2000)) is also covered by our spectroscopic survey, however, the K-band spectrum is partly saturated. Spectral modelling by Clark et al. (2009) of the K-band spectrum of this source shows that LS1 is a P Cygni type supergiant with an expanding envelope (see also Okumura et al. 2000). Star #1 is also included in Figuerêdo et al. (2008) as star #44 in their paper, classified as an O5 star. While in our analysis it was classified as O7-O8 due to the very faint HeII line at 2.189 μm.

4.3.3 YSO

According to the location of the YSO in the CCD (red star symbol in Fig 4.5, panel e), with an $H-K$ color larger than 2 mag, it is located significantly below the reddened main sequence. Nevertheless, its location in Fig. 4.4 implies similar extinction as for the other stars #1, #2, #4 and #5, which are located in the same HII region. This supports its characterization as an intrinsic infrared excess source reddened by the circumstellar material. The details of this kind of objects are discussed in Sect. 3.3.2.

Similar to star #4 in W49 (see Sect. 3.3.2), this YSO exhibits CO overtone bands at around 2.3 μm in emission as they are the most obvious feature of a YSO (Fig 4.7). The CO overtone in emission comes from the inner parts of an accretion disk, and is associated with the presence of an

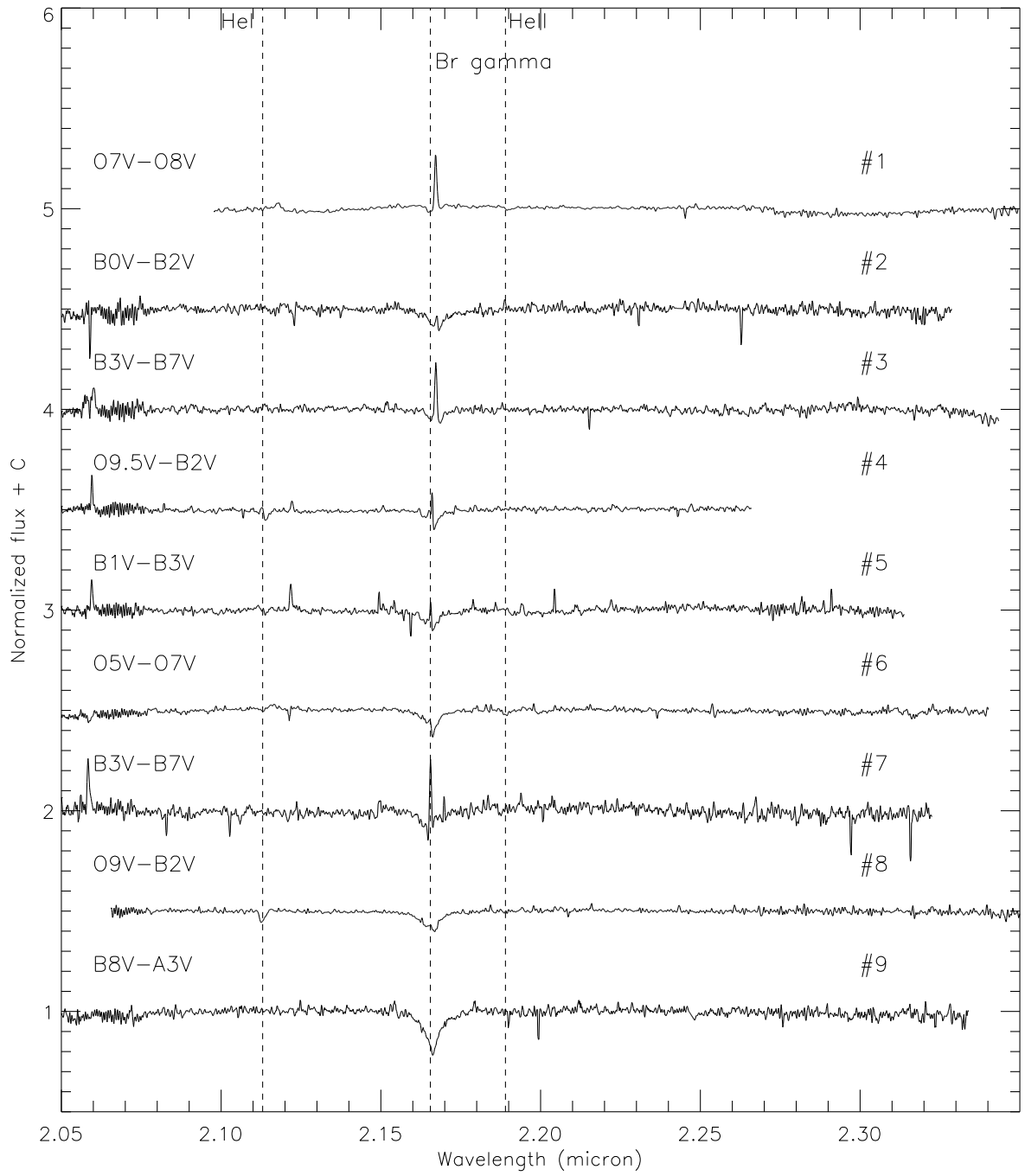

Figure 4.6: Normalized *K*-band spectra of OB-type stars as taken with the multi-object mode of LUCI. The star number and the spectral type based on the spectroscopic classification described in the text are indicated above with the corresponding spectrum. Indicated with dashed lines are the diagnostic lines crucial for spectroscopic classification

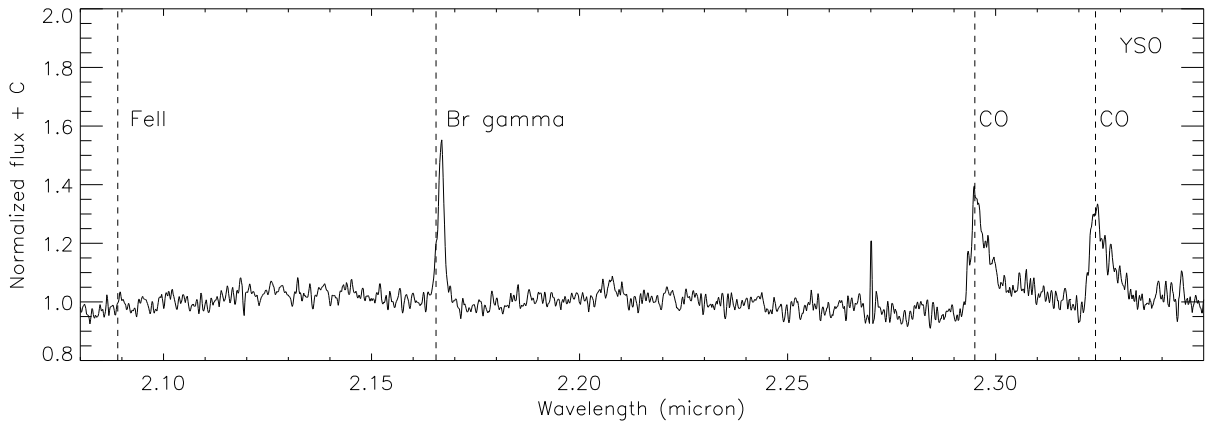

Figure 4.7: Normalized K-band spectrum of the star identified as YSO. Indicated with dashed lines are CO emission lines at the long wavelength end of its K-band spectrum. Locations of other possible diagnostic lines of YSO such as FeII and Brγ are also indicated.

YSO according to previous studies (Bik & Thi 2004; Blum et al. 2004). In addition to CO lines, the YSO in W51 also shows Brγ and faint FeII in emission. The origin of Brγ emission is either the surrounding HII region or the ionised regions of the circumstellar disk. The FeII emission might be caused by UV fluorescence of high-luminosity objects (McGregor et al. 1988). As we have little knowledge on the photosphere of this star itself, the spectral type of the central star is hard to determine. But the presence of Brγ and faint FeII lines suggest it is a hot and massive star (Bik et al. 2006).

4.3.4 HRD

After having properly classified the spectral types of the OB-type main sequence stars, we can put them in the HRD with the help of stellar atmosphere models. The effective temperature of O-type main sequence stars is taken from Martins et al. (2005), while the bolometric correction and the intrinsic $H-K$ colors are from Martins & Plez (2006). The effective temperature, bolometric correction and the intrinsic $H-K$ colors of B type main sequence stars are from Pecaut & Mamajek (2013), since the models by Martins do not include B type stars. By assuming the Indebetouw et al. (2005) extinction law, the extinction (A_K) was derived. The absolute K-band magnitudes were calculated by subtracting A_K and the distance modulus from the apparent magnitudes. Considering the bolometric correction from stellar models we can get the bolometric magnitudes and then derive the luminosity of the OB stars, and thus place them in the HRD.

In Fig. 4.8, the OB stars discovered in our spectroscopic survey are indicated with red and blue

dots refering to the regions they are associated with (Stars indicated with red dots are in G49.5-0.4 of W51A, stars with blue dots are in G49.2-0.3 of W51B). The very luminous source, named LS1 in Okumura et al. (2000), is presented with a yellow dot in the HRD. Apart from the observed stars, we overplot the ZAMS isochrone from Lejeune & Schaerer (2001) and main sequence isochrones for 1, 2, 3 and 5 Myrs from Ekström et al. (2012) and Yusof et al. (2013) with dashed lines, together with the PMS isochrones of 1 and 2 Myrs from Tognelli et al. (2011) with dashed-dotted lines.

Inspecting Fig 4.8 shows that the location of the stars cannot be fit by one single isochrone. The most luminous star (#1) is located between the 1 and 2 Myrs isochrone, similar to #9, near the 1-2 Myrs PMS isochrone. On the other hand, the location of LS1 is close to the 5 Myrs isochrone, consistent with the age derived by Clark et al. (2009). Several other stars in our sample might have a similar age. This suggests that star formation in W51 has been active for at least 5 Myrs. We do not find any clear distinction between different regions, though this might in part be due to our small sample size.

In Fig. 4.9, the stellar evolution tracks from Geneva models (Ekström et al. 2012; Yusof et al. 2013) are plotted in solid lines. By comparing the locations of OB stars in Fig. 4.9, the masses of OB stars are derived with a rang from a few to over one hundred $M_{\odot}$. The physical parameters discussed above are summarized in Table. 4.2.

4.4 Discussion and Summary

4.4.1 Notes on individual clusters

G49.5-0.4

G49.5-0.4 is the most well studied region and the most luminous region in W51. It contains several strong radio sources: W51h (covered by Box 1 of our observation), W51f/g (Box3_NE), W51d/e (Box3_SW) (Mehringer 1994). Two embedded clusters indicated by infrared sources IRS1 and IRS2 are associated with W51e and W51d (Kumar et al. 2004), respectively. This fact implies the clusters are embedded in gas and dust of the W51 GMC.

Numerous studies have been performed on W51d/IRS2 using data from a wide wavelength range. Using mm continuum observations, Zapata et al. (2009) reported the presence of a dusty circum-stellar disk and outflow perpendicular to it in IRS2, suggesting a single very massive protostar with a central stellar mass of more than 60 $M_{\odot}$. The two bright sources IRS2E and IRS2W were identified from low resolution NIR images, and IRSE was suggested to be a small cluster

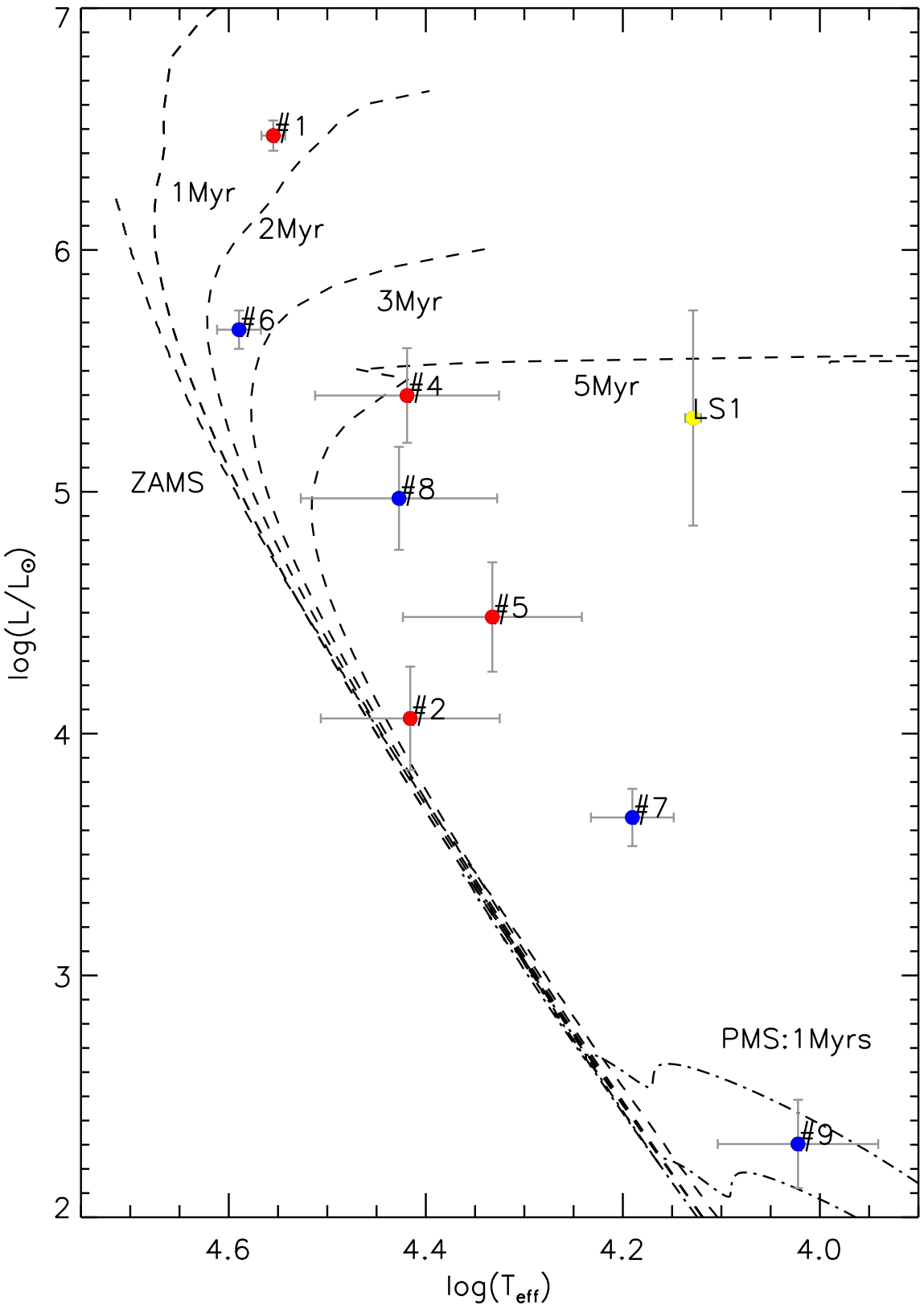

Figure 4.8: HRD of stars identified as OB stars in our spectroscopic survey. The dashed lines represent the ZAMS isochrone from Lejeune & Schaerer (2001) and main-sequence isochrones for 1, 2, 3 and 5 Myrs from Ekström et al. (2012) and Yusof et al. (2013). The dash-dot lines represent the PMS isochrones of 1 and 2 Myrs from Tognelli et al. (2011). The stars are de-reddened using the extinction law of Indebetouw et al. (2005). The location of LS1 (Okumura et al. 2000) is marked with a yellow dot.

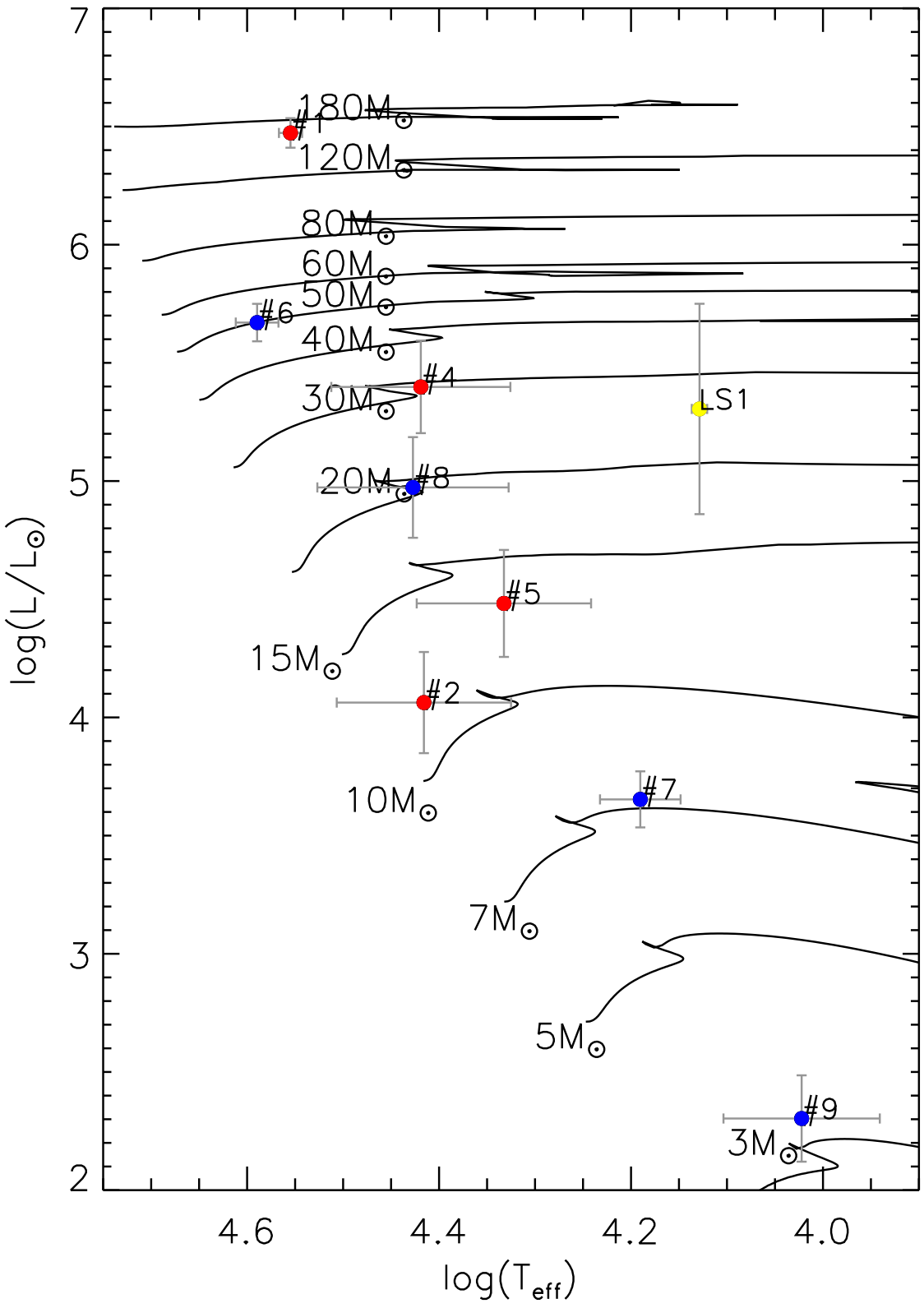

Figure 4.9: HRD of stars identified as OB stars in our spectroscopic survey. The solid lines represent the evolutionary tracks from Ekström et al. (2012) and Yusof et al. (2013). The stars symbols have the same meaning with in Fig. 4.8.

of stars (Goldader & Wynn-Williams 1994). High resolution imaging reveals that IRS2E as a single unresolved source (Figuerêdo et al. 2008). The spectrum of IRS2E shown in Figuerêdo et al. (2008) may reflect the nebular nature, when considering its similarity with the UCHII region G25.2-1.74 (Bik et al. 2005). Mid-infrared (7.8-13.5 μm) observations resolved IRS 2 into seven sources, including four UCHII regions and an embedded protostar (Okamoto et al. 2001). Spectral types of the central ionizing sources derived from mid-infrared data are later than those from the radio continuum flux.

Two very luminous stars (LS1 and LS2) were discovered by Okumura et al. (2000). A high resolution K-band spectrum of LS1 (marked in Box 1 of Fig. 4.3) identifies it as a P Cygni supergiant (Clark et al. 2009). This suggests star formation might be externally triggered instead of simply proceeding sequentially (Kumar et al. 2004).

G49.2-0.3

G49.2-0.3 is the largest and brightest HII region of W51B, which is a long filamentary structure including three other UCHII regions (G49.1-0.4, G49.0-0.3 and G48.9-0.3) not covered by our spectroscopic survey. The four UCHII regions are located almost in a line parallel to the Galactic plane (Koo 1999). G49.2-0.3 is associated with the cloud NE, while the other three UCHII regions are associated with the cloud SW according to their positions and velocities. The radio continuum morphology suggest G49.2-0.3 to be a "blister" type HII region formed near the edge of a molecular cloud (Koo 1999).

The shape of the G49.2-0.3 region are suggested to be the product of shock wave interaction between the supernova remnant W51C and the GMC (Kumar et al. 2004). OH masers observed in the vicinity of G49.2-0.3 provide evidence for this interaction (Brogan et al. 2013). To the southeast of G49.2-0.3 the pulsar wind nebula candidate CXO J192318.5+1403035 found (Koo et al. 2005; Aleksić et al. 2012; Brogan et al. 2013) to be associated with the supernova remnant. The K-band nebulosity shown in Box 5 of Fig. 4.3 reveals a shell like morphology similar to what is observed in the 21-cm continuum (Koo & Moon 1997).

4.4.2 Spatial distribution of the massive stars in GMC region

The locations of our star sample comprising eight OB stars and a YSO might suggest different star formation processes. In G49.5-0.4, the massive stars identified by our NIR observation (Box 3_SW region) do not reside in the very central part of the clusters. The only exception is an O-type star (#1,associated with W51e/IRS1), which is the most massive star identified in our study. The other three stars (#2,#4 and #5) are all of early B type with much lower masses, and

are associated with the nebulosity structures in the outskirt of the compact centres. This may hint at the presence of mass segregation. The location in the HRD (Fig. 4.8) suggest an age for star #1 of 1-2 Myrs, which is younger than the age estimate for the three B stars. The YSO detected in our spectroscopic survey resides on the edge of the cluster in the centre of Box 3 (Fig. 4.3), outside of our sampling region for the photometric analysis.

In G49.2-0.3, which is covered by Box 5 in our observation, the most massive star (#6) is found again in the dense centre of the cluster. Star #7 and #8 sit in the southeast part of the HII region, where the brightness of radio continuum decrease smoothly (Koo 1999), though their extinction is comparable with star #6, which resides in the densest HII region. Star #9, located in the northwest part of the HII region, suffers from much lower extinction because it is less obscured by the cloud. Star #7 and #9 are located far from the main sequence isochrones in Fig. 4.8. Star #9 falls on the region of PMS star isochrones with an age between 1 and 2 Myrs. Star #7, which is also falls above the main sequence, could be an intermediate-mass PMS star (see, e.g., Bik et al. (2012)). Usually PMS stars located above the "birth line" (Bik et al. 2012, Fig. 4) are not visible in the optical, but the ability of penetrating with NIR observations might make this kind of objects detectable in our observation. However, star #7 could also be a fore/background star with a much older age since the cluster membership is difficult to confirm. To conclude, the morphology of the HII region together with the distributions of stars of different kinds, including a younger O star (#6), an older B star (#8), a PMS star (#9) and a possible intermediate-mass PMS star, make the formation of this region more complicated than in the region of G49.5-0.4.

4.4.3 Star formation history

Sequential star formation in G49.5-0.4 was claimed by Okumura et al. (2000). By investigating their NIR photometry, an age spread between region 1, 2 and 3 in their paper has been found, implying the internal triggered star formation from north to south. Clark et al. (2009) object against this hypothesis because if region 1 triggered similar star formation activity in region 3, then we might expect to see a large wind blown cavity in mid-IR created by stars like LS1 in region 1. But Spitzer observations reveal that IRS2 does not resides on the boundaries of any wind bubble, implying IRS2 formed independently of the effect of other regions. Thus no evidence of internal triggering was found and the star formation event of W51 might be a result of a large scale external trigger (Kumar et al. 2004).

On the other side of the W51 GMC is G49.2-0.3, which was thought to be triggered by the interaction between the supernova shock wave and the cloud. With four stars identified in this region through our spectroscopic study, the stars ranging from PMS (#9) to the main sequence star (with star #8 as the oldest one having an age of $\sim$ 5 Myrs). Considering the estimated age

of the supernova remnant W51C of only 30 kyr (Koo et al. 1995), the formation of the stars we observed in G49.2-0.3 cannot have been triggered by the supernova event. This instead supports that star formation originated at multiple sites. The appearance of LS1, a P Cygni-type supergiant (Okumura et al. 2000) in W51A suggests the star formation has been underway for at least 5 Myrs (Clark et al. 2009).

4.4.4 Distinct star formation histories in W51 and W49

W51 and W49, two of the most massive and luminous star forming regions in our Galaxy have a lot of features in common. Both region are located in the galactic plane inside a spiral arm. The parental GMCs have very similar total gas masses of 1.1×10^6 $M_\odot$ for W49 (Galvan-Madrid et al. 2013) and 1.2×10^6 $M_\odot$ for W51 (Carpenter & Sanders 1998). The estimated total stellar masses of $5-7 \times 10^4$ $M_\odot$ for W49 (Homeier & Alves 2005) and $\sim 10^4$ $M_\odot$ for W51 (Kumar et al. 2004) are also on the same order. The lower stellar mass and thus lower star-forming efficiency in W51 might be related to the more widely spread-out star-forming regions, and the lack of a central massive cluster.

Nevertheless, the similar initial conditions of these two regions do not result in similar morphologies and forming clusters with similar properties. On the contrary, their formation scenarios have obvious distinctions, implying two completely different star-forming patterns. By looking at the results of our spectroscopic surveys of W51 (Table. 4.2) and W49 (Table. 3.2), the stellar populations are found to be very different. In W51, we find no VMS while in W49 three VMSs with stellar wind features are found. In addition, stars observed in W49 are more massive and have earlier spectral types than stars found in W51 in general. What is the reason of the absence of VMSs in W51? The most direct explanation might be different scales they are in, compared to the very compact central region of W49, which harbours the major part of the mass of the GMC, W51 has a more extended shape elongated along the galactic plane with a length of ~ 60 pc, more than 10 times the size of W49. Star formation in W51 seems to have been seeded on multiple locations. This suggests independent cloud fragmentation at different sites, and individual collapses on their own. As a consequence, the physical interaction between different subregions was very weak. Clark et al. (2009) found no evidence of internally trigged, sequential star formation within W51, and favour the scenario that star formation happened at multiple independent sites within the GMC, triggered by a Galactic spiral density wave Kumar et al. (2004). In W49, on the other hand, the most massive stars reside in the central cluster and quite likely provide feedback to further star formation activities like those identified in the "Welch ring" (Sect. 3.4.3).

The fact that both W51 and W49 have supernova remnants close to the GMCs is another very interesting common point. In W49, we do not find a signature of supernova remnant (W49B)

interacting with the star-forming region. In the case of the supernova remnant W51C, an interaction with GMC is taking place, and might be responsible for triggering future star formation e.g. in the vicinity of the HII region G49.2-0.3 (Brogan et al. 2013). Our investigation suggests a longer lasting star formation history as stars with ages considerably older than the supernova remnant are present, resulting in a complex star formation history and future of the G49.2-0.3 region.

To summarize, two types of star formation patterns have been observed in W51 and W49. The wide spread, multiple seeds star formation in W51 is triggered and affected mainly by external effects such as galactic density wave and the current interaction with a supernova shock wave. Its lower star formation efficiency compare to W49 might be a result of the star formation activities in more distributed regions (Bonnell et al. 2011). The end products of such kind of regions might be OB associations (Clark et al. 2005b). In W49 with its central massive cluster, where the gravity of the central region dominants the evolution, internal triggers seem to play a more important role.

4.5 Conclusions

In this Chapter, we present the JHK_s imaging form NTT/SOFI and K-band spectroscopy from LBT/LUCI on stellar content in the star-forming region of W51. Nine OB-type stars have been identified from spectroscopic classification by means of the diagnostic lines in their K-band spectra. A YSO is found with the circumstellar disk features shown in its spectrum.

By investigating the CMDs and CCDs of the entire region W51 and subregions indicated in Fig. 4.3 assuming a distance of 5.4 kpc (Sato et al. 2010) and an extinction law of Indebetouw et al. (2005), stellar populations at low and high extinctions are visible. In the compact centre of G49.5-0.4 the extinction go as high as $\sim$ 4.7 (Star #1), while star #9 resides on the "back" of a HII region not embedded in the molecular clouds.

The most massive star discovered by our spectroscopic survey is star #1 (with an estimated mass over 100 $M_\odot$) falls in the compact centre of HII region G49.5-0.4, with a very young age (1-2 Myrs). While other three stars classified as B type stars, located in the outskirt of the same region with an older age ($\sim$ 5 Myrs). Additionally, the location of the YSO is on the edge of the HII region even out of the sampling region of the photometry analysis, implying complex star formation history in this region. In another HII region investigated in this chapter, G49.2-0.3, stars ranging from mid-O to PMS are observed and signatures of interaction between the supernova remnant and GMC are found.

By studying the physical parameters and the spatial distributions of the stellar population in W51,

the property and environment of this region are analysed. The star formation history of W51 is discussed and compared to the star forming region we studied in the previous chapter of W49. With similar physical conditions in the mass of gas and locations on the galactic plane, W51 and W49 show distinct morphologies and stellar content. The possibility that different star formation patterns might be applied in the their star formation histories are discussed.

Chapter 5

Summary and Future Prospect

5.1 Summary

In this thesis, I aim to investigate the star formation mechanisms of different star-forming regions in our Galaxy by NIR spectroscopic studies on their massive stellar content. I focus on two of the most massive and luminous regions: W49 and W51. Both of them are with abundant reservoir of gas, and high total stellar mass, but result in different stellar populations and morphologies. The thesis consists of three major parts:

In Chapter 2, a VMS (M > 100 $M_\odot$) is identified in the central cluster of W49. VMSs are very rare objects, but have a strong influence on their environment. The formation of this kind of objects is of prime importance in star formation, but observationally still poorly constrained. We investigate near-infrared K-band spectroscopic observations of W49 from VLT/ISAAC together with JHK images obtained with NTT/SOFI and LBT/LUCI. On the basis of its K-band spectrum, W49nr1 is classified as an O2-3.5If* star with a K-band absolute magnitude of -6.27±0.10 mag according to classification criteria based on the equivalent widths of Brγ and He II given by Crowther & Walborn (2011). The effective temperature and bolometric correction are estimated from stars of similar spectral type. After comparison to the Geneva evolutionary models, we find an initial mass between 100 $M_\odot$ and 180 $M_\odot$. The effect of variations in the extinction law on the stellar parameters result in a large initial mass range of 90 - 250 $M_\odot$.

In Chapter 3, the NIR K-band spectroscopic observation of W49 from LBT/LUCI combined with JHK images obtained with NTT/SOFI and LBT/LUCI are analysed. High extinction (on average $A_K \sim 3$ mag) as well as large extinction variations are confirmed in this region. Thirteen O-type stars as well as two YSOs are identified according to the features presented in their K-band spectra. Based on JHK-band photometry and K-band spectroscopy the massive stars are placed in a HRD. By comparing with evolutionary models their age, and hence the star formation history of W49 can be investigated. Ten O-stars are main sequence stars with subtypes ranging

from O9.5V to O3V, and with masses ranging from ~ 20 $M_\odot$ to ~ 120 $M_\odot$. Three of the O stars show strong wind features, and are considered to be Of type supergiants with masses beyond 100 $M_\odot$. Two YSOs show CO emission, indicative for the presence of circumstellar disks in the central region of the massive cluster. The age of the cluster is estimated as ~ 1.5 Myrs, with star formation still ongoing in different parts of the region. The ionising photons from the central massive stars have not yet cleared the molecular cocoon surrounding the cluster. W49 is comparable to extragalactic star-forming regions and provides us with an unique possibility to study a starburst in detail.

In Chapter 4, the JHK_s imaging obtained with NTT/SOFI and K-band spectroscopy obtained with LBT/LUCI on stellar content in the star-forming region of W51 are presented. Nine OB-type stars have been identified from spectroscopic classification by means of the diagnostic lines in their K-band spectra. A YSO is found with spectral signatures of CO, indicative of the presence of a circumstellar disk. Five of the OB stars are associated with HII region G49.5-0.4 in the brightest region of W51A, while four OB stars are associated with G49.2-0.3 in the brightest region of W51B. Based on the analysis of the HRD with our limited sample, I find no obvious age difference between different subclusters. The star formation in W51 has started ~ 5 Myrs ago and still ongoing until now. Both the star formation history and the stellar population of W51 seems to differ from W49. The possibility of different star formation mechanisms in these two regions is discussed.

My investigation of two of the major star-forming regions located in spiral arms in our Galaxy has revealed their massive stellar populations in greater detail. This results in clues on the past and future evolution of these regions, and – perhaps even more importantly – indicates that different star formation mechanisms have been at work in the parental GMCs of W49 and W51.

5.2 Future

While considerable new insights are revealed on the star formation activities in W49 and W51 by the spectroscopic survey, also new questions are raised. Some of these questions may be answered by a continuation of the present surveys or its extension to multi-wavelength studies, while other questions will require future observational instruments.

5.2.1 Immediate plans

Within both W49 and W51 regions, dozens of infrared excess sources are identified with the K-band excess based on the CCDs of the stellar clusters. The infrared excess implies the presence of

disks around the stellar objects in the star forming regions. In order to determine the disk fraction for each of the clusters, observations extending into the mid-infrared, starting with the L'-band, are required. As the inclusion of L'-band observations have been proven to more sensitive than simple JHK excess measurements, this will provide a better estimate of the true disk fraction for each of the clusters. With the observed spatial distributions of the excess sources, we will learn how disks evolve within different environments through external effects like photo evaporation and gravitational interactions, which can boost the dispersion of disks.

It is well known that the multiplicity of massive stars is higher than for low mass stars. For the massive stars discovered in our spectroscopic survey, it is quite possible that most of them are actually binary or multiple systems. The likelihood of VMSs discovered in W49 to be binaries are discussed in Sect. 3.3.4. The X-ray counterparts at the same positions of massive stars provide a sign of multiplicity, but the further confirmation relies on the more detailed and specific observations toward our massive star samples in X-ray.

In addition, a program operated by VLT/K-band Multi Object Spectrograph (KMOS) is ongoing (PI: A. Bik) to explore the feedback processes from young massive stars to their parental HII regions. Observational constraints will be put on the various feedback mechanisms by investigating three giant HII regions: G333.6-0.2, M8 and NGC 6357. The unique ability of KMOS to perform spectroscopy for multiple targets simultaneously are utilized. A large program covering the full sample of nearby giant HII regions is also in planning.

5.2.2 Long term prospect

The next generation high resolution instrument E-ELT (Fig. 5.1, right panel) is a ground based 40-m class telescope currently being built by ESO, and the first light is targeted for 2024. Located on top of Cerro Armazones in the Atacama Desert of northern Chile, it will provide high resolution optical and NIR spectra of stars using the planned instrument named High Angular Resolution Monolithic Optical and Near-infrared Integral field spectrograph (HARMONI). With the extreme large diameter, the E-ELT will have the capability of catching the light from extra-galactic stellar clusters and more important, resolve the stellar content inside them. These studies promise to reveal unprecedented details and to deliver new (and perhaps unexpected) insights into those extra-galactic stellar objects. With the higher spatial resolution, direct imaging and identification of those multiple systems will become possible in the crowded star fields like centres of stellar clusters. Furthermore, higher spectral resolution will reduce the nebular contamination in the observed spectra and hence improve the spectral classification of the embedded stellar objects.

A little bit closer in time, the next generation space observatory, JWST (Fig. 5.1, left panel), is

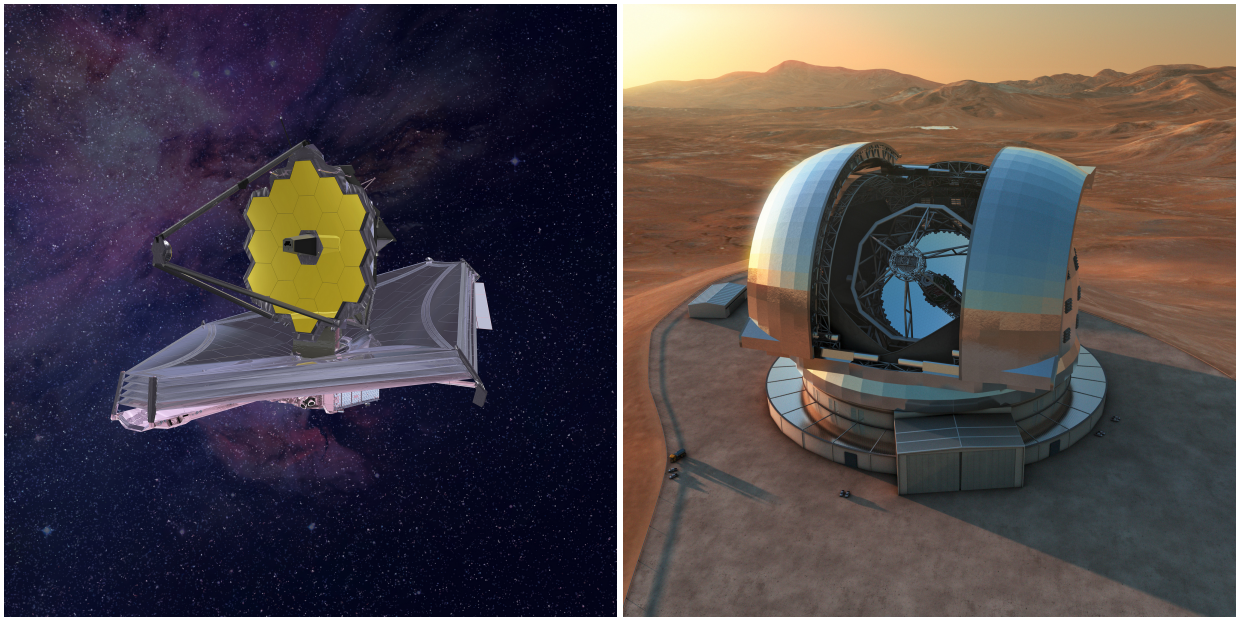

Figure 5.1: *Left:* The artist's impression of JWST from its homepage (http://www.jwst.nasa.gov/) *Right:* The artist's impression of E-ELT from its homepage (http://www.eso.org/public/teles-instr/e-elt/)

scheduled to launch in 2018. Compared to E-ELT, it offers lower angular, but higher sensitivity observations, in particular in the wavelengths regions in the near- and mid-infrared, which are outside of the atmospheric windows of Earth. The longer wavelength range will provide a chance to look closely into the protostar populations in young star-forming regions. Through observations in mid-infrared bands, the earlier stage of star formation can be revealed.

Acknowledgments

First, I would like to acknowledge Thomas Henning, for providing me the precious opportunity to start my PhD in MPIA. Thomas has taught me a lot, not only on science, but also on how to be a good scientist. He always give important directions for my work, and encouraged me to be more positive. I am and will keep learning from his expertise and insights, and most important, passion for Astronomy.

I am particularly grateful to Arjan Bik for all the time and energy he spent on me during the last three years. Without his help, the works in this thesis can not be completed. He was always patient and willing to help me no matter how stupid the questions I asked and how horrible my writing skill was. He is the nicest advisor I can imagine, provide good advices, encourage me all the time, and respond to my requests always in short times. It was my luck to work with Arjan.

I want to thank Anna Pasquali and Wolfgang Brandner for being my thesis committee members. Their kindly help and suggestions on my work are indispensable.

Many thanks to Thomas Henning and Ralf Klessen for being the referees of this thesis, and Mario Trieloff and Arjan Bik for being the examiners of my thesis defense.

Thanks a lot to other collaborators including Andrea Stolte, Joachim Bestenlehner and Miaomiao Zhang for helping improve my papers significantly.

I am grateful to Christian Fendt for his contributions to IMPRS. It is such a lovely program with so many interesting people in. The seminars, retreats and travels with my dear follows will be on of my most precious memories in Heidelberg. I am grateful to Matthias Samland and Wolfgang Brandner for their help with translating the abstract into german. Many tanks to Arjan Bik and Wolfgang Brandner for their comments and suggestions during writing of this thesis. Thanks to Aida Ahmadi for proof-reading part of this thesis.

I am especially indebted to my family. Special thanks to my father Shi-Xian Wu and my mother

Chun Chang for their consistent support for so many years. My wife Fei Wu is the one who has done most for me during my pursuit of my PhD, especially after our daughter, Rui-Xin Wu, was born. The little one caused many troubles but providing more joys for our family lives. Without their company, it is impossible for me to make any achievement.

Bibliography

Ageorges, N., Seifert, W., Jütte, M., et al. 2010, Proc. SPIE, 7735, 53

Aleksić, J., Alvarez, E. A., Antonelli, L. A., et al. 2012, A&A, 541, A13

Allison, R. J., Goodwin, S. P., Parker, R. J., et al. 2009, ApJ, 700, L99

Alves, J. & Homeier, N. 2003, ApJ, 589, L45

Ascenso, J., Alves, J., Beletsky, Y., & Lago, M. T. V. T. 2007a, A&A, 466, 137

Ascenso, J., Alves, J., Vicente, S., & Lago, M. T. V. T. 2007b, A&A, 476, 199

Bally, J., Anderson, L. D., Battersby, C., et al. 2010, A&A, 518, L90

Banerjee, S., Kroupa, P., & Oh, S. 2012, ApJ, 746, 15

Barbosa, C. L., Blum, R. D., Conti, P. S., Damineli, A., & Figuerêdo, E. 2008, ApJ, 678, L55

Bastian, N., Covey, K. R., & Meyer, M. R. 2010, ARA&A, 48, 339

Bestenlehner, J. M., Vink, J. S., Gräfener, G., et al. 2011, A&A, 530, L14

Bik, A., Henning, T., Stolte, A., et al. 2012, ApJ, 744, 87

Bik, A., Kaper, L., Hanson, M. M., & Smits, M. 2005, A&A, 440, 121

Bik, A., Kaper, L., & Waters, L. B. F. M. 2006, A&A, 455, 561

Bik, A., Stolte, A., Gennaro, M., et al. 2014, A&A, 561, A12

Bik, A. & Thi, W. F. 2004, A&A, 427, L13

Blaauw, A. 1961, Bull. Astron. Inst. Netherlands, 15, 265

Blaauw, A. 1991, in NATO Advanced Science Institutes (ASI) Series C, Vol. 342, NATO Advanced Science Institutes (ASI) Series C, ed. C. J. Lada & N. D. Kylafis, 125

Blum, R. D., Barbosa, C. L., Damineli, A., Conti, P. S., & Ridgway, S. 2004, ApJ, 617, 1167

Blum, R. D., Damineli, A., & Conti, P. S. 1999, AJ, 117, 1392

Bonnell, I. A. & Bate, M. R. 2005, MNRAS, 362, 915

Bonnell, I. A., Smith, R. J., Clark, P. C., & Bate, M. R. 2011, MNRAS, 410, 2339

Bonnell, I. A., Vine, S. G., & Bate, M. R. 2004, MNRAS, 349, 735

Bouret, J.-C., Lanz, T., Hillier, D. J., et al. 2003, ApJ, 595, 1182

Brandner, W., Clark, J. S., Stolte, A., et al. 2008, A&A, 478, 137

Bressert, E., Bastian, N., Evans, C. J., et al. 2012, A&A, 542, A49

Brogan, C. L., Goss, W. M., Hunter, T. R., et al. 2013, ApJ, 771, 91

Buschkamp, P., Hofmann, R., Gemperlein, H., et al. 2010, Proc. SPIE, 7735, 236

Cardelli, J. A., Clayton, G. C., & Mathis, J. S. 1989, ApJ, 345, 245

Carpenter, J. M. & Sanders, D. B. 1998, AJ, 116, 1856

Casali, M., Adamson, A., Alves de Oliveira, C., et al. 2007, A&A, 467, 777

Chlebowski, T., Harnden, Jr., F. R., & Sciortino, S. 1989, ApJ, 341, 427

Clark, J. S., Davies, B., Najarro, F., et al. 2009, A&A, 504, 429

Clark, J. S., Negueruela, I., Crowther, P. A., & Goodwin, S. P. 2005a, A&A, 434, 949

Clark, P. C., Bonnell, I. A., Zinnecker, H., & Bate, M. R. 2005b, MNRAS, 359, 809

Conti, P. S. & Blum, R. D. 2002, ApJ, 564, 827

Crowther, P. A., Hadfield, L. J., Clark, J. S., Negueruela, I., & Vacca, W. D. 2006, MNRAS, 372, 1407

Crowther, P. A., Schnurr, O., Hirschi, R., et al. 2010, MNRAS, 408, 731

Crowther, P. A. & Walborn, N. R. 2011, MNRAS, 416, 1311

Dale, J. E., Ngoumou, J., Ercolano, B., & Bonnell, I. A. 2013, MNRAS, 436, 3430

Dale, J. E., Ngoumou, J., Ercolano, B., & Bonnell, I. A. 2014, MNRAS, 442, 694

Davies, R. I. 2007, MNRAS, 375, 1099

de Pree, C. G., Mehringer, D. M., & Goss, W. M. 1997, ApJ, 482, 307

de Wit, W. J., Testi, L., Palla, F., Vanzi, L., & Zinnecker, H. 2004, A&A, 425, 937

de Wit, W. J., Testi, L., Palla, F., & Zinnecker, H. 2005, A&A, 437, 247

de Zeeuw, P. T., Hoogerwerf, R., de Bruijne, J. H. J., Brown, A. G. A., & Blaauw, A. 1999, AJ, 117, 354

Devillard, N. 2001, in Astronomical Society of the Pacific Conference Series, Vol. 238, Astronomical Data Analysis Software and Systems X, ed. F. R. Harnden, Jr., F. A. Primini, & H. E. Payne, 525

Ekström, S., Georgy, C., Eggenberger, P., et al. 2012, A&A, 537, A146

Fang, M., van Boekel, R., King, R. R., et al. 2012, A&A, 539, A119

Fazio, G. G., Hora, J. L., Allen, L. E., et al. 2004, ApJS, 154, 10

Figer, D. F. 2005, Nature, 434, 192

Figuerêdo, E., Blum, R. D., Damineli, A., Conti, P. S., & Barbosa, C. L. 2008, AJ, 136, 221

Fitzpatrick, E. L. 1999, PASP, 111, 63

Fukui, Y., Ohama, A., Hanaoka, N., et al. 2014, ApJ, 780, 36

Galvan-Madrid, R., Liu, H. B., Zhang, Z.-Y., et al. 2013, ArXiv e-prints

Gennaro, M., Bik, A., Brandner, W., et al. 2012, A&A, 542, A74

Gennaro, M., Brandner, W., Stolte, A., & Henning, T. 2011, MNRAS, 412, 2469

Ginsburg, A., Bally, J., Battersby, C., et al. 2015, A&A, 573, A106

Goldader, J. D. & Wynn-Williams, C. G. 1994, ApJ, 433, 164

Grabelsky, D. A., Cohen, R. S., Bronfman, L., & Thaddeus, P. 1988, ApJ, 331, 181

Gräfener, G., Vink, J. S., de Koter, A., & Langer, N. 2011, A&A, 535, A56

Gvaramadze, V. V., Kroupa, P., & Pflamm-Altenburg, J. 2010, A&A, 519, A33

Hambly, N. C., Collins, R. S., Cross, N. J. G., et al. 2008, MNRAS, 384, 637

Hanson, M. M., Conti, P. S., & Rieke, M. J. 1996, ApJS, 107, 281

Hanson, M. M., Kudritzki, R.-P., Kenworthy, M. A., Puls, J., & Tokunaga, A. T. 2005, ApJS, 161, 154

Hernández, J., Hartmann, L., Calvet, N., et al. 2008, ApJ, 686, 1195

Hewett, P. C., Warren, S. J., Leggett, S. K., & Hodgkin, S. T. 2006, MNRAS, 367, 454

Hilditch, R. W., Howarth, I. D., & Harries, T. J. 2005, MNRAS, 357, 304

Hill, J. M., Green, R. F., & Slagle, J. H. 2006, Proc. SPIE, 6267, 31

Hillier, D. J. & Miller, D. L. 1998, ApJ, 496, 407

Hollenbach, D. J., Yorke, H. W., & Johnstone, D. 2000, Protostars and Planets IV, 401

Homeier, N. L. & Alves, J. 2005, A&A, 430, 481

Hoogerwerf, R., de Bruijne, J. H. J., & de Zeeuw, P. T. 2001, A&A, 365, 49

Indebetouw, R., Mathis, J. S., Babler, B. L., et al. 2005, ApJ, 619, 931

Irwin, M. J. 2008, in 2007 ESO Instrument Calibration Workshop, ed. A. Kaufer & F. Kerber, 541

Johnston, K. G., Beuther, H., Linz, H., et al. 2014, A&A, 568, A56

Kausch, W., Noll, S., Smette, A., et al. 2015, A&A, 576, A78

Kennicutt, Jr., R. C. 1984, ApJ, 287, 116

Koen, C. 2006, MNRAS, 365, 590

Koo, B.-C. 1999, ApJ, 518, 760

Koo, B.-C., Kim, K.-T., & Seward, F. D. 1995, ApJ, 447, 211

Koo, B.-C., Lee, J.-J., Seward, F. D., & Moon, D.-S. 2005, ApJ, 633, 946

Koo, B.-C. & Moon, D.-S. 1997, ApJ, 475, 194

Kroupa, P. 2001, MNRAS, 322, 231

Krumholz, M. R. 2014, in Very Massive Stars in the Local Universe, 3417

Kudryavtseva, N., Brandner, W., Gennaro, M., et al. 2012, ApJ, 750, L44

Kuiper, R., Klahr, H., Beuther, H., & Henning, T. 2010, ApJ, 722, 1556

Kuiper, R., Klahr, H., Beuther, H., & Henning, T. 2011, ApJ, 732, 20

Kuiper, R., Klahr, H., Beuther, H., & Henning, T. 2012, A&A, 537, A122

Kumar, M. S. N., Kamath, U. S., & Davis, C. J. 2004, MNRAS, 353, 1025

Kurtz, S. E., Churchwell, E. B., & Wood, D. O. S. 1994, ApJS, 91, 659

Lada, C. J. & Lada, E. A. 2003, ARA&A, 41, 57

Larson, R. B. 1969, MNRAS, 145, 271

Lawrence, A., Warren, S. J., Almaini, O., et al. 2007, MNRAS, 379, 1599

Lejeune, T. & Schaerer, D. 2001, A&A, 366, 538

Longmore, S. N., Kruijssen, J. M. D., Bastian, N., et al. 2014, Protostars and Planets VI, 291

Lucas, P. W., Hoare, M. G., Longmore, A., et al. 2008, MNRAS, 391, 136

Martins, F. & Plez, B. 2006, A&A, 457, 637

Martins, F., Schaerer, D., & Hillier, D. J. 2005, A&A, 436, 1049

McGregor, P. J., Hyland, A. R., & Hillier, D. J. 1988, ApJ, 324, 1071

Mehringer, D. M. 1994, ApJS, 91, 713

Moffat, A. F. J., Drissen, L., & Shara, M. M. 1994, ApJ, 436, 183

Moorwood, A., Cuby, J.-G., & Lidman, C. 1998, The Messenger, 91, 9

Nagy, Z., van der Tak, F. F. S., Fuller, G. A., & Plume, R. 2015, A&A, 577, 127

Nagy, Z., van der Tak, F. F. S., Fuller, G. A., Spaans, M., & Plume, R. 2012, A&A, 542, 6

Negueruela, I., Clark, J. S., & Ritchie, B. W. 2010, A&A, 516, A78

Nishiyama, S., Tamura, M., Hatano, H., et al. 2009, ApJ, 696, 1407

Okamoto, Y. K., Kataza, H., Yamashita, T., Miyata, T., & Onaka, T. 2001, ApJ, 553, 254

Okumura, S.-i., Mori, A., Nishihara, E., Watanabe, E., & Yamashita, T. 2000, ApJ, 543, 799

Olczak, C., Pfalzner, S., & Eckart, A. 2010, A&A, 509, A63

Pasquali, A., Bik, A., Zibetti, S., et al. 2011, AJ, 141, 132

Pecaut, M. J. & Mamajek, E. E. 2013, ApJS, 208, 9

Peng, T.-C., Wyrowski, F., van der Tak, F. F. S., Menten, K. M., & Walmsley, C. M. 2010, A&A, 520, A84

Philp, C. J., Evans, C. R., Leonard, P. J. T., & Frail, D. A. 1996, AJ, 111, 1220

Preibisch, T., Roccatagliata, V., Gaczkowski, B., & Ratzka, T. 2012, A&A, 541, A132

Rieke, G. H. & Lebofsky, M. J. 1985, ApJ, 288, 618

Roberts, H., van der Tak, F. F. S., Fuller, G. A., Plume, R., & Bayet, E. 2011, A&A, 525, A107

Rochau, B., Brandner, W., Stolte, A., et al. 2010, ApJ, 716, L90

Román-Zúñiga, C. G., Lada, C. J., Muench, A., & Alves, J. F. 2007, ApJ, 664, 357

Sabbi, E., Sirianni, M., Nota, A., et al. 2008, AJ, 135, 173

Salpeter, E. E. 1955, ApJ, 121, 161

Saral, G., Hora, J. L., Willis, S. E., et al. 2015, ArXiv e-prints

Sato, M., Reid, M. J., Brunthaler, A., & Menten, K. M. 2010, ApJ, 720, 1055

Seifert, W., Ageorges, N., Lehmitz, M., et al. 2010, Proc. SPIE, 7735, 256

Shu, F. H., Adams, F. C., & Lizano, S. 1987, ARA&A, 25, 23

Skrutskie, M. F., Cutri, R. M., Stiening, R., et al. 2006, AJ, 131, 1163

Smette, A., Sana, H., Noll, S., et al. 2015, A&A, 576, A77

Sollins, P. K., Zhang, Q., & Ho, P. T. P. 2004, ApJ, 606, 943

Stetson, P. B. 1987, PASP, 99, 191

Stevens, I. R., Blondin, J. M., & Pollock, A. M. T. 1992, ApJ, 386, 265

Stolte, A., Brandner, W., Brandl, B., Zinnecker, H., & Grebel, E. K. 2004, AJ, 128, 765

Stolte, A., Hussmann, B., Olczak, C., et al. 2015, eprint arXiv

Stolte, A., Morris, M. R., Ghez, A. M., et al. 2010, ApJ, 718, 810

Tognelli, E., Prada Moroni, P. G., & Degl'Innocenti, S. 2011, A&A, 533, A109

Vargas Álvarez, C. A., Kobulnicky, H. A., Bradley, D. R., et al. 2013, AJ, 145, 125

Warren, S. J., Cross, N. J. G., Dye, S., et al. 2007, ArXiv Astrophysics e-prints

Weidner, C., Kroupa, P., & Bonnell, I. A. D. 2010, MNRAS, 401, 275

Welch, W. J., Dreher, J. W., Jackson, J. M., Terebey, S., & Vogel, S. N. 1987, Science, 238, 1550

Wheelwright, H. E., Oudmaijer, R. D., de Wit, W.-J., et al. 2010, MNRAS, 408, 1840

Wu, S.-W., Bik, A., Henning, T., et al. 2014, A&A, 568, L13

Yusof, N., Hirschi, R., Meynet, G., et al. 2013, MNRAS, 433, 1114

Zapata, L. A., Ho, P. T. P., Schilke, P., et al. 2009, ApJ, 698, 1422

Zhang, B., Moscadelli, L., Sato, M., et al. 2014, ApJ, 781, 89

Zhang, B., Reid, M. J., Menten, K. M., et al. 2013, ApJ, 775, 79

Zinnecker, H. & Yorke, H. W. 2007, ARA&A, 45, 481

Acronyms

CCD	Color-Color Diagram
CMD	Color-Magnitude Diagram
DIT	detector integration time
E-ELT	European Extremely Large Telescope
ESO	European Southern Observatory
EW	Equivalent Width
FWHM	Full Width at Half Maximum
GMC	Giant Molecular Cloud
HARMONI	High Angular Resolution Monolithic Optical and Near-infrared Integral field spectrograph
HRD	Hertzsprung-Russell Diagram
IMF	Initial Mass Function
ISAAC	Infrared Spectrometer And Array Camera
ISM	interstellar medium
JWST	James Webb Space Telescope
KMOS	K-band Multi Object Spectrograph
LBT	Large Binocular Telescope
LOBSTAR	LUCI OBservation of STARburst regions
LUCI	LBT NIR Spectroscopic Utility with Camera and Integral field unit
MOS	Multi-Object Spectroscopy
NDIT	number of integrations
NIR	near-infrared
NTT	New Technology Telescope

PMS pre-main-sequence

PSF point spread function

SNR Sinal-to-Noise Ratio

SOFI Son of ISAAC

UCHII Ultracompact HII

VLT Very Large Telescope

VMS very massive star

Wd1 Westerlund 1

YMC Young Massive Cluster

YSO Young Stellar Object

ZAMS Zero Age Main Sequence